REPORT DOCUMENTATION PAGE

Form Approved OMB No. 0704-0188

1. REPORT DATE *(DD-MM-YYYY)*	2. REPORT TYPE	3. DATES COVERED *(From – To)*
08-08-2005	Final Report	30 May 2003 - 27-Dec-05

4. TITLE AND SUBTITLE

Modification of Aerodynamic Surfaces Using Plasma

5a. CONTRACT NUMBER
FA8655-03-D-0001, Delivery Order 0005

5b. GRANT NUMBER

5c. PROGRAM ELEMENT NUMBER

6. AUTHOR(S)

Professor Igor Mikhailovich Minaev

5d. PROJECT NUMBER

5d. TASK NUMBER

5e. WORK UNIT NUMBER

7. PERFORMING ORGANIZATION NAME(S) AND ADDRESS(ES)

M.V. Lomonosov Moscow State University (MSU)
Leninskie Gory
Moscow 119992
Russia

8. PERFORMING ORGANIZATION REPORT NUMBER

N/A

9. SPONSORING/MONITORING AGENCY NAME(S) AND ADDRESS(ES)

EOARD
PSC 802 BOX 14
FPO 09499-0014

10. SPONSOR/MONITOR'S ACRONYM(S)

11. SPONSOR/MONITOR'S REPORT NUMBER(S)
EOARD Task 02-9005

12. DISTRIBUTION/AVAILABILITY STATEMENT

Approved for public release; distribution is unlimited.

13. SUPPLEMENTARY NOTES

14. ABSTRACT

This report results from a contract tasking M.V. Lomonosov Moscow State University (MSU) as follows: The contractor will accomplish the following: (1) develop and manufacture a compact plasma generator; (2) manufacture various geometric shaped wind tunnel models; (3) investigate the propagation of electric fields and discharges over the models; (4) conduct aerodynamic wind tunnel testing; (5) investigate the effect of the plasma on aerodynamic performance and assess sensitivities to plasma discharge parameters; (6) Experimental optimization of the plasma boundary layer; (7) Theoretical analysis of the gas discharge and aerodynamic interaction and the effect on drag and heat transfer.

15. SUBJECT TERMS
EOARD, Flow Control, Plasma Aerodynamics

16. SECURITY CLASSIFICATION OF:			17. LIMITATION OF ABSTRACT	18, NUMBER OF PAGES	19a. NAME OF RESPONSIBLE PERSON
a. REPORT	b. ABSTRACT	c. THIS PAGE			SURYA SURAMPUDI
UNCLAS	UNCLAS	UNCLAS	UL	110	19b. TELEPHONE NUMBER *(Include area code)* +44 (0)20 7514 4299

U.S. CIVILIAN RESEARCH AND DEVELOPMENT FOUNDATION FOR THE INDEPENDENT STATES OF THE FORMER SOVIET UNION

GRANT ASSISTANCE PROGRAM

FINAL TECHNICAL REPORT

Project Title: **"Modification of Aerodynamic Surfaces Using Plasma"**

CRDF Project #: RPO-1382-MO-03

Principal Organization: Faculty of Physics of Moscow State University

Project Director:  **I.M. Minaev .**
(instead of I.B. Timofeev)

Reporting Period: **.May 30, 2003 – May 30, 2005**

Moscow
July 2005

Partner - EOARD

Phone /Fax: (095) 4686849 / 939-17-87 E-mail: bychvl@orc.ru

Contents

Summary

Investigations of sliding discharge plasma influence on a character and structure of a picture of the working model streamlining by an incident flow at the flow velocity corresponding to the Mach number M =3 have been carried out for the first time. The sliding discharge was initiated on a surface of the working model in a boundary layer. Conditions have been determined at which stable

development of the sliding discharge over a separation boundary of two dielectrics with different dielectric permittivity (two solid dielectrics and solid and liquid dielectrics) is observed. Sliding discharge characteristics in different conditions have been determined (at different pressures, in gas flow and without flow in wind tunnel). Pressure measurements on the working model surface has been made before and after a boundary layer disturbance by the sliding discharge. Change of gas flow around character was detected at minimal energy put of ~ 0.1 J/cm^3 to the discharge (boundary layer thickness change, inclination angle change of disturbances lines, turbulization of a boundary layer, changing of static pressure behind the excitation zone). We undertook investigation of gas flow streamlining character of two types of working models: a flat plane and a cylinder.

Theoretical analysis of sliding discharge physical model has been made. High temperature plasma layer influence on a value of a friction tension has been considered. Analysis of sliding discharge plasma influence on character of vortices forming in a boundary layer has been made. Numerical modeling of flat plane streamlining character has been made for the case of a heat source on the plane surface. Numerical modeling of a streamlining character has been made for pulse thermal source. Obtained new experimental and theoretical results allow to estimate area of further experimental and theoretical investigations and practical applications of the sliding discharge in the plasma aerodynamics.

INTRODUCTION

An opportunity for using of gas discharges in high-speed vehicle aerodynamics opens nowadays. Works in this direction were discussed in details during «Weakly Ionized Gases Workshop» from 1-st, in 1997 to 5-th in 2005 in USA. Basic areas of gas discharge applications in aerodynamics were outlined: drag reduction of vehicles and influence on the aerodynamic characteristics of streamline bodies, creation of lift forces, improvement of burning conditions of fuel mixtures, suppression of engine noise, decrease of sound impact, etc

Analysis of literature data shows that application of gas discharge different types can substantially influence oncoming supersonic flow structure as well as aerodynamic characteristics of flying vehicles. In so doing one of mostly convenient and energy profitable discharge type – a sliding discharge proved still not to be called for solution of plasma aerodynamic problems.

A sliding discharge possess a number of unique properties (simplicity of realization, comparably low energy usage necessary for its forming over large surfaces, insensibility to a supersonic flow) making it rather prospectus for applications in practical aerodynamics.

Experimental investigations in the presented Project included: 1.Development and manufacturing of power source for a sliding discharge; manufacturing of aerodynamic models; test experiments on formation of a sliding discharge over a flat plate 100×300×3 mm.; 2. Diagnostics of a sliding discharge. 3.Determination of temperature and charged particle concentration distributions in a discharge plasma; 4. Assembling of a diagnostic stand for measuring of sliding discharge's parameters in a supersonic flow; 5. Analysis of discharge power characteristics and investigation of sub-layer material effect on the discharge properties. 6. Test experiments on sliding discharge's forming at a curvilinear surface (half-cylinder of 50 mm diameter, 300 mm length, 3 mm width); 7. Realization of plasma aerodynamic experiment: visualization of turbulent boundary layer near flat and curvilinear surfaces, visualization of plasma boundary layer.

Theoretical investigations included: 1. Development of a discharge physical model. 2. Development of a computer code of non-stationary turbulent boundary layer over a plate at presence of pulse energy sources in it. 3. Development of a discharge physical model over a curvilinear surface. 4. Preliminary analysis of sliding discharge effect on friction and thermal exchange at the plate in a turbulent boundary layer. 5. Theoretical investigations of plasma boundary layer over a flat plate effect on flow characteristics. 6. Undertaking of multiple calculations and analysis of obtained results. 7. Adoption of the developed code for description of viscous gas flow over curvilinear surfaces at presence of energy release sources in a flow.

Experimental investigations were carried out at flow Mach number M = 0.8 or 0.9 in subsonic mode and M=3 in a supersonic mode, typical size of flat and curvilinear plates 100 × 300 mm, curvature radius of half tubes R = 25 mm., power of electric source is up to 5 kW.

Overall purposes were:

1. Corroboration of the opportunity of large plasma leaf creation on a dielectric or metallic surface in supersonic flows. Realization of plasma aerodynamic experiment: visualization of turbulent boundary layer over a surface, visualization of plasma boundary layer.
2. Collection of experimental data about sliding discharge parameters and energy characteristics in a supersonic flow at different values of static pressure and Mach number. Optimization of power source with respect to external conditions.
3. Development of a discharge physical model. Development of a computer code for description of non-stationary turbulent boundary layer at a plate at presence of pulsed periodic energy sources in it. Obtained results would find applications in practical aerodynamics.

PART I. EXPERIMENTAL INVESTIGATIONS (Task 1, Task 2)

§1.1. Power supply unit for the sliding discharge

In Fig. 1.1 one can see an electric scheme of the set up for generating of the sliding discharge. In Fig.2 a schematic draft of the discharge unit is represented.

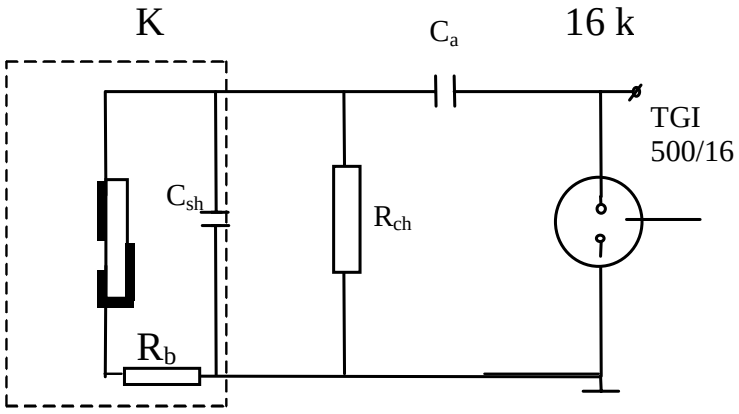

Fig. 1.1. Principle electric scheme of the sliding discharge.
C_a – accumulating capacitor; C_{sh} – sharpening capacitor; R_{ch} – charging resistance;
R_b – ballast resistance; TGI-500/16- starting thyratron; K – discharge unit.

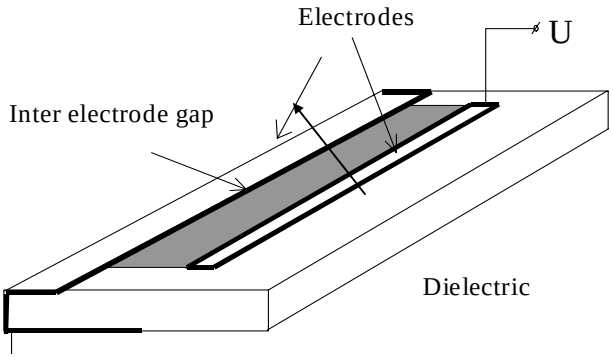

Fig 1.2. Typical discharge unit for creation of the sliding discharge

The principle of the scheme operation is the following: the thyratron TGI is closed in initial state, and the accumulating capacitor (C_a – up to 2 nF) is charged up to the voltage of the power supply source (about of 16 кВ). The thyratron opens at the giving on it the starting pulse, and the capacitor voltage is applied to the discharge gap. The sharpening capacitor (C_{sh} – 0,2 nF) is used for rising of the applied voltage front steepness, This insures the breakdown over the dielectric surface (see. Fig.1.2). By this means the forming of the sliding discharge over the dielectric surface takes place. The discharge duration is dependent on the scheme parameters and equals to 100-200 ns.

The system is supplied by the power source (Power supply unit) with the maximum voltage up to 30 kV and the power up to 1 kW. The starting of the thyratron is realized by the pulse of the positive polarity of $t_{pulse.}$ = 3 μs and the amplitude of $U_{pulse.}$ = 300 V.

The starting pulse is given by the special synchronizing scheme assembled on a basis of two generators: the supporting and the outlet one. The supporting generator allows to obtain the starting pulses both in the single mode of the operation and in the periodic mode with the maximum frequency of f_{puse} = 10^4 Hz, which is governed by conditions of the sliding discharge operation. Besides, pulses of different additional devices are obtained from the synchronizing system (starting of the light source for a shadow system, pulse of CD-camera –starting, etc.)

The power supply source of the sliding discharge was manufactured. It was adapted for an application in the aerodynamical experiment in the wind tunnel A-7. (The appearance of the power source is represented in the Fig. 1.3. [1]).

§1.2.Choice of materials for manufacturing of aerodynamic models, current carrying units. Ordering and purchasing of materials and components for manufacturing of aerodynamic model.

1.2.1. Sliding discharge over a separation boundary of two solid dielectrics.

In some cases it can be observed that the flowing around surface (dielectric substrate) is covered by water or ice layer. This takes place in wind tunnel experiments on investigation of plasma surface created over the dielectric substrate flown around by the incident gas flow. So there is actual interest in investigations of sliding discharge realization possibility in these conditions.

In Fig.1.3. one can see a scheme of sliding discharge development over the separation boundary of two solid dielectrics, where earlier investigated gaseous dielectric is changed for the solid one (ice, epoxy rosin, etc) [1].

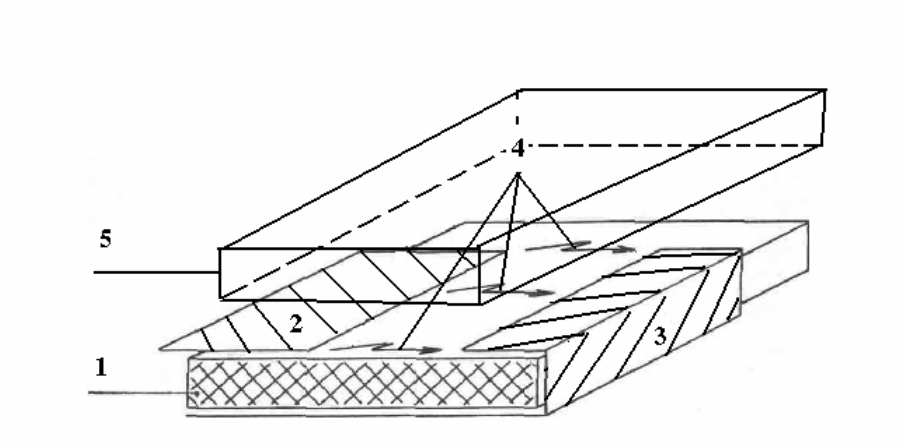

Fig.1.3. Sliding discharge over separation boundary of two solid dielectrics.
1- dielectric with $\acute{\varepsilon}_1$, 2- initiating electrode, 3- main electrode, 4- sliding discharge (plasma leaf) , 5 – dielectric with c $\acute{\varepsilon}_2$.

In our experiments we created electrode configuration of sliding discharge with contact boundaries organic glass-epoxy rosin and glass fiber plastic –ice.

The plasma layer was created at the boundary of the area 50 x 50 mm^2 at the voltage of about 40 kV, its specific energy put was ~ 0.1 J/cm^2. This energy put proved to be sufficient to realize the separation of the upper dielectric layer over the whole contact boundary area. This took place because of energy release in small volume of the contact layer. Observed effect can be used for getting rid of ice covering of construction elements being in humid medium at low temperatures. Diffuse or multi channel sliding discharge is developed over this boundary because of small electric strength of the contact boundary of two dielectrics.

We have to note that standard lacquer coating can be used for the dielectric substrate. For validation of this possibility we made experiments on sliding discharge realization over the surface of metallic plate covered by standard lacquer coating. At that the sliding discharge was developing over the paint surface starting at initiating electrode voltage about 1 kV. Electric strength of this coating proved to be sufficient for insuring of sliding discharge realization with frequency up to 1500 Hz without irreversible damage of the paint layer.

1.2.2. Sliding discharge over liquid dielectric surface.

We undertook experiments for determination of conditions and realization possibility of sliding discharge over surfaces of dielectric liquids (water) [2]. Experimental set up scheme is represented in Fig.1.4.

Standard sliding discharge electrodes configuration has the following features. The grounded electrode is the metallic substrate for the dielectric layer. A small resistance R_{mes} is placed in the break of the grounded electrode. This resistance is used for determination of existence of the finished stage of the sliding discharge over liquid dielectric surface. This is caused by the fact that it is visually difficult to detect the existence of the finished state of the sliding discharge over the surface of a liquid because there is a possibility of thin liquid layer breakdown from the fore front of unfinished sliding discharge stage to the grounded substrate.

The second feature is the capability to change the dielectric type for observation of comparable discharge characteristics. In Fig.1.4. in circles one can see the following types dielectrics in the discharge gap: a-is the glass layer of 1.8 mm thickness, b is the glass layer with liquid layer deposited on its surface, and c – dielectric liquid layer of 1-2 mm thickness in the discharge gap.

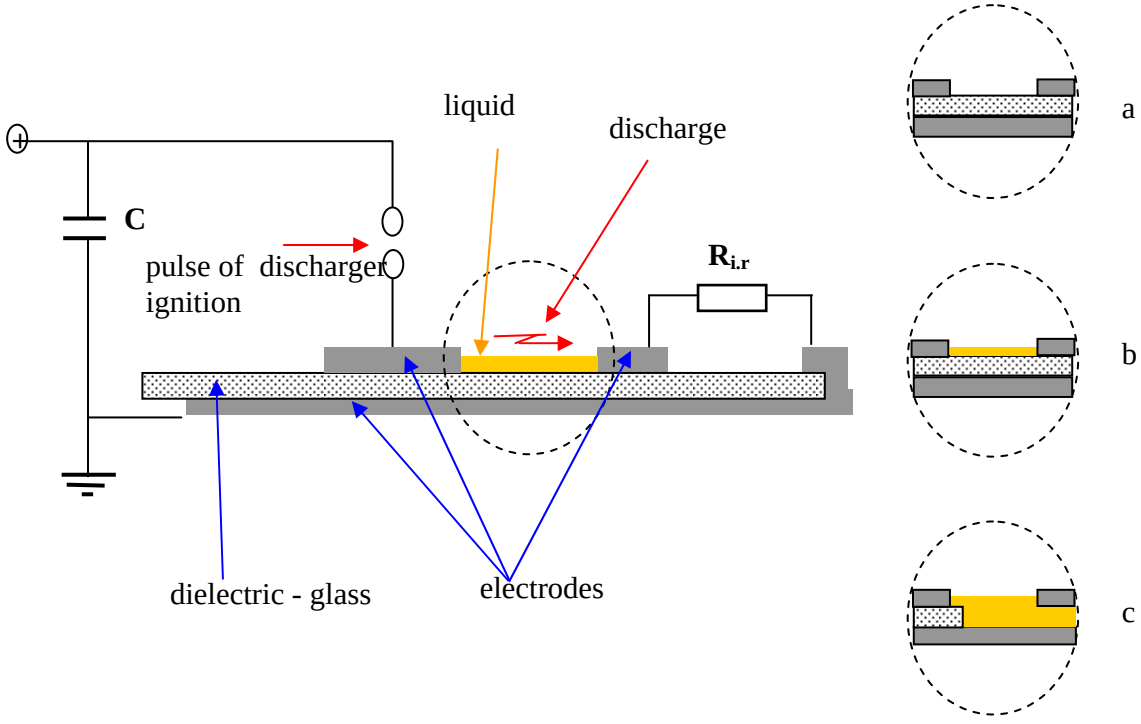

Fig.1.4. Scheme of experimental set up: C = 1 nF – accumulating capacitor, charging voltage U_c = 15 kV;
$R_{i.r}$ - instrument resistor (instrument shunt) for measurement of discharge current (R_{mes}).
a, b, c – configurations of electrode units: (a) without liquid dielectric,
(b, c) with liquid dielectrics
a is a glass layer of 1.8 mm thickness, b is a glass layer with dielectric liquid deposited on its surface; c – dielectric liquid layer of 2 mm thickness.

In Fig.1.5. one can see waveforms of the voltage at the initiating electrode and the current through R_{mes} for all three cases at the voltage of 15 kV at the accumulating capacity.

Comparison of these waveforms shows that there the finished discharge stage with approximately same temporary characteristics took place in all three cases. Initial negative current jump corresponds to the process of the capacity charging i.e. bias current.. This capacity is created by the high voltage electrode and grounded substrate with the dielectric streak. One can see that the charging current somehow smaller in the case of the dielectric layer created by only liquid with the glass substrate (waveform (c)), this was expected because the capacity formed in this case is smaller than in the cases (a) and (b).

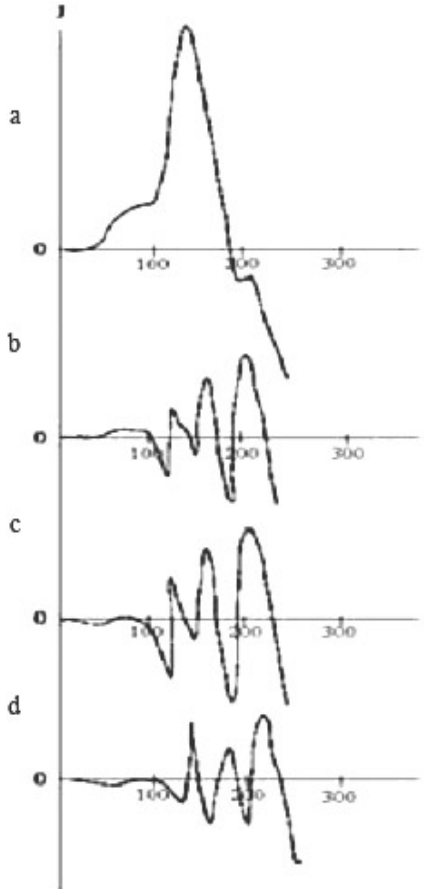

Fig.1.5. Waveforms of the voltage (d) and current through R_{mes}: a- the dielectric without liquid layer; b- liquid layer on the dielectric; c- liquid layer without of the dielectric.

In a photo of Fig.1.6. one can see the typical discharge over the liquid surface appearance at voltage pulse repetition frequency 10 kHz.

One can see that the unfinished discharge stage has the spread to all sides from the initiating electrode and the discharge length corresponds to the length of

the discharge gap for the finished stage. This is the consequence of the fact that sharp voltage drop takes place at the initiating electrode at closing of the discharge gap.

So we showed that the sliding discharge can be realized over the surface of thin (approximately 1 mm thickness) dielectric liquid layer without presence of electrically strong dielectric substrate. It follows from said above that experiments on external aerodynamics can be undertaken at different temperatures and humidity of airflow in wind tunnel.

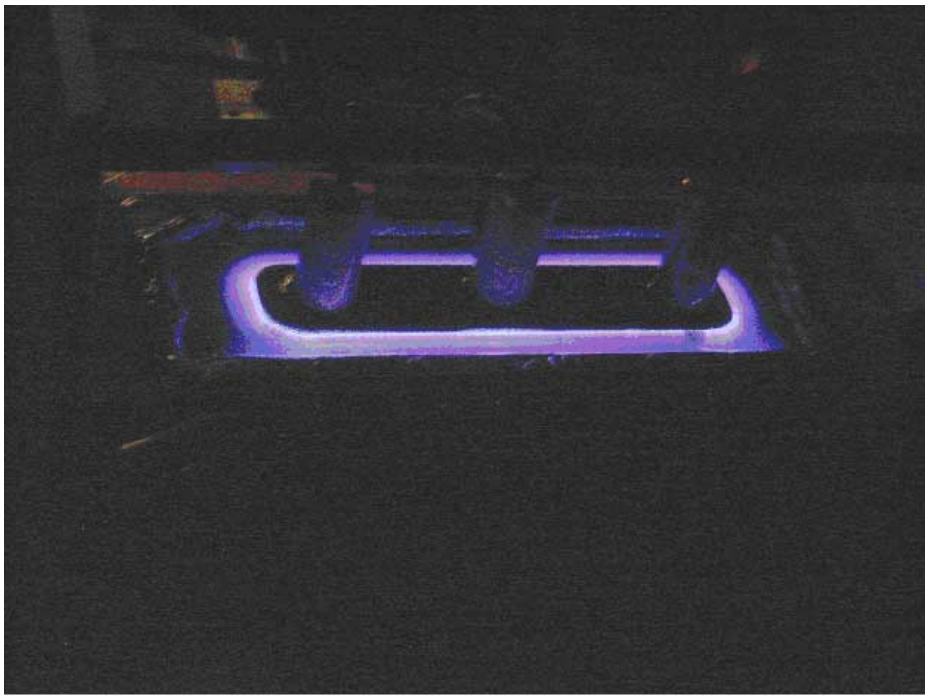

Fig.1.6. Typical appearance of the discharge over the liquid surface at voltage pulse repetition frequency 10 kHz.

§1.3. Aerodynamic models

Two designs of models have been developed for experiments in the wind tunnel A-7, the sliding discharge is to be ignited on their surfaces. The first one (see Fig.1.4. [1]) is aimed to organize the longitudinal (oriented along a flow) pulse-periodic sliding discharge, the second one (see Fig.1.5. [1]) is for organizing the transversal (oriented perpendicular to a flow) sliding discharge. The model bodies are to be made of dielectric materials (caprolactam, fluoroplastic, textolite) and the electrodes are to be made of brass. Glass as a dielectric is to be used for forming of the sliding discharge. The typical sizes of the models are of the order $10 \times 25 \times 3$ cm.

The appearance of the model for the realization of the longitudinal sliding discharge in the plasma aerodynamical experiment is represented in Fig.1.7. (f – top view, b – side view), it was made just before the finishing grinding of the model surface. The nose part is made of duralumin, the angle in the top of the wedge is 20°. The model body is made of the organic glass. The glass of the 1 mm thickness is used for the dielectric on the surface of which the sliding discharge is formed.

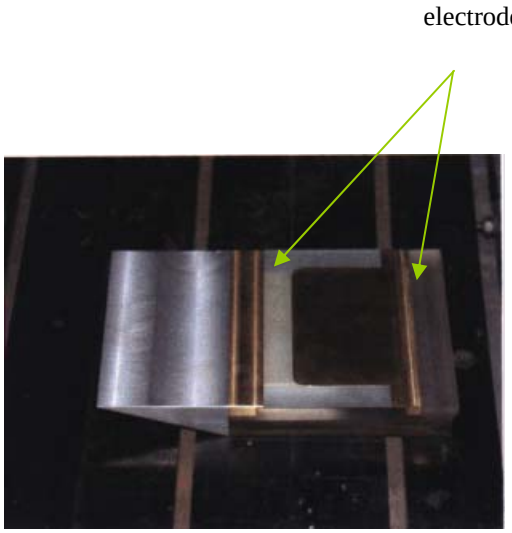

Fig.1.7..

The power source tests have been made at this stage and the preliminary investigations on the sliding discharge formation over the plane plate in the pressure chamber (at pressures of 0.1 and 0.15 atm) as well.

In Fig.1.8. one can see the sliding discharge in the motionless air. The discharge was formed over the plane plate 30 cm long and 3 cm wide, the plate thickness was 3 mm. The pulse repetition rate was - 1 kHz.

..

Fig.1.8.

The discharge proved to burn stably in these conditions. Its glow is practically uniform over the whole subjacent dielectric surface. The starting-up and adjustment works have been made in the wind tunnel A-7. They were connected with blowing of the models electric discharge exact copies at the Mach number value of the flow M = 0,8. (Fig. 1.9.)

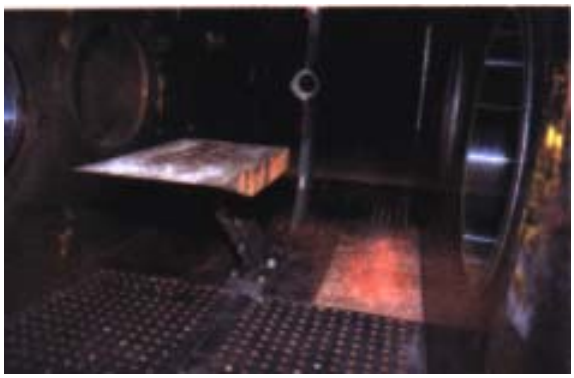

a

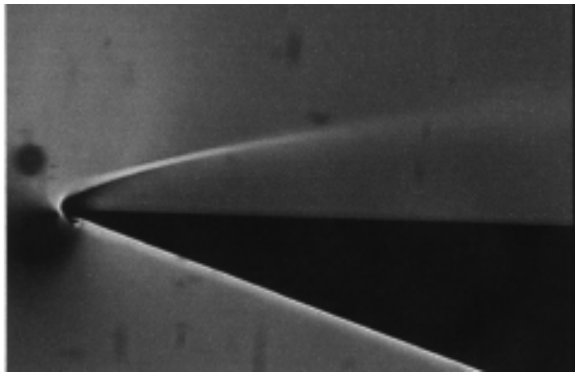

b

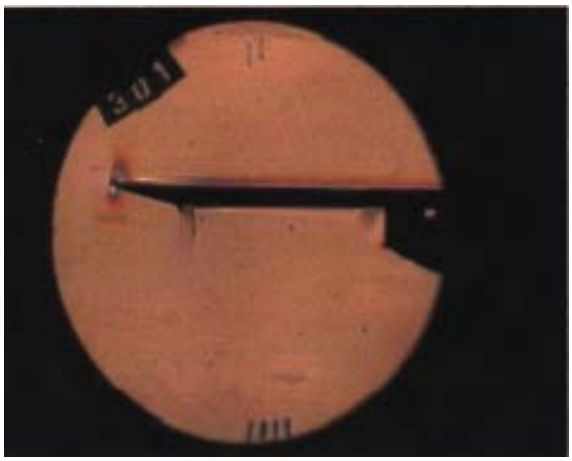

c

Fig.19.5.
a – The model in the wind tunnel A-7;
b – the flow visualizing over the model;
c – the boundary layer visualizing over the plate.

Main attention during the next stage of works will be paid to the debugging and increasing of the sensitivity of the flow structure visualization optical system at the Mach numbers M = 0,9 and M = 3.

§1.4. Experimental investigations in a wind-tunnel A7

Wind-Tunnel. We suppose to apply available wind tunnel **A7** for undertaking of experimental investigations in the high-speed flow. It is the supersonic aerodynamic set up with changeable density, the velocity range corresponds to Mach numbers from M = 0,4 to 4.

The wind-tunnel A7 is equipped with the forcing and suction ejectors allowing to make tests in a wide range of Reynolds numbers, and to model a wide

range of flight heights. The closed tube working part is of the square cross section 0,6 × 0,6 m, 1.5 m long.

Models. Several variants of plates were manufactured for fulfillment of methodical experiments. Following features were foreseen at designing and manufacturing of models:

- Brining of minimum disturbances to a flow at the subsonic speeds (M = 0.8),
- Insurance of the attached density shock to the first edge of the wedge at the supersonic speeds (M = 3.0).

One of the model copies the wedge model configuration with the discharge source located in it. (A photo of this model placed in the working part of the set up A-7 is represented in Fig.1.9. [1]).

We plan to undertake experiments with several model types for the investigation of discharges on the plane (the plate 100 mm width and 300 mm long) and curvilinear surfaces.

Detection of the flow parameters. Flow parameters measuring system of detection is based on an application of standard pressure sensors (pressure in the fore chamber and the static pressure in the working section of the tube). An operator during the experiment undertakes the mode of the flow parameters over the indicators of the wind-tunnel control desk. The flow parameters detection is realized with a help of measuring system on the computer base. The detection program is realized in language of Graphical programming LabView of National Instruments Company. The flow parameters calculations are made at the end of the experiment with the application of the calibration tables, and the experimental data is written to the file for the further analysis.

Flow structure visualization. Tepler device is used for fulfillment of investigations on the discharge influence of a flow in the boundary layer (for studies of the boundary layer variation and transition from the laminar flow mode to the turbulent one). The visualizing system is based on one channel of the interferometer used as the devise of the “shadow method”. The beam aperture of the diagnosing ray is 230 mm. The focusing range is spread over the full width of the working part (about 600 mm). The standard objective with the focus distance of 150 mm was used for the image formation. The optical system of the device forms the image of the diagnostic beam to the circle of 20 mm diameter, it corresponds to the full format frame of 36 mm photo film.

The detection of the flow picture will be executed with a help of the follows equipment:

1. Special digital camera Nikon;
2. High-speed digital detector VS-CCT-075 .

Test experiments. Tests were undertaken for detection of the boundary layer on the plate without a discharge (time of detection is 0.5 μs). The exposure time of the single frame can be of 1/4000 seconds, it allows to consider the recorded frame as the momentary flow picture.

In Fig.1.10. – 1.13. one can see a set of photos obtained with a help of the digital camera in the case of the plate flowing around by the supersonic flow with the Mach number M = 3.0.

The target of these experiments was to increase of the turbulent boundary layer width for more precise estimate of the discharge influence. Conventional experimental means were used for influencing on the boundary layer width: putting of obstacles in the fore part of the plate that turbulize and thicken the boundary layer. The following variants are shown: the clear plate; the plate with the wire (of d=1 mm diameter) placed across the flow at the distance of 30 mm from the front edge of the plate; the plate with the plane strip glued to it (scotch tape), the strip width is 05 mm and its width 10 mm; and the plate with deposited rough layer of small sand particles of 0.5 mm diameter.

It follows from the represented photos that addition of the turbulizing coatings leads to the boundary layer increase. In next experiments it is reasonable to consider the boundary layer structure in more details with numerical measurement of its width.

Fig.1.10.

Fig. 1.11.

Fig. 1.12.

Fig. 1.13.

§1.5. Parameters of sliding discharge in immovable air at atmospheric pressure.

General scheme of the discharge Ampere-Volt characteristics measurements is represented in Fig. 1.14.

Volt-ampere characteristics were investigated for sliding discharge in air at atmospheric pressure (unfinished discharge - a) and at pressure 0,2 atm. in a vacuum chamber (finished discharge - b). These types of discharges are present in Fig.1.15.

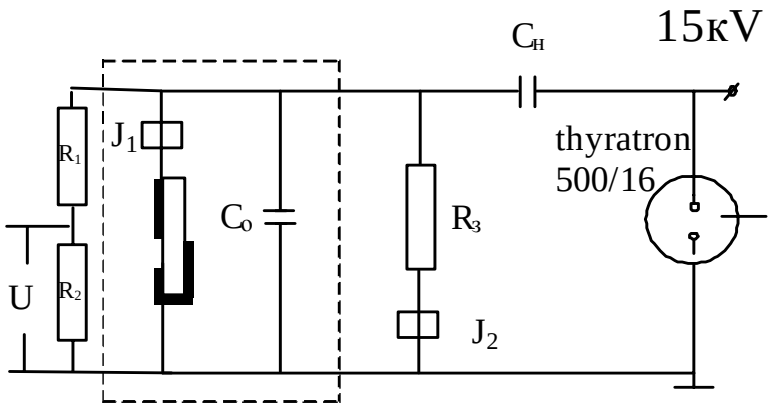

Fig. 1.14. Sliding discharge Ampere-Volt characteristics measuring scheme

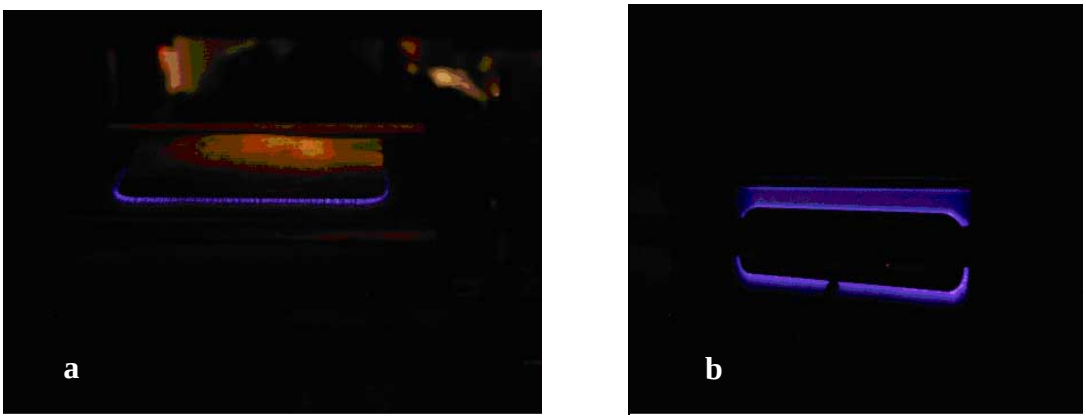

Fig.1.15. Sliding discharge for aerodynamics experiments.
a -Unfinished sliding discharge, pulse repetition rate is 1000 Hz. The discharge is in air. The discharge gap length is 20 mm. The plasma layer thickness in this conditions is about of 0.5 mm.
b - Finished sliding discharge, discharge gap length is 10 mm.

Typical discharge Ampere-Volt characteristics are represented in Fig.1.16.

The discharge characteristic were obtained at air atmospheric pressure at the pulse repetition frequency f = 10 Hz at the charging voltage in the range 15 kV. The current on the discharge gap and on the charging gap was measured with a help of Rogovsky belt with the converting coefficient 1A = 64.062 mV. The voltage on the discharge gap was measured by the ohmic divider with the division coefficient k = 948.4. One can see that the discharge current during the first half period (during 30 ns) reaches 400 A during a pulse. The voltage on the discharge gap rises during this time period and reaches 4 kV. The current practically does not change during 10 ns after reaching the maximum. The voltage continues to rise, reaches the value of 9 kV before the beginning of the current decreasing, and reaches its maximum of 14 kV at 70 ns. Then the vibration process of recharging takes place.

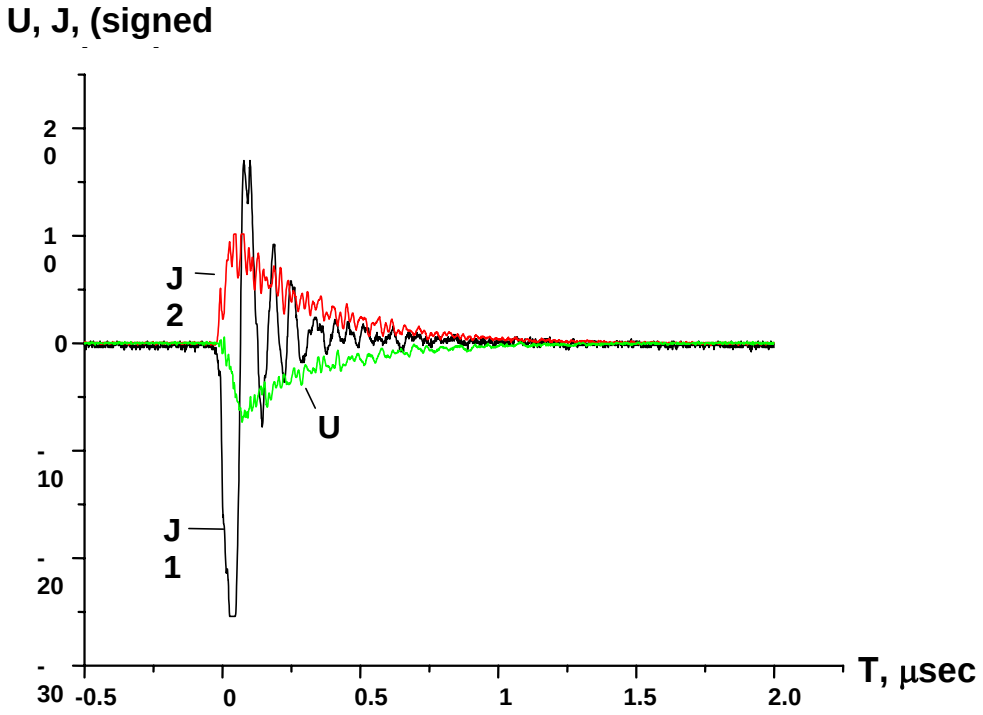

Fig.1.16. Unfinished sliding discharge Ampere-Volt characteristics at atmospheric
U- a voltage on the discharge gap
J_1- a current on the discharge gap

The stored energy equals to 112 mJ at the charging voltage 15 kV and storing capacity of 1 nF. The consumption power equals to 112 W at the frequency of 1000 Hz.

Unfinished sliding discharge, pulse repetition rate 1000 Hz. The discharge is in air at 1 atm. The discharge gap is 20 mm. The plasma layer with is about 5 mm in these conditions.

The finished discharge, the discharge gap length is 10 mm. The sliding discharge with the gap length of 20 mm will have the same appearance at lower pressure, but it Ampere –Volt characteristics have another form.

Following problems were solved during experiments:

1. Pressure measurements in non-disturbed flow Pст., P_0', P_0 and on the model with pressure difference ΔP between two points P_1 , P_2 (reference pressure was the pressure in the point P_1).
2. Detection of deviation angles of disturbance lines on the model by the optical method.

3. High-speed recording of the flow structure at airflow flowing around the working chamber.

§1.6. Pressure measurements in undisturbed flow Pst., P_0', P_0 and on the model between two points P_1 , P_2

The working model in version of longitudinal sliding discharge was located in the working part of the tunnel on oblique pylon. Observations were carried out through the illuminator with a help of optic device "Tepler", images were recorded by video and photo cameras. Detailed description of measuring complex is given in [1].

Following pressures were measured during experiments: P_0 – pressure in fore chamber in wind tunnel, Pst.- static pressure of undisturbed flow on a wall of working part of the tunnel, P_0'- stagnation pressure of incident flow, P_1 and P_2 – pressures on the surface in the fore and base parts of the model. Position of drainage points for measurements of pressure and geometrical sizes of the model are represented in Fig.1.17.

Pressure difference ΔP between points P_1 and P_2 was measured by U type water manometer for exclusion of high voltage discharge noise. Airflow velocity was maintained during experiments at a level corresponding to Mach number M=3, and the velocity flow (pressure in velocity flow): $q=7.1$ kg/cm^2.

Pressure recording was realized by pressure sensors IPS (Inductive Pressure Sensor) included to measuring complex on PC base. Measurements data are represented in Fig.1.19.

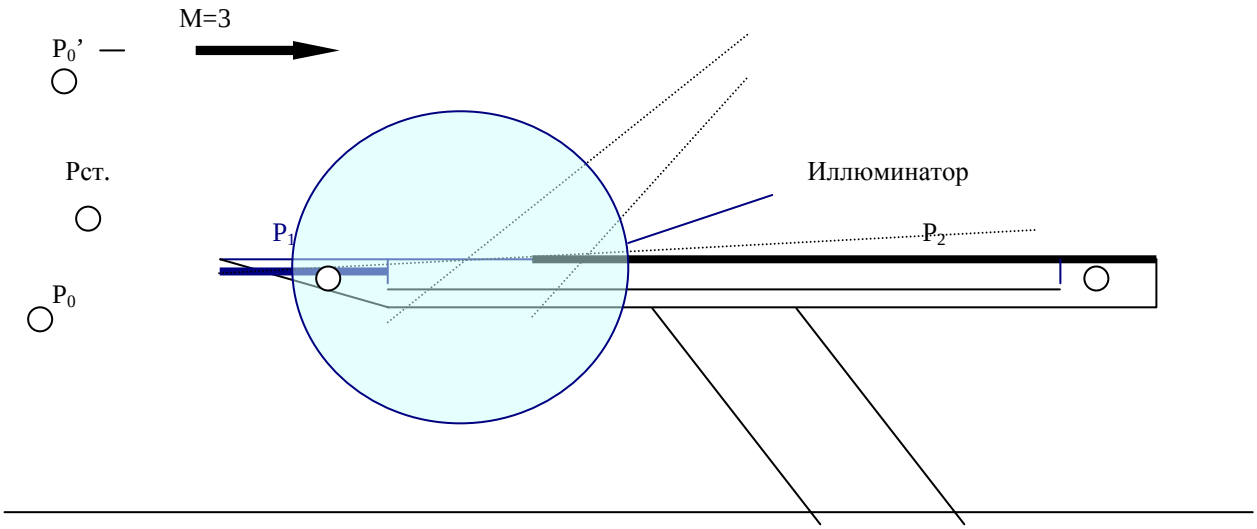

Fig.117. Drainage points location for pressure measurements

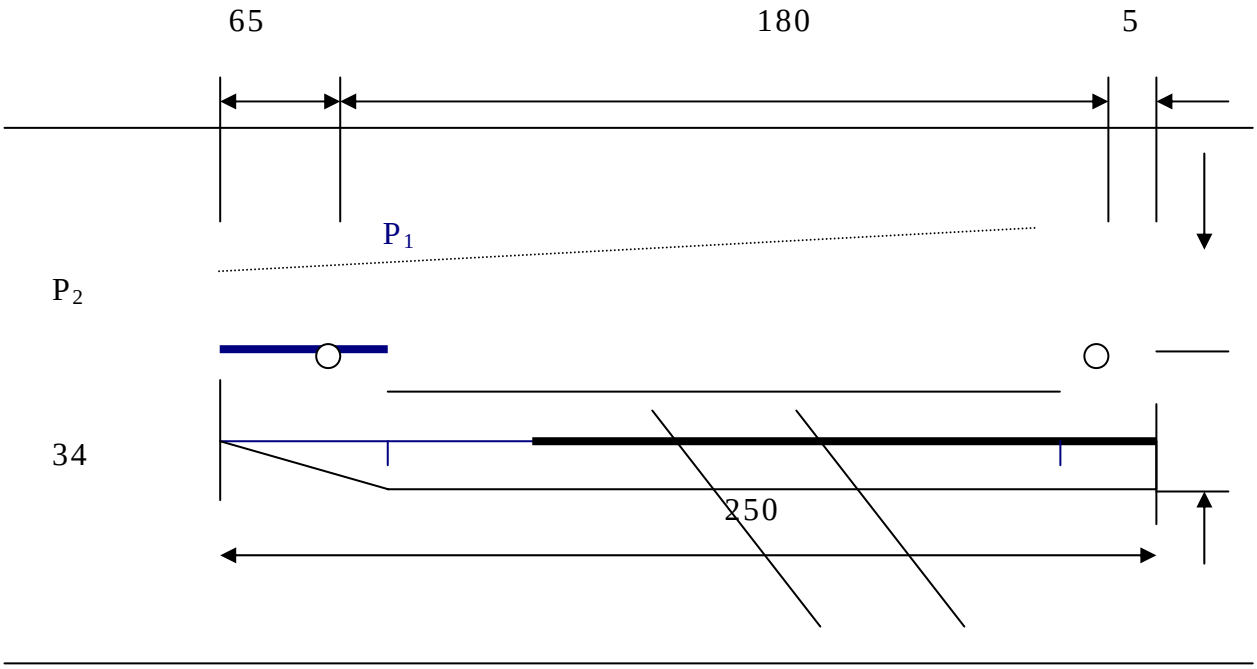

Model width is 180 mm

Fig.1.18. Geometrical sizes of the model.

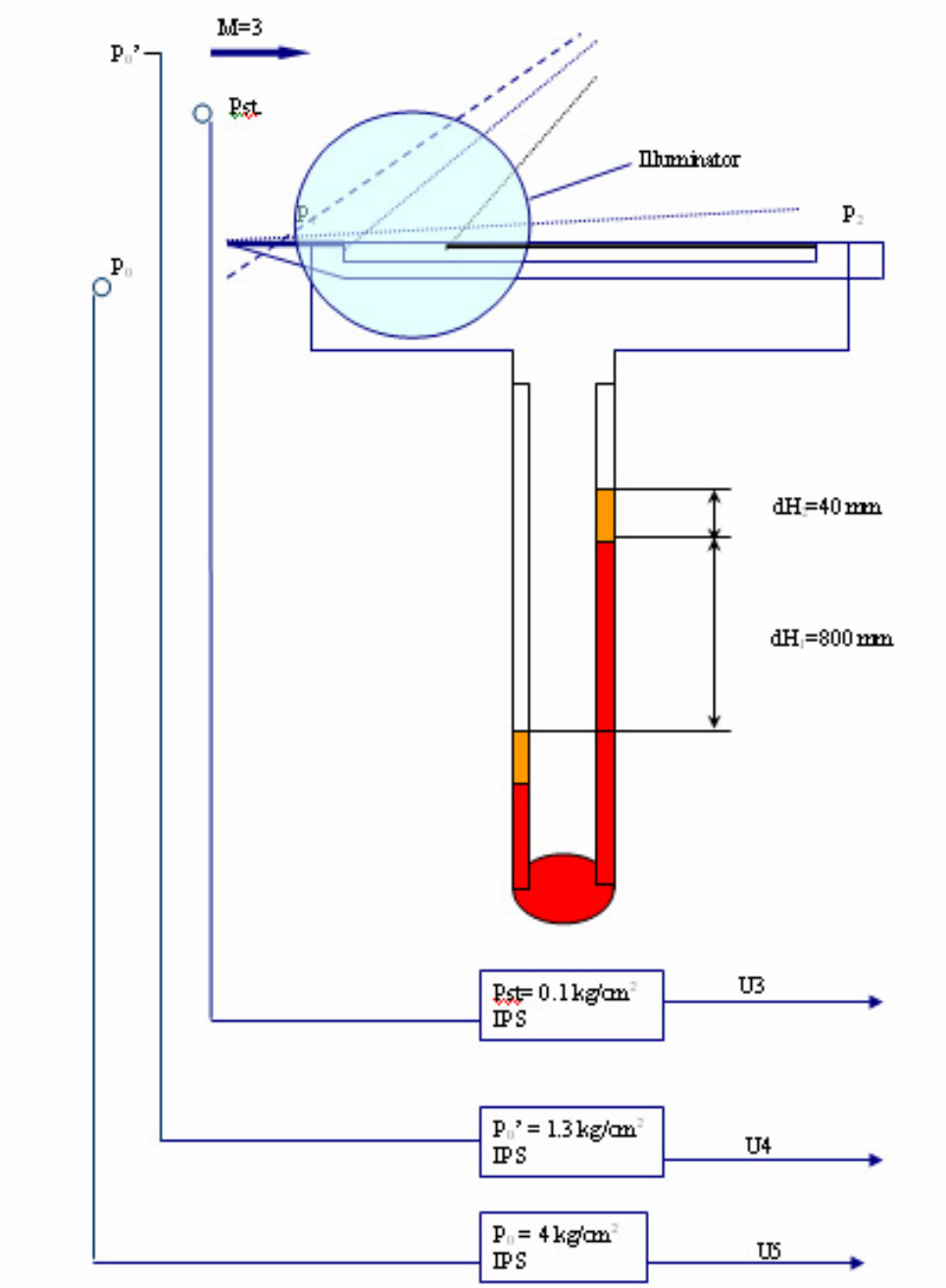

Fig. 1.19. Pressures measured data P_0, Pst, P_0', P_1, P_2 .

§1.7. Choice of detection mode of sliding discharge influence on a character of airflow flowing around the working model with velocity corresponding to Mach number M=3.

Test detection modes of sliding discharge recording were realized at the set up A – 7. Investigations were carried out in the working part of set up A – 7 without a flow. The goal of investigations was detection of discharge recording modes by the “Tepler” device.

Different installation-specific settings were used in the optical part of the “Tepler” device (width of the slit, light source brightness, location of knife). Different video and photo cameras [1] were applied for images recording. Different detection devices allowed to detect settings range of recording equipment.

1. High voltage scheme of discharge voltage formation has inductive delay at coming out to the mode. It was discovered at high-speed recording (285 frames per second.) that the discharge power gradually rises at the system switching on, and it comes to normal mode after (8 frames × 1/285 s) 0,028 s after voltage delivering to the high voltage scheme.

2. Time of discharge existence is about 100 ns, frequency of discharges running is adjusted from 500 to 1000 pulses per second. Detection of more than one discharge takes place at setting of the frame exposure time smaller than 1/1000 (or 1/500) second.

3. Considerable influence on a image has total flash of the working area at the frame exposure time more than the discharge existence time.

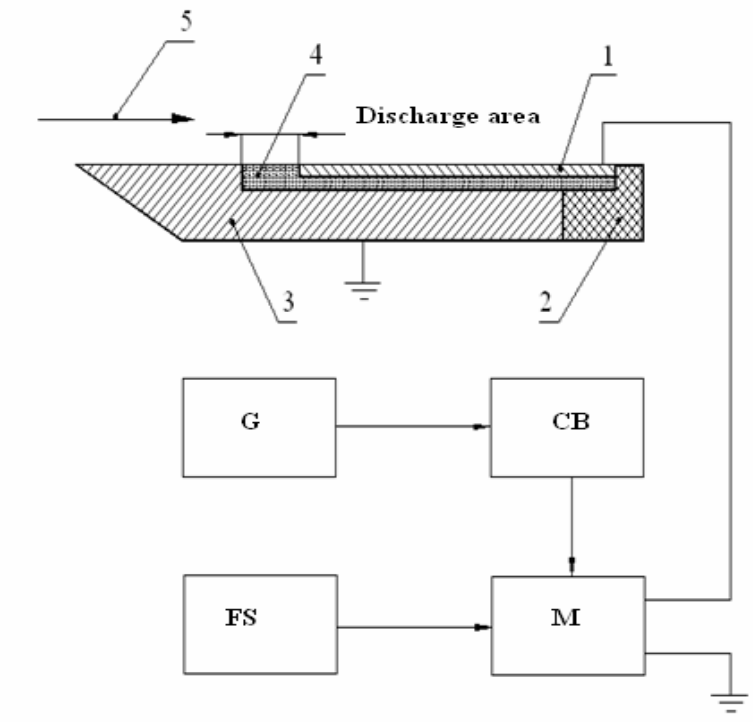

Fig.1.20.16. Electrical functioning scheme

1.High Voltage electrode; 2. Isolator; 3. Grounded electrode; 4. Dielectric; 5.Non-disturbed incident air flow (M=3). FS – feeding source 5 kW (with controlled voltage of 0-30 kV). G - Starting generator (500-1000 Hz). CB – block of modulator controlling (it forms pulses of 800V amplitude and 1μs duration. M – modulator (transforms FS voltage in pulse mode of ~1 μs duration, forefront ~10 ns and current up to ~ 500 A).

§1.8. Sliding discharge on the model without a flow

Recording settings of the discharge in wind tunnel A-7 have been made.

The work was realized after precise mounting of the model plane along the "Tepler" device axis.

Vertical stripe on the screen is a marker of the discharge area. Vertical marker height is 30 mm.

Recording of discharge development was made by the camera "Video eye". 285 photos of medium disturbance development process caused by the sliding discharge in the working area were made. We represent most typical moments corresponding to 222, 224 and 230 frames.

Experiments were carried out in the tunnel without organization of the flow.

Fig. 1.21. – record of the working model location without a discharge. Photo 222

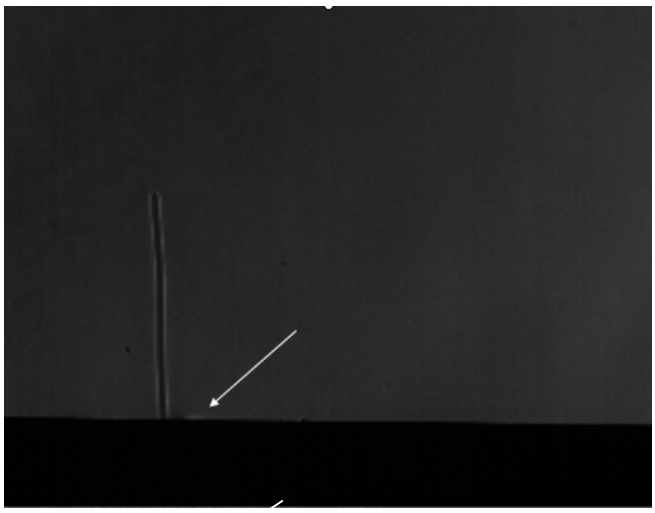

Fig. 1.22. First discharge on the working model. Photo 224
Arrow indicates location of the disturbance origin in dead gas Pulse repetition frequency 1000 Hz. Discharge voltage 11 kV.
Frame exposure time– 1/10000 s. Frames frequency 285 frames/s.

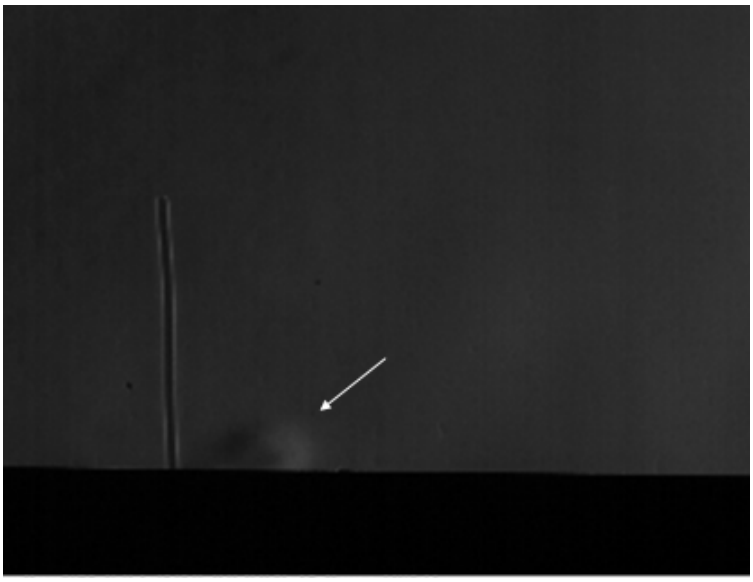

Fig.1.23.Two successive discharges pictures during exposure time. Photo 230.
Arrow indicates location of the disturbance after 18 ms from the pulse beginning in dead air. Pulse repetition frequency 1000 Hz. Discharge voltage 11 kV. Arrow indicates location of the disturbance origin in dead gas. Frame exposure time– 1/10000 s. Frames frequency 285 frames/s.

Detection details: Camera Metracom-4000; Frames frequency 285 frames per second. Frame exposure time– 1/1700 s. Pixel frame size 280 × 180.Results obtained from analysis of photos (see Fig.1.22. and Fig.1.23.) show that the sliding discharge initiated in dead atmosphere causes thermal disturbance of the surrounding gas, which boundary moves from the discharge area with velocity ~ 30 cm/s.

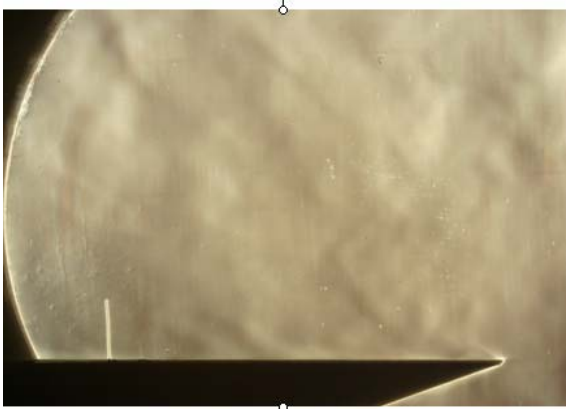

Fig.1.24. Picture without a flow and a discharge.

Fig.1.25. Picture without a flow but with the discharge of 10 kV.

Fig.1.26. Picture without a flow but with the discharge of 11 kV.

The model located in the working part of wind tunnel.

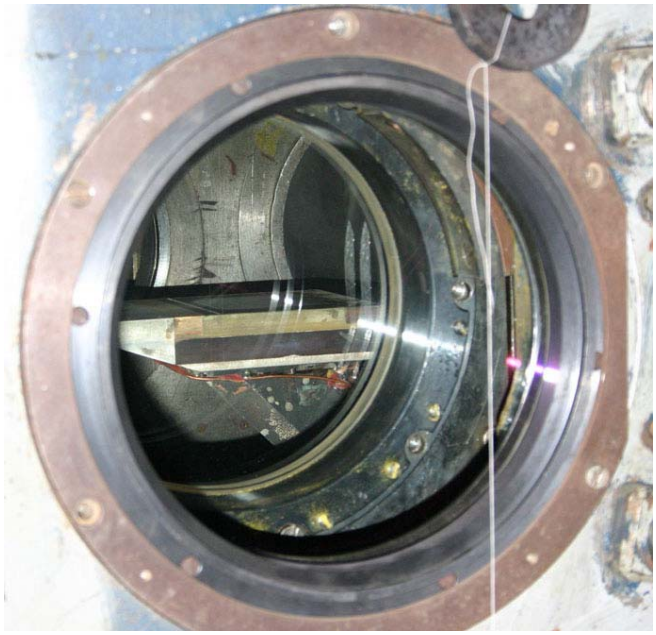

Fig.1.27. The model without a discharge.

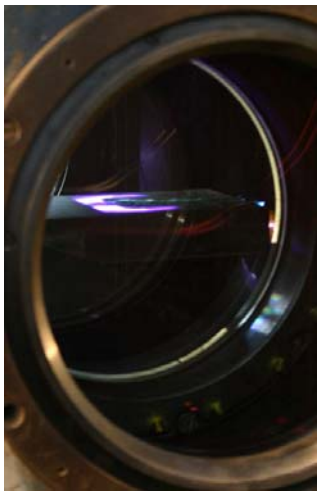

Fig.1.28. The model with the discharge

§1.9. Sliding discharge on the model in the flow

Recording settings of the device for detection of the sliding discharge influence on the character of airflow around the working model in wind tunnel A-7 have been made.

The work was realized after precise mounting of the model plane along the “Tepler” device axis.

Experiments were carried out without discharge realization and with discharge realization in the working zone.

Comparison of compression shocks pictures originating at airflow around the working model at the flow velocity corresponding to Mach number M=3 was made in these conditions.

Video recording of the medium disturbances development process in the working zone cause by the sliding discharge was made during experiments.

We represent most typical investigation moments.

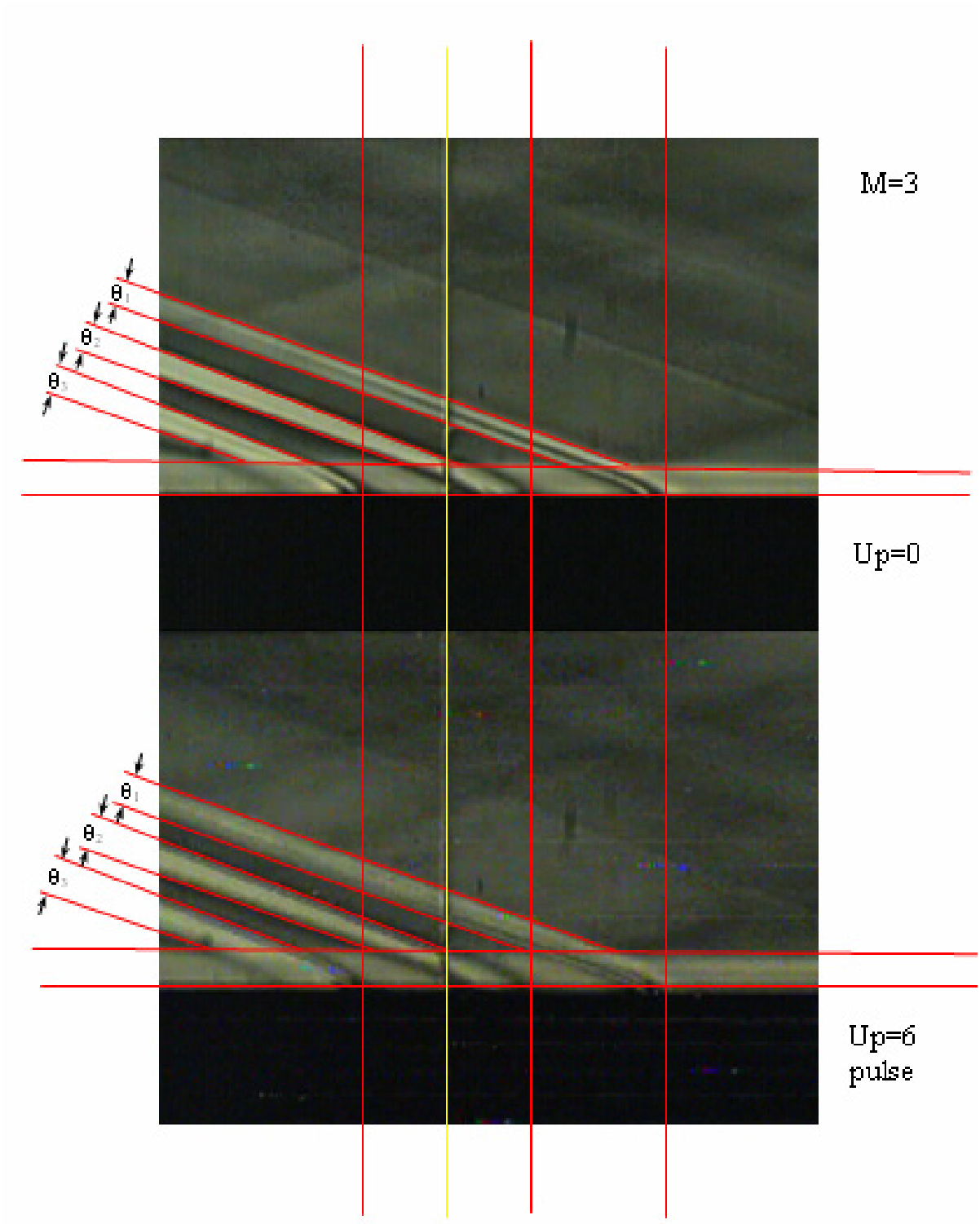

Fig.1.29. Picture of the boundary layer and of compression shocks system a) without a discharge (upper); b) with the discharge (lower) U p= 6 kV.

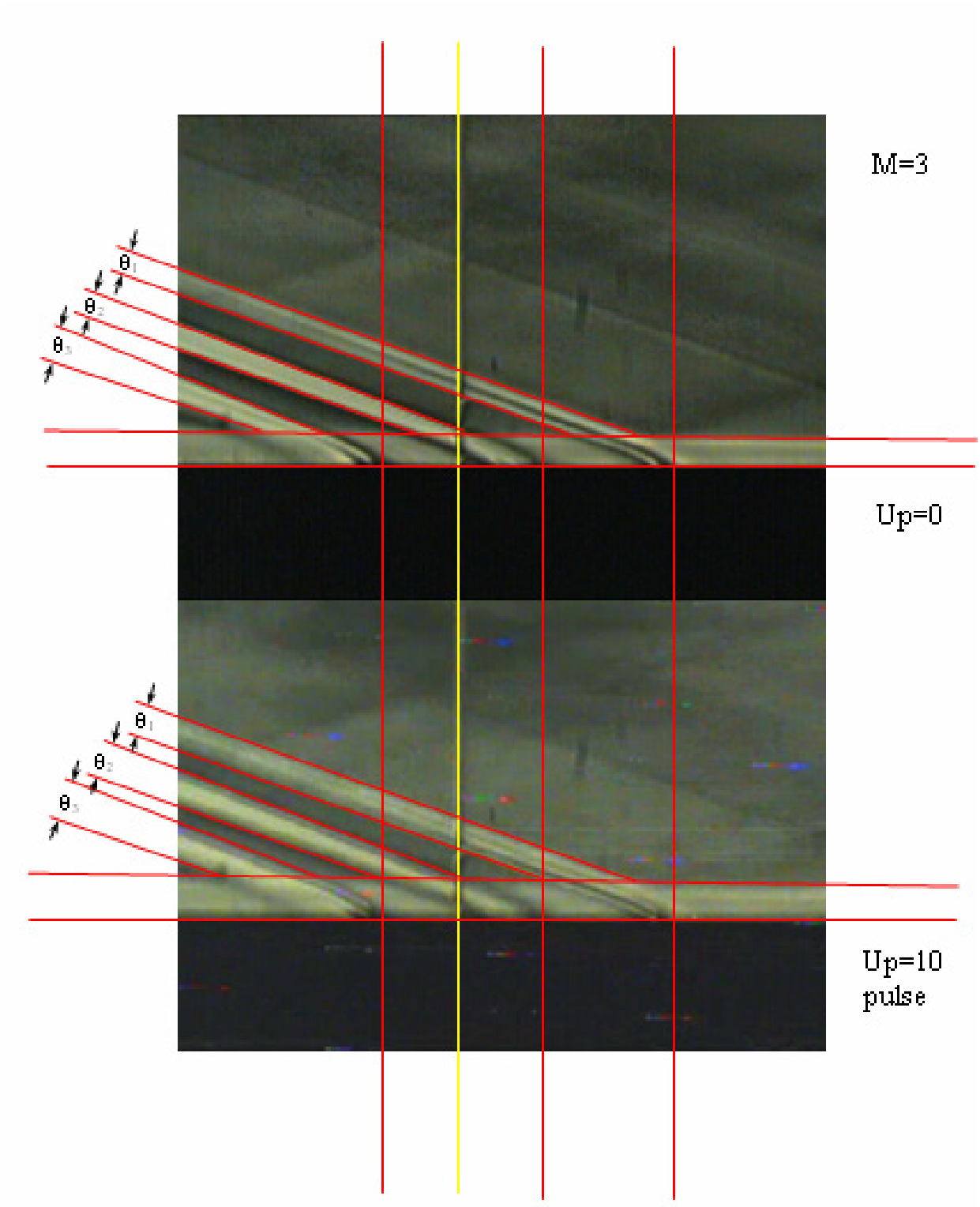

Fig.1.30. Picture of the boundary layer and of compression shocks system a) without a discharge (upper); b) with the discharge (lower) U p=10 kV.

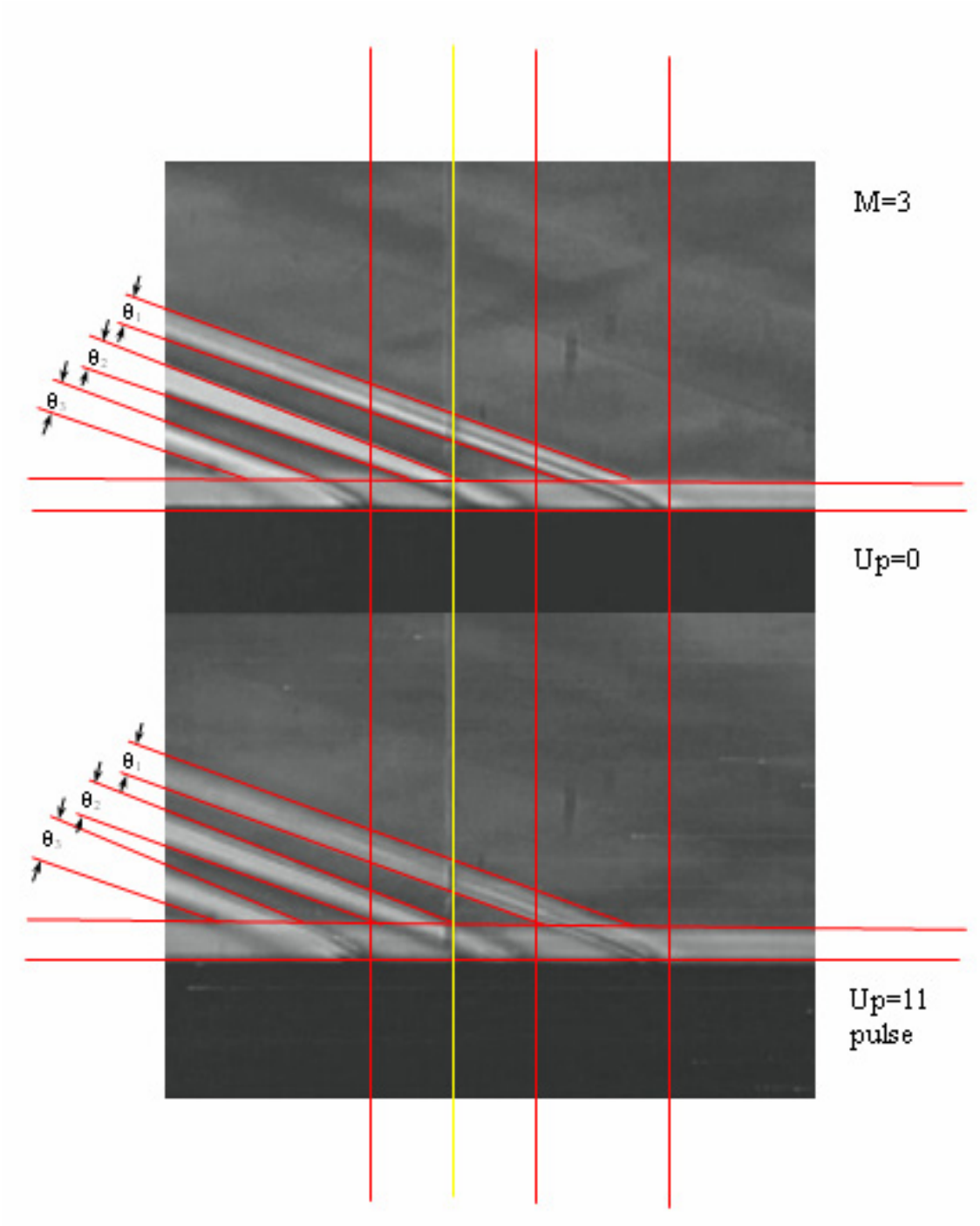

Fig.1.31. Picture of the boundary layer and of compression shocks system
a) without a discharge (upper); b) with the discharge (lower) U p=11 kV.

1.10. Discussion of experimental results.

1) Measurements of pressure along the model without the discharge and with the discharge were made during experiments.

Obtained results show that pressure P_2 drops down at initiation of the sliding discharge in comparison with pressure in the same point without the discharge ;

2) Investigations of the discharge without a flow showed the following. Analysis of results represented in photos (see Fig.6 and Fig.7) revealed that the sliding discharge initiated in the working area of the model in dead atmosphere causes thermal disturbance of the surrounding gas, and its boundary moves from the discharge area with the velocity of ~ 30 cm/s.;

3) Character of airflow around the model at the sliding discharge initiation on the model surface obtained during present experiments. First of all we have note that there is no synchronizing frame of the video recording with the initiation moment of the sliding discharge in the working area. As a result in video frame we have a fragment of the discharge aftereffect on the character of flow around. Comparison of pictures in Fig.13 a) and b) shows that the discharge initiation on the model surface leads: first - to widening of the boundary layer width, second – to smoothing of second and third shocks. Widening of the boundary layer width is caused by temperature rise in the layer due to energy release of the discharge. Smoothing of second and third shocks can be explained by the following: the flow velocity drops down after the first shock at sharp rise of gas temperature during discharge action, and shock angle of slope increases. Smoothing of the third shock has the same reason. More detailed picture of compression shocks structure and air flow around the working model at sliding discharge initiation will be given in the next report (experiment and numerical simulation).

Here we will make an estimate of possible due to indicated reasons widening of boundary layer thickness.

Relative change of boundary layer thickness at temperature variation for ΔT can be estimated as in [2]

$$\delta_{гг} = \text{const} \sqrt[4]{T} \qquad (1)$$

Considering that all discharge energy transforms to heat we obtain the estimate for gas temperature.

$$\Delta T = \Delta Q / C_v \qquad m \qquad (2)$$

here ΔT is a value of gas temperature change after discharge shut down;

ΔQ is discharge energy put to the gas, $\Delta Q = CU^2/2$; C is capacitor capacity (C= 1nF);

U – voltage at the capacitor (U = 11 kV); C_v - specific heat capacity at constant volume (C_v = 0,72 J/(g K); m is the heat by the discharge gas mass, m = ρV (ρ=1,29 10^{-3} g / cm^3 , V = 5 10^{-1} cm^3).

Inserting these values to (2) we get ΔT =100 K. Model temperature before the discharge was ~273 K in experimental conditions. Boundary layer width without sliding discharge was ~ 3 mm (see Fig.13 (a)), boundary layer thickness after the discharge shut down was ~ 3,4 mm (see Fig.13 (b)).

Determining value of the const from (1) for the new temperature value one obtains the new value $\delta_{тт}$ =3,3 mm, it is in sufficiently good agreement with experimental results.

§1.11. Investigation of sliding discharge effect on viscous gas flow at flow around a plate and curvilinear surfaces.

Investigation of sliding discharges effect on viscous gas flow at flow around a plate and curvilinear surfaces. Visualization of turbulent boundary layer, visualization of plasma boundary layer.

In the present section of the Report we represent results of investigations of working model (wedge or cone) flow around character. The working model appearance – the cylinder with the cone in the nose part is represented in Fig.1.32. Discharge gap working zone is situated over the generatrix of the cylinder.

Fig.1.32. Working model appearance : the cylinder and the cone are in the nose part.

In this Report we represent disturbance picture recording for the case when it is detected directly during the moment of discharge initiation, i.e. during first

5 μs, in difference with results represented in the Report #6. Reconstruction of flow character in the disturbance zone, change of inclination angles of disturbance lines, appearing at uniformities in the disturbance area (discharge) in the result of velocity profile change over the boundary layer cross section, see Fig.1.33. and Fig.1.34. take place during this time.

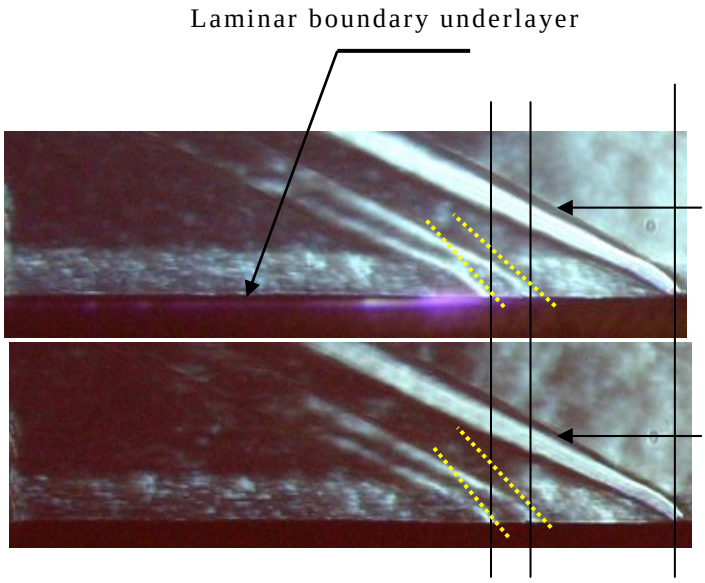

Fig.1.33. Disturbances picture (flat model with wedge type nose part) for the case when the sliding discharge is initiated over the surface of the model (a). (b) is a picture of flow streamlining in the discharge absence

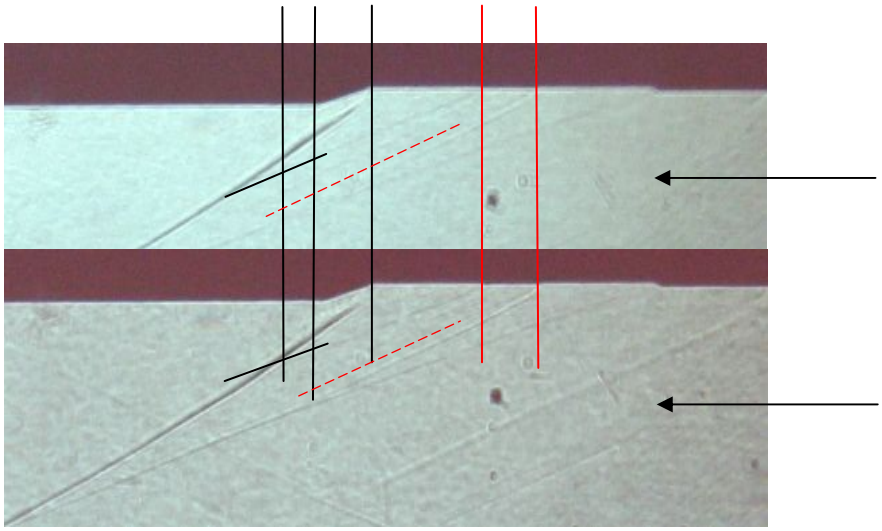

Fig.1.34. Disturbances picture (the cylinder with the cone in the nose part) for the case when the sliding discharge is initiated over the surface of the model (a). (b) is a picture of flow streamlining in the discharge absence.

In Fig.1.33. one can see photos of the disturbances picture at airflow around the working model (a wedge) at flow velocity corresponding to Mach number M=3. In Fig1.33. (a) there is the disturbances picture for the case when the sliding discharge is initiated over the surface of the model. In

Fig.1.33. (.b) there is picture of the flow streamlining in the discharge absence. Comparison of figures (a) and (b) shows that decrease of inclination angle of initial area of the disturbance lines takes place at sliding discharge initiation in the working zone of the model. One can see the disturbance of the first and second lines along the flow at the disturbance specially prepared in the discharge area (polyethylene film 15 μm thickness glued to the dielectric substrate). Variation of the inclination angle can be explained by the following. Variation of temperature takes place in the boundary layer at sliding discharge initiation in the area of the boundary layer. This leads to variation of velocities distribution profile over the boundary layer cross section. This effect was considered in details in the Report № 5 in the section devoted to tangential discontinuity of velocities.

We formulated a problem: by some visual method to detect features of the flat plate flowing around at creation and influencing of surface discharge on the boundary layer. Investigations were carried out in the wind tunnel (WT) A-7 Imec MSU. It is a short time operation WT of half circle type with the incident flow corresponding to Mach number M=3.

Pressure in the fore chamber and static pressure of undisturbed flow in WT were measured by sensors of IKD-27 type. Sensor feeding was realized by the voltage of 27 V from the stabilized constant current feeding source B5-45. Electrical signals from the sensors were detected and analyzed by PC.

Flow parameters were the follows:

Pressure in the fore chamber Po=4.344 kg/cm^2 ,

Static pressure of undisturbed flow P=0.1173 kg/cm^2,

Stagnation pressure of the incident flow Po'=1.3 kg/cm^2,

Mach number $M_\infty = \sqrt{5 \cdot \left[\left(\frac{P_o}{P_\infty} \right)^{0.28571} - 1 \right]} = 3$

Velocity head $q_\infty = 0.7 M_\infty^2 \cdot P_\infty =$ 0.7415 kg/cm^2,

Sound velocity a = 198.259 m/s,

Flow velocity V = 595.77 m/s,

Static temperature in undisturbed flow T = 97.291^0 K

Reynolds number $\mathrm{Re} = \frac{\mathrm{Re}\infty \cdot 10^{-6}}{L} = \frac{26814.819 \cdot P_\infty M_\infty}{(1 + 0.2 M_\infty^2)^{2.25} \cdot T_o^{1.25}} = 3.0953$, at L=0.1m.

Pressure sensors accuracy in the complex of measuring equipment was determined at pressure sensors calibration. Measurements accuracy was ~ 3%.

Flow structure investigations were made with a help of optical device IT-14 with spark source application.

Spectra of models streamlining (plane with wedge type fore part, cylinder with cone-type fore part) were obtained with a help of digital photo camera.

Models were located in the working part of WT on a pylon with zero angle of attack.

Flow parameters were detected and analyzed with a help of PC. Recording of flow parameters by electrical sensors was made in the absence of the discharge in order to exclude electrical noise.

Let us stop at flow feature determination on the surface without the discharge; it is required for analysis of the flow appearing in the result of boundary layer interaction with the discharge.

A shock-wave structure is absent in the experiments, this corresponds to flow around the plate with sharp fore edge at zero angle of attack. We observed so called weak disturbance waves from the fore edge of the model – the turbulizer (it is the polyethylene film of 15 μm thickness that is glued to the dielectric substrate in the discharge gap) and joint of electrodes with the isolator on the model surface.

Thing mixing turbulent layer gradually increases along the plate. This is agreement with boundary layer theory and computed values for laminar incident flow (the level of initial turbulence in the working part of AT is E=2% at M=3 according with methodical measurements).

Turbulent mixing takes place on a background of weak disturbances on the plate, and intensity of these disturbances decreases due to turbulization processes.

Boundary layer and weak shock waves structure has a stationary picture without sharp variations of inclination waves of disturbances and boundary layer thickness.

Flow transition through a row of disturbances along the flow and increase of boundary layer thickness cause insignificant pressure increase in the base drainage point in comparison with the front point where the pressure equals to the static pressure of undisturbed flow.

Results of investigations at the discharge realization showed typical flow features in the sliding discharge area.

From visual experimental results one can see that a flow in the boundary layer has more smooth and filled structure of the boundary layer. The pressure in the base point insignificantly decreases by a value comparably with measuring accuracy but with sufficiently clear revealing of pressure gradual decrease feature in the base point during the time of the discharge realization.

Disturbance lines from the turbulizer undergo a change. Decline angle decreases and weak disturbance shock wave zone of interaction with the boundary layer somehow moves down the flow.

Non stationarity of origin point of the disturbance line with the boundary layer (smooth basement of the disturbance wave) attracts attention. Sharp boundary between the laminar flow and turbulent boundary layer is observed directly on the model surface (in the form of light stripe) and there is formation of near wall layer with more low viscosity due to high temperature on the model surface.

The density in the boundary layer is lower at the discharge presence than in the case without it, as it was determined by light intensity character.

PART II. THE PHYSICAL MODEL OF THE SLIDING DISCHARGE

(Task 3)

§2.1. Development of discharge physical model. General properties of sliding discharge

Sliding discharge over a separating surface between a solid and a gaseous dielectrics has a special place between the open high current discharges [8]. An electric spark is formed not in the open gas volume, but on the surface of the dielectric material when the high voltage pulse is applied to the electrode system, which is represented in **Fig. 2.1**.

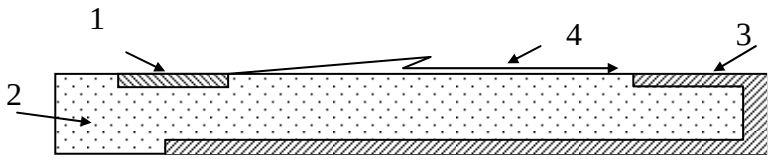

Fig.2.1. Electrode scheme of sliding discharge: 1 - initiating electrode, 2 - dielectric substrate, 3 - metallic substrate (second electrode), 4 - sliding discharge.

An electric field in such a discharge gap is value E is characterized by the ratio of the applied voltage and the dielectric width and is practically independent of the gap size between the ionizing 1 and closing electrode 2 along the dielectric surface. Since the electric strength of modern isolating materials can exceed 10^6 V/cm (for example, lavsan) then the E value can be 10^6 V/cm the hazard of dielectric substrate damaging. It is important that such a high electric field E, which is sufficient for a gas ionization, can be reached at small dielectric material width, and hence at rather moderate amplitudes of the high voltage pulses feeding the discharge. High field non uniformity with the component, which value is independent of the discharge gap length, and presence of distributed capacity of the dielectric substrate, which is charged during the discharge development, conditions the specific form of the breakdown characteristics of the sliding discharge that are not satisfy the Paschen law [9].

In Fig. 2.2 one can see dependencies of the ignition voltage via the gap size between the initiating and closing electrodes, taken from [10]. One can see that the same voltage dependence in case of the spark and the sliding discharges take place only at the discharge gap value of 1-2 cm. The breakdown voltage changes weakly in case of the sliding discharge at increasing of the inter electrode gap size or a gas pressure above some value dependent of a gas composition, width and dielectric constant of the isolating material. This circumstance allows to insure the breakdown of the discharge gap of one meter and more at moderate voltages (see Fig.2.2).

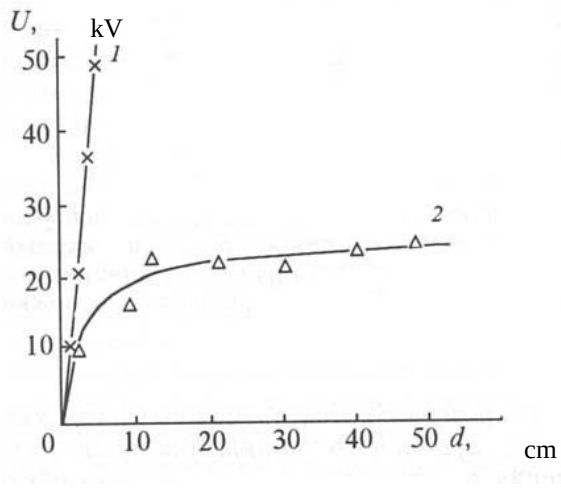

Fig.2.2. Dependence of the ignition voltage via inter electrode gap size in air: 1- static breakdown, 2 – sliding discharge.

Besides low breakdown voltages the sliding discharge has additional peculiarity, it is connected with the high voltage of the normal component of the electric field. The point is that the conditions typical for nanosecond breakdown of highly over voltage spark gaps are created at the action of the high voltage pulse (with the amplitude no less than 10^4-10^5 V with the rising velocity no less than 10^{11}-10^{12} V/s) on the electrode system of the sliding discharge. Electric field strength in a gap can be increased by 10^2 times on the surface micro imperfections of the dielectric material and [11]. At that the time of the discharge development becomes comparable with the typical time of elementary processes in a plasma. This leads to deviation from the Tawnsend and streamer mechanisms [12] and the absence of the discharge channel even at high currents of about 10^5 A. The channel can be formed after reaching of the maximum current value, and not a single one, but several [13]. Avalanches radiation created in these condition contains an intense short wave radiation, which lies in the region of the vacuum ultra violet [14] or even in the region of the soft X-radiation [15]. This radiation, which intensity rises with increasing of the field strength, can produce free photo electrons at distances much greater than the sizes of initial avalanches, this conditions the diffuse and multi channel discharge forms. The multi channel sliding discharge structure can be cause by the following. The distributed capacity of the dielectric substrate play a role of the great number of capacitors that separate with respect to feeding the isolated regions of the extended initiating electrode during the discharge forming. The leader channel growth along the discharge gap is connected with the transport of the electric charge some value, so the higher value of the specific capacity of the dielectric $C \sim \varepsilon / \Delta$ (ε - is the dielectric permeability, Δ - is the dielectric width) then from the smaller part of the electrode the separate channel will start to develop, without the

interference to the neighboring channel growth. It means that the number of plasma channels forming the plasma sheet on the dielectric surface increases.

The phase of the sliding discharge is called incomplete if the edge of the sliding discharge is closed by the isolating material so that the leader channels do not close the gap when they reach the end of the dielectric channels. The incomplete sliding discharge appears at the voltage insufficient for the discharge gap breakdown. The absence of the high current phase conditions high uniformity of the plasma sheet created by the discharge. It is necessary to note that the main channel developed perpendicular to the edge of the initiating electrode has many junctions. So the whole dielectric surface is covered by the plasma, which density becomes higher in the place of main channel location.

The current of the incomplete sliding discharge is limited by the distributed capacity of the dielectric substrate and equals to

$$i = \frac{\partial (CU)}{\partial t} = U\frac{\partial C}{\partial t} + C\frac{\partial U}{\partial t} \qquad (2.1)$$

Here U — is the voltage between the plasma and the sliding electrode, C is the capacity of the capacitor, which is created by the sheet plasma and the sliding electrode. U , generally speaking, has to be a function of the applied radiation and the coordinate on the dielectric surface. But since the potential of the initiating electrode is transferred to the leader head practically unchanged [16], so this potential can be considered as the voltage applied between electrodes. The value C is proportional to the length of the leader channel, and so it is the time function during the discharge development. The first item in the equation for the current (3.1) can be great due to the high speed of the sliding discharge development 10^6-10^8 cm/s [17], and it insures rapid rise of the current. The current of the incomplete sliding discharge is determined only by the bias current $C\frac{\partial U}{\partial t}$ after filling of the dielectric surface by the plasma. One can expect this discharge to be rather economic source of the intense ionizing radiation in spite of its small energy input in comparison with the high current discharges. First, the head part of the propagating channel has to radiate intensely in the ultra violet range of the spectrum, there the non equilibrium processes of the discharge plasma forming in the strong electric field take place. Second, the bias current continues to heat the channel after its forming. At that the reached temperature is relatively not high $(2\text{-}3)\cdot 10^3$ K [18], but the intensity of the ionizing radiation can be large due to the large area of the luminous surface.

The discharge gap is closed by a system of parallel brightly luminous channels of the complete sliding discharge at reaching by the leader channels the edge of the sliding electrode. The brightness temperature of the discharge can be much higher than 10^4 K [19]. The plasma channel density of the

complete sliding discharge, and hence the uniformity of created plasma sheet are determined not only by the density of the plasma channel distribution over the surface but the equality of their propagation velocity. The leader that propagates with the highest velocity will be the first to close the discharge gap and this will cause fast decrease of the voltage on it, and extinction of other leaders. Increasing of the growth steepness and of the applied voltage pulse amplitude leads to the synchronizing the velocity of their development [20].

Deposition of coatings containing fine disperse powders of graphite barium and copper to the dielectric surface create a multitude of auto emission sources facilitating the sliding discharge development. By deposition of these compounds on the surface in a form of regularly alternating strips one can put in order the location of channels and equalize velocities of their development at somehow reduced requirement to the voltage pulse [21].

The specific property of the sliding discharge is determined by the active interaction of the discharge plasma with the dielectric surface. The cross section of the sliding discharge channel, widening of which is bounded by the dielectric surface has an oval form elongated along this surface, and the smaller area in comparison with usual spark at the same current [22-24]. The complete sliding discharge channel has larger linear resistance in comparison with the spark, which stay large during the whole discharge time and it insures liberation in the channel of up to 97% of energy stored in feeding accumulator [25].

The intense evaporation of the dielectric substrate takes place under the action of the sliding discharge plasma action and vapors enter the plasma in the channel. This causes increasing of the plasma density and leads to higher velocity of the light flux growth at the specific radiation luminosity of the channel length unit by 2-3 times greater than of the spark in the visible region of the spectrum [26].

So one can see that the sliding discharge as the source of the prior ionizing of powerful discharge devices exceeds other types of open discharges by luminescence, electric and energy properties. The possibility of creation of rather uniform brightly luminous large size plasma surfaces with a help of the sliding discharge in incomplete and complete forms at rather moderate requirements to the feeding source allows to use this discharge for creation of plasma cathodes and heating devices, which possibilities for plasma aerodynamics were discussed in [27].

§2.2. Parameters of the sliding discharge. Electric field dependencies

Consequent analysis of the sliding discharge properties represents a complicated two dimensional electrodynamics problem of the propagation of the sliding discharge as two dimensional ionization wave in the non homogeneous external electric field [28-29]. A complete model describing a

propagation of two dimensional ionization wave in helium is represented [28-29] with solution of electrodynamics and kinetics. However such computations for the sliding discharge in air are absent now, and it is connected with the difficulty of electrodynamics and kinetics processes in the chemically active medium. In this case we will apply a simplified approach developed in references [13,17] на on a basis of experiments realized by the authors of these publications, this approach proved to be applicable for discharges in nitrogen, air and helium.

A discharge proves to be localized in some area near a dielectric surface in case of the sliding discharge over a plane dielectric. In this situation one can use the telegraph equations of the type [30] for a description of the potential U and a current I distributions in a circuit created of the linear capacity C_d of the dielectric, its linear resistance R_d and linear inductance of the area near the dielectric

$$-\partial U / \partial z = L_d \, \partial I / \partial t + R_d \, I \,,$$

$$-\partial I / \partial z = \partial (U C_d) / \partial t \,, \qquad (2.2)$$

where an axis z is directed along the dielectric from the high voltage electrode to the grounded one.

This system of equations has to be supplemented with an equation for determination of electron concentration N_e, with it one can determine a resistance of the plasma channel from the equation

$$R_d = R / l = \frac{m \nu_{ea}}{e^2 N_e S} \qquad (2.2a)$$

(m, e – are electron mass and its charge, S – area of the plasma channel, l – its length, ν_{ea}- frequency of elastic scattering of electrons in collisions with molecules), and which in case of air at the discharge development during hundreds of nanoseconds has a form:

$$dN_e / dt = q + (\nu_i - \nu_{att}) N_e \qquad (2.3)$$

where N_e – is electron density, q – velocity of appearance of slow electrons due to fast background electrons in air , ν_i- ionization frequency in a process $e + M_2 \rightarrow M_2^+ + 2e$ (M_2= N_2, O_2), ν_{att}- attachment frequency in a $e + O_2 \rightarrow O^- + O$. At that an initial electron density is determined on a basis of the equation:

$$N_{e0} = q / (k_{tb} \cdot N_{O2}^2), \qquad (2.3a)$$

where k_{tb} – is a rate constant of the three-body attachment in a process $e + O_2 + O_2 \rightarrow O_2^- + O_2$ [24].

The equation (3.3) has an analytic solution at $\nu_i > \nu_{att}$, at the constant value of the E/N parameter (where E – is an electric field strength in the discharge channel, N is a concentration of a gas molecules:

$$N_e = N_{e0} \cdot exp((\nu_i - \nu_{att})\Delta t) + \frac{q(exp((\nu_i - \nu_{att})\Delta t) - 1)}{(\nu_i - \nu_{att})}, \qquad (2.4)$$

here Δt- the time of the ionization.

It is difficult to simplify the system of equations (3.2)-(3.3) in case of air so to get an analytic solution, but computer simulations were not supposed at this stage of investigations.

In this section we use results of the experiments [13,17] nitrogen, air and helium for getting of estimating equations. There the discharge chamber was made of the teflon with the window of CaF_2 with sizes 120×60 mm ^{2}. A discharge was created in the chamber at pressure of 0,1 MPa. The electrode system consisted of a grounded electrode covered by a plane dielectric plate, a high voltage electrode was located on its surface. The system was manufactured by etching of the glass fiber laminate covered by a foil on both sides. Experimental data was obtained in case of the discharge gap of l = 10 cm length and H = 4 cm width.

The electric discharge system for realizing of the sliding discharge is represented in **Fig. 2.3.** Two variants of the electric discharge scheme were used, they differed by the voltage growth velocity in the discharge: with a shunting capacity c C_0 (C_0 = 15 nF, C = 30 nF, L_0≈200 nH) and without it (C_0 = 0, C= 30 nF, $L + L_0$≈200 nH). The accumulating capacity C was charged up to the voltage U_0 through the resistance R and it was commutated by the nitrogen high pressure discharger P with the own conductance ~25 nH. Experiments were carried out at negative polarity of the high voltage electrode. The discharge voltage was measured with a help of the ohmic dividers. The disturbance of the voltage rectangular pulse front by the dividers did not exceed 3 ns. The voltage in the inter electrode gap was measured with a help of probes, they represented the foil strips 0,2 mm wide. The probes were located at the dielectric surface parallel to the electrodes at a given distance from the latter. Usually the probe part of 1 mm length was in the discharge region. The full current through a discharge was measured by the low inductive current shunt. Signals were detected by the oscilloscope C 1-26.

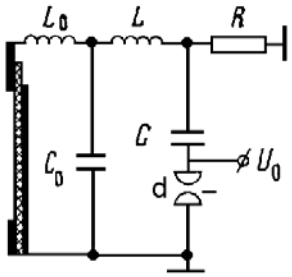

Fig.2.3. Electrode scheme for creation of sliding discharge [13,17].

The experiments showed that the current passing in the sliding discharge can take place during one or two stages. The first stage is characterized by a small discharge current ($I \approx \partial(C_d U)/\partial t$), which is the main current of the dielectric distributed capacity C_d charging and it changes from 10 to 200 A. The second stage represents the breakdown of the previously at the first stage ionized of a gas layer near the dielectric surface and it is characterized by the sharp current rise up to 10 kA. In **Fig. 2.4** one can see the waveforms of the full current, voltage at the high voltage electrode and at the probe (**Fig. 2.5**), placed at a distance of 9,3 cm from the high voltage electrode (l =10 cm).

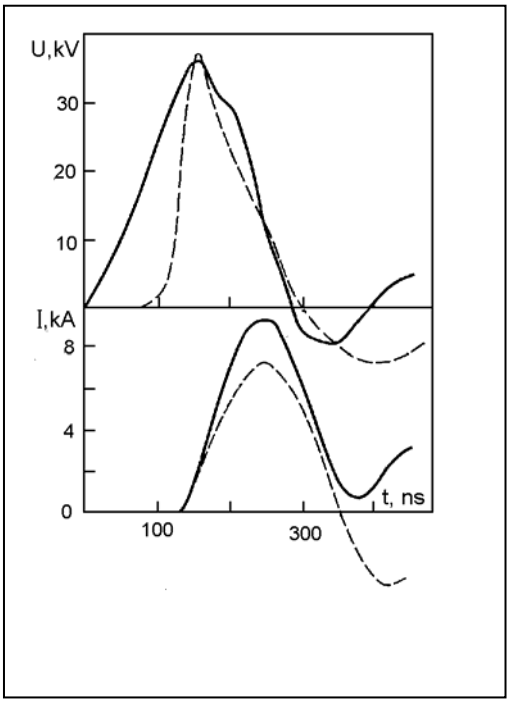

Fig.2.4. Waveforms of the discharge voltage and current at U_0 =40 kV for C_0=0 (dashed line) and C_0= 15 nF (solid line) [10].

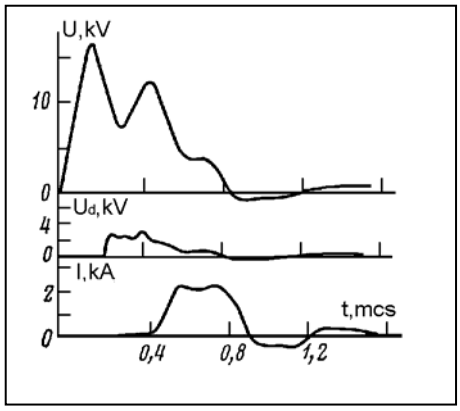

Fig.2.5. Waveforms of the discharge voltage $U_,$ at the probe U_z and current I at U_0 =17 kV and C_0= 15 nF [10].

The voltage pulse reaches the probe already during the first stage. The propagation velocity of the voltage wave is V≈5·10^7 cm/s. The full current at this stage did not exceed 100 A. However, gas ionization by a strong field in a layer near the dielectric, which appears due to vibrations of the

surface discharge of the dielectric, can lead to a breakdown (second stage of the current passing) after a definite time τ1 μs (see Fig. 3.2) at the voltage much smaller than those in the first peak. The temporary rapprochement of these two stages takes place at the increasing of the charging voltage U_0. The breakdown takes place practically at the moment of the voltage wave coming to the grounded electrode at high values of U_0 and at reaching of the maximum voltage at the high voltage electrode (see **Fig.2.4**).

For studies of the voltage pulse initial front steepness influencing on the sliding discharge dynamics the parameters of the electric discharge circuit in the both variants of the electric scheme were chosen so that the voltage amplitude U in the discharge and the duration of the current (energy input) were the same. The peak voltage at the discharge was $U > U_0$ for both variants of the scheme at variation of U_0 from 20 to 50 kV, and the steepness of the voltage pulses differed approximately by 5 times (**Fig. 2.4**).

Measurements showed that the velocity of growth of $\partial U / \partial t$ and the propagation velocity of the voltage pulse substantially change with the voltage pulse propagation over the dielectric. Investigations showed that the field $E_z = \left|\partial U / \partial z\right|$ increases with the increase of z before the breakdown, and weakly changes along the discharge after the breakdown. The voltage pulses with high growth of rising have the higher velocity of the propagation v. The velocity does not change at variation of the dielectric width d.

Experiments showed that a ratio $(1/v)(\partial U / \partial t)$ is practically independent of applied electric discharge system, i.e. of $(\partial U / \partial t)$ and weakly (for 40%) rises at substantial increase (from 20 to 50 kV) of the voltage amplitude in the discharge U.

Measurements showed that the magnitude of $(1/Nv)(\partial U / \partial t)$ is weakly dependent of a gas pressure ant it is $> 2 \cdot 10^{-16}$ V·cm^2 for a discharge in helium and $> 16 \cdot 10^{-16}$ V·cm^2 in nitrogen.

It is rather difficult to make well-grounded estimates of all processes roles that form the sliding discharge. Suppose that the main mechanism of electron multiplication at initial moment of the voltage wave coming is the direct ionization by electrons of a gas atoms and molecules (Tawnsend mechanism) near the dielectric surface. At that the roles of ionization by fast electrons, photo ionization, attachment, etc. come (see (2.3.a, 2.4)) to change of initial electron concentration in front of the voltage wave. The absence of the voltage dependence at probes on the length of probes shows that the propagation of the voltage wave takes place uniformly over the dielectric width. So, basing on it, let us consider the linear capacity of the dielectric to be constant in the system of equations (2.2), and we omit the inductance in the consideration because the linear

resistance is great at initial breakdown stage, and it mainly depends on the electron concentration N_e (3.2a) in the plasma layer near the dielectric.

Typical value of the *E/N* parameter in some point near the dielectric surface can be calculated using the following equation:

$$E / N = (1/ N)\sqrt{(\partial U / \partial x)^2 + (\partial U / \partial y)^2 + (\partial U / \partial z)^2} \qquad (2.5)$$

here U – is a voltage in a given point, the axis y is directed normally to the surface, the axis x is directed over the dielectric width

$$\partial U / \partial z \cong (1/ v)(\partial U / \partial t) \qquad (2.6)$$

here $\partial U / \partial t$ - is a velocity of a field potential variation in a point at the moment of the voltage wave coming; v – is a velocity of this wave propagation скорость; $\partial U / \partial x \cong 0$ (as showed measurements with probes of different length).

We have from the experiments that the width Δ of the sliding discharge layer is Δ<0,1 cm, and it is much smaller that the typical size of U variation with respect to z (i. e. $U /(\partial U / \partial z) \cong 10$ cm >>Δ). This allows to obtain a connection of normal components of the electric field strength (directed along the axis y) using the boundary conditions on the separation surface between a dielectric and a plasma of the sliding discharge in a form [30]

$$4\pi\sigma E_{py} = \partial(\varepsilon E_{dy} - E_{py}) / \partial t .$$

We suppose that $E_{py} = \partial U / \partial y$ and it does not change in the layer Δ. Here E_{dy} and E_{py} – are electric field strengths in the dielectric and in the plasma layer near the dielectric; σ -is the conductivity of the plasma layer. Using the condition

$$U = E_{py} \cdot \Delta + E_{dy} \cdot d$$

one can obtain an equation for a magnitude of $\partial U / \partial y$ and to approximately estimate a value of the parameter *E/N* in the rather general case in the sliding discharge plasma

$$E / N = (1/ N)\sqrt{\left\{U / \left[\Delta + \frac{d}{\varepsilon} \cdot \frac{4\pi\sigma + \partial \ln(\partial U / \partial y) / \partial t}{\partial \ln(u - \Delta \partial U / \partial y) / \partial t}\right]\right\}^2 + \left(\frac{\partial U}{\partial t} \cdot \frac{1}{v}\right)^2} \qquad (2.7)$$

Note that in the potential approximation (when rot *E*=0) [30]

$$\frac{\partial \ln(\partial U / \partial y) / \partial t}{\partial \ln(u - \Delta \partial U / \partial y) / \partial t} = 1 ,$$

and it can be applied for the experiments description.

From equations (3.5) and (3.7), which determine an approximate value of the *E/N* parameter, follows that if the plasma conductivity σ is small then

$$E / N \cong (1/ N)\sqrt{\left\{U / \left[\Delta + \frac{d}{\varepsilon}\right]\right\}^2 + (\frac{\partial U}{\partial t} \cdot \frac{1}{v})^2} \qquad (2.8)$$

Now let us suppose that the gas conductivity σ near the dielectric surface is considered in the high current sliding discharge with high values of U and $\partial U / \partial t$, and at the moment of the voltage coming it considerably increases up to values $\sigma >> (\varepsilon / 4\pi d)\partial ln(u - \Delta \partial U / \partial y) / \partial t$ during the times much smaller then the voltage rise time in this point. In this case the electric field strength E magnitude at the voltage wave front (excluding probably the initial front part) is determined by the E_z and according with (3.5) and (3.6) is

$$E / N \cong (1/(N v))(\partial U / \partial t) \qquad (2.9)$$

As showed experiments with the high current uniform discharge in helium $(1/(N v))(\partial U / \partial t) \cong 2 \cdot 10^{-16}$ V·cm^2, and in nitrogen (and air) $(1/(N v))(\partial U / \partial t) \cong 16 \cdot 10^{-16}$ V·cm^2 (remind that the breakdown voltage in glow and volume discharges in air is $E/N > (11\text{-}12 \cdot 10^{-16})$ V·cm^2 .

A development of the high current sliding discharge takes place in two stages. At the first stage, which is characterized by high uniformity, the linear capacity process of charging takes place. At the second stage takes place a self maintained breakdown of the inter electrode gap.

In general case the *E/N* parameter depends on the linear dielectric capacity magnitude, gas pressure value over the dielectric, an amplitude and a velocity of applied voltage rising, etc. Changing of main parameters depends on the sliding discharge organization.

An important difference of the sliding discharge over the dielectric surface from other discharges is the possibility of its realization at different *E/N* values, which depend or do not depend on plasma conductivity. Ionization processes at the front of the high current uniform sliding discharge, which condition the propagation of the voltage wave, are determined by the parameter $E / N \cong (1/(N v))(\partial U / \partial t) \approx const$

The *E/N* value is determined by the sort of a gas, and is close to the maximum values of those in the pulse volume discharges as experiments showed.

§ 2.3. Discharge channel characteristics

Using the data about the discharge plasma and adduced formulas let us determine the possible radius of the separate channel of the sliding discharge. For this let us use an equation connecting

ionization and attachment processes with electron diffusion D_e from the discharge channel of R_0 radius, as it can be made in case of air [31-32]:

$$\nu_i \sim \nu_{att} + 6D_e / R_0^2,$$

or

$$R_0 \sim \sqrt{6D_e /(\nu_i \sim \nu_{att})} . \qquad (2.10)$$

Let us use the rate constants for ionization and attachment k_i-$k_{att}\approx(1\text{-}2)\cdot10^{-12}$ cm^3/s, and electron diffusion $D_e\approx(0{,}2\text{-}0{,}3)\cdot$ m^2/s at air breakdown at air temperature T≈2000 K (fit to experiments [13]) [33], there special computations of electron distribution function were made for hot air conditions. Using (3.10) we obtain that the effective diameter of a channel is $2R_0$~1. -1.5 mm.

One can obtain an estimate of the gas heating in the channel, considering the channel diameter, average voltage and current to be constant during the typical time of the discharge pulse on the basis of equation

$$\frac{7}{2} N k_B \frac{dT}{dt} = \frac{\bar{I}\,\overline{U}}{Sh}$$

where k_B- is the Boltzmann constant $\bar{I}$, $\overline{U}$ - are the average values of the discharge voltage and current during the discharge pulse Δt , or

$$\Delta T = \frac{\bar{I}\,\overline{U}\,\Delta t}{Sh\frac{7}{2}N k_B}$$

Using the average values of the current and voltage during the pulse with its duration from [6, 10] , $\bar{I} \approx 3$ kA, $\overline{U} \approx 20$ kV, $\Delta t = 10^{-7}$ s, $h=2R_0$=1-1,5 mm, and the surface area of the discharge S=4×10 см^2 [13, 17] one can obtain $\Delta T\sim(1.8\text{-}2.7)\cdot10^3$ K, that is in good agreement with the experimental value $T=2.\cdot10^3$ K even at such a rough consideration.

The undertaken approximate analysis shows that the sliding discharge plasma layer of 1-1,5 mm width is heated up to the temperature $\Delta T\sim(2\text{-}3)\cdot10^3$ K during the pulse time of the discharge of about hundreds of nanoseconds, obtained characteristics can be used as initial ones for the gasdynamic analysis.

§ 2.4. Theoretical investigation of plasma boundary layer effect on flow parameters. Character of sliding discharge distribution over a surface.

This section is devoted to sliding discharge properties, which influence the sliding discharge difference from plasma boundary layer. Usually the area covered by a plasma discharge consists of plasma channels developing along the dielectric surface [1-2] the increasing of channel numbers

increases its resemblance with boundary layer. This section is devoted to questions of channels and their development in the sliding discharge, analysis of conditions for a uniform sliding discharge development over a dielectric surface in gases.

Experimental data. Uniformity of a sliding discharge determines an efficiency of its application. For a purpose of channel density increasing it was proposed to insert emission centers with a small work function to the dielectric surface [3] in a sliding discharge. For the purpose of a uniform discharge creation also pulsed transformers were applied with an putting out voltage up to 200 kV [3, 4], however a channel density of the sliding discharge did not exceed 1-2 channel/cm (ch/cm)in this case.

It was marked in [3, 5-7] it was marked that the sliding discharge generation in helium and air is difficult. Its effective application for solution of internal combustion problems supposes its uniform formation namely in mixtures with air (air) at moderate voltages (<50 кВ) and voltage rising rates $<10^{12}$ V/s on the discharge.

A sliding discharge in references [5-7] was created in a chamber made of fluoroplastic -4. A gas pressure was usually - 750 Torr (with the exception of several cases). The discharge was observed through a window made of CaF_2 with sizes 12×6 cm^2. An electrode system consisted of a grounded electrode covered by plane dielectric plate, a high voltage electrode was located on it. Fluoroplastic, glass textolite and ceramics based on titanium oxide were used as a dielectric. In the references [5-7] one can find results obtained at the discharge gap sizes 10×4 and 4×10 cm^2. Discharge gap sizes in several experiments changed up to a length L=15 cm and up to H=1 m in a width.

A scheme of the sliding discharge creation is represented in **Fig.2.6.** Two variants of the scheme were applied: with a sharpening capacity C_0=0,12·C and without it (C_0=0). A storing capacity C=0,1 μF was charged up to a voltage of U_0 through a capacity *R*. A current commutation was realized by a high pressure discharger. Usually inductances L_0 and *L* were 40 and 70 nH. Experiments were carried out at negative polarity of a high voltage electrode. A current and a discharge voltage were detected by an oscilloscope C1-26. An integral discharge luminosity was detected by a photographic method. Discharge channel width was determined with a help of blow – up photos and densitygrams and was averaged over a discharge gap.

The investigations showed that the sliding discharge characteristics and its uniformity depend on a number of parameters, and in particular by its amplitude *U* and by a velocity of a voltage rising on a discharge $\partial U/\partial t$. The discharge consists of one stage, the charging stage of distributed capacity of a dielectric C_d , at values of *U* smaller than those of the breakdown voltage U_{min} of the inter electrode gap. The second stage is realized at $U > U_{min}$, which represents a

breakdown of preliminary ionized during the first stage gas near a dielectric surface. It is characterized by a sharp current rise up to 40 kA. The breakdown at $U_{min} \leq U \leq U_{max}$, (where U_{max} – some typical value of an applied voltage ($U_{max} \approx 3\ U_{min}$ in given experiments) takes place 0,1-1,0 μs after the discharge gap is passed by the voltage wave and at reaching of the voltage maximum on it. The breakdown takes place at$U \geq U_{max}$ practically at the moment of the voltage wave coming to the grounded electrode.

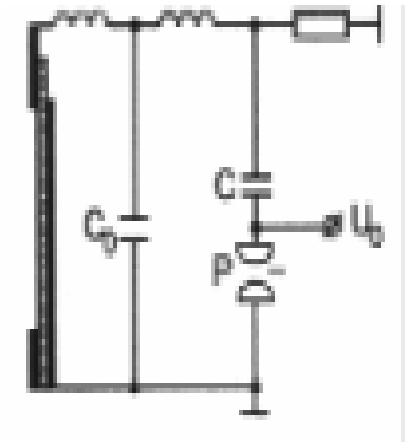

Fig.2.6. Electrode scheme for creation of sliding discharge [5-7].

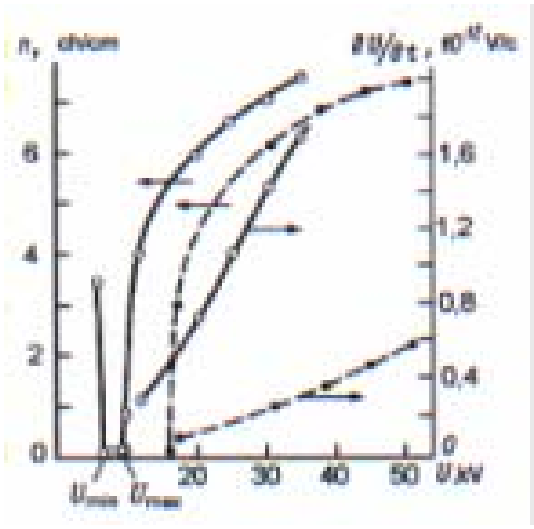

Fig.2.7. Dependencies of n channels and $\partial U / \partial t$ on U for feeding schemes with sharpening capacity (dashed lines) and without it (solid lines).

In **Fig. 2.7** one can see dependencies of sliding discharge channel density n and voltage rising velocity $\partial U/\partial t$ via an applied voltage in helium. In his case in the experiments the textolite was used as a dielectric, its thickness was d = l mm; and area - L×H=4×10 cm^2. In a series of experiments at $U = U_{min}$ were observed both the uniform discharge, in which only the first stage is realized, and the gap breakdown by one channel. The breakdown took place by one or two bright channels in the voltage region $U_{min} \leq U \leq U_{max}$, independently of H (up to 1 m), the second stage was realized with a delay. The area of U, in which the non uniform sliding discharge development takes place ($U_{min} \leq U \leq U_{max}$), is determined by the discharge gap length L, value of $\partial U/\partial t$ and the gas type. Dependencies of U_{min} , U_{max} via a dielectric permeability ε and a dielectric thickness is not so essential. The analysis of [6] shows that an application of other inert gases instead of helium, decreasing of L and d, and increasing of ε leads to the decrease of U_{min} , U_{max} values. Dependencies comparison (**Fig. 2.7**) shows that the channel density n weakly depends on U and $\partial U/\partial t$ at rather high U values. High channel density (>6 ch/cm) was reached in discharges at small charging voltages (U_0 β25 kV).

A discharge circuit conductance value is one of important parameters in real devices for the sliding discharge creation. In **Fig.2.8** one can see dependencies of n, U and $\partial U/\partial t$ via the inductance value. These dependencies show that increasing of L_{ind} causes the decrease of $\partial U/\partial t$ and it decreases the channel density n respectively. Discharge channel luminosity intensity is about the same at L_{ind} β 1 μH, and at Lρ3 μH (at long typical times of the discharge development) discharge channel luminosity intensity of separate channels differs drastically (for ~25% of the total number).

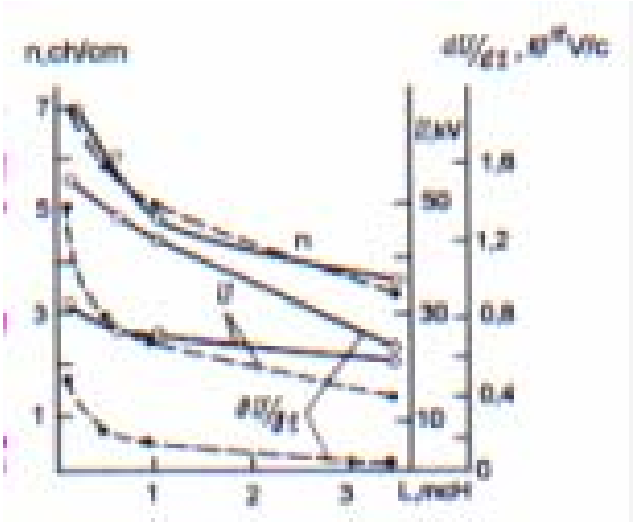

Fig.2.8. Dependencies of n, U and $\partial U/\partial t$ on L for feeding schemes with sharpening capacity (dashed lines) and without it (solid lines).

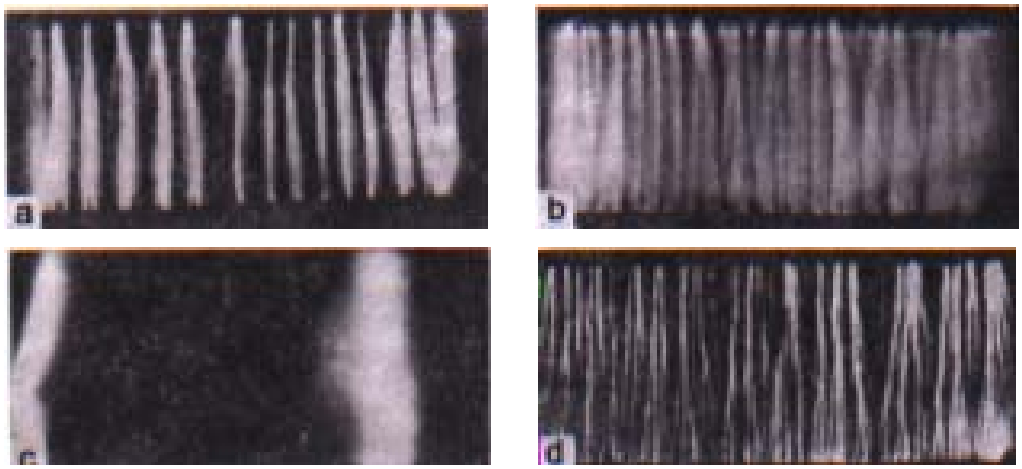

Fig.2.9. Photos of sliding discharge plasma integral luminescence at $L \times H$=4×10 cm^2 and d=6 mm: a – He, ε ≈4; b - He, ε ≈250; c- air, ε ≈4; d - air, ε ≈250.

In **Fig. 2.9** one can see photos of the sliding discharge over dielectrics with ε≈4 and ε≈250 for helium and air. The discharge in air over the textolite surface (ε≈4) 6 mm thickness developed by two arcs over edges of electrodes. Increasing of ε allowed to realize the multi channel discharge at the same thickness. A comparison of discharge luminosity in air and in helium shows that plasma filling of a discharge gap is better then in air, however a channel density in helium is smaller than in

air. Let us imply under an uniformity improvement the simultaneous increasing of a channel density *n* and of a coefficient of discharge plasma filling of a dielectric $K=\Delta n$, where Δ- is a transversal channel size averaged over the discharge gap. Sliding discharge uniformity in air slightly changed at increasing of a dielectric permeability higher than ε≈150. A discharge uniformity in helium slightly changed in the whole range of ε investigated values: from ε≈3 (fluoroplastic -4) to ε≈250 (ceramics).

Investigations showed that a dielectric thickness exerts substantial influence on an uniformity of a sliding discharge. In **Fig.2.10** one can see *n* and *K* dependencies upon 1/*d* value for helium and air для. A textolixe plate of 0,4- 5 mm thickness was used as a dielectric. It can be seen that the channel density inversely depends on the dielectric thickness in the conditions of the experiments.

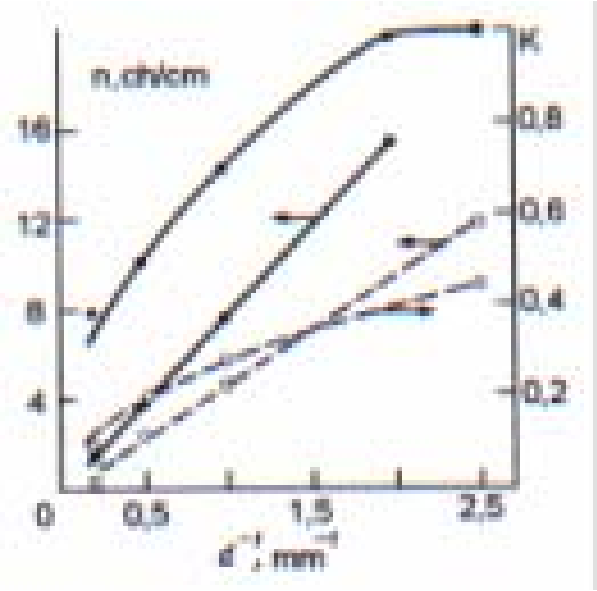

Fig. 2.10. Dependencies of n, and filling coefficient K via d^{-1} for He (solid lines) and air (dashed lines).

K and *d* connection can be obtained on a bases of following considerations. Supposing that main energy putted in a discharge is an energy of brightly luminous channels one can write an approximate ratio:

$$En \approx En_0 (nDS),$$

where *En* is a mean energy of a gas unit volume in a channel; En_0 is total energy putted in the discharge; *D* is an area of the discharge gap, *S* is the channel cross section. The channel cross section over a dielectric surface (in air, Ar and He) is close to a semicircle according to [8]. Basing on it $S \approx \Delta^2$, where Δ is averaged channel width. So one has

$$\Delta \approx \sqrt{En_0 /(nDEn)} \qquad (2.11)$$

A luminosity of a cooling channel at an expansion is detected up to some definite temperature in a channel (~2000 K) connected with a speed of a film. Supposing that a temperature changes slightly over a channel cross section (with the exception of a small area near its boundary) then the detected channel width is constant (for a given gas) at a constant value of *En*. Measurements showed that the energy put in En_0 does not depend on a dielectric thickness within an accuracy of 15% (the accuracy of measurements). Hence with accounting of a dependence $n \sim d^{-1}$ obtained in the experiments one has

$$\Delta \sim d^{1/2},\ K \sim d^{-1/2} \quad . \qquad (2.12)$$

In **Fig.2.10** dependencies (2) are represented the dependencies (2) going through measured values of *K* at *d*=1 mm. The discharge plasma in He completely fills the dielectric at the dielectric thickness d=0,5 mm, the coefficient *K* reaches its maximum value equal to unity and then it stays constant at decreasing of *d*. Sliding discharge photos in helium and air (**Fig.2.10**) at different *d* illustrate a sharp dependence of the sliding discharge uniformity on a dielectric thickness.

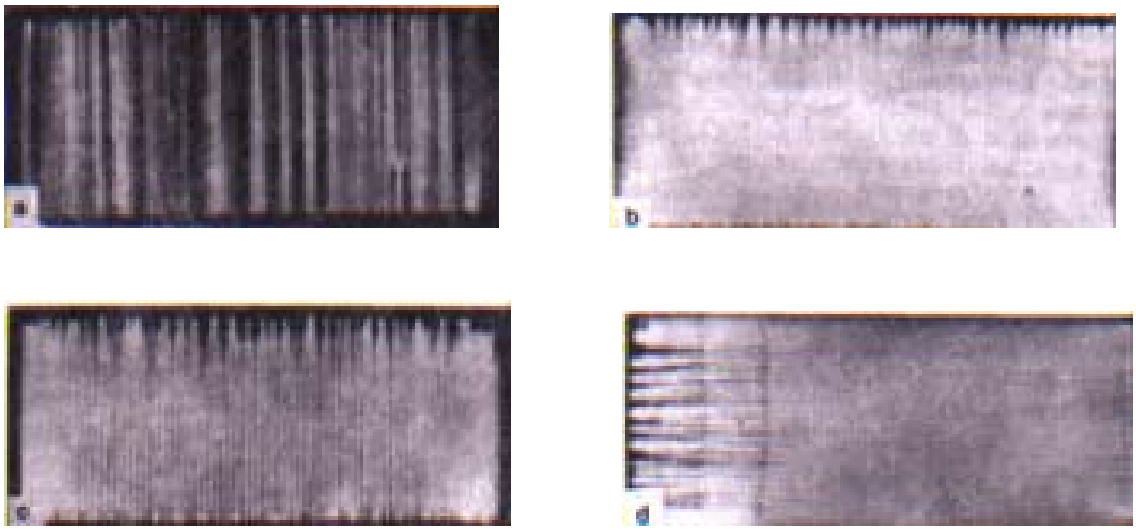

Fig.2.11. Photos of sliding discharge plasma integral luminescence at U_0 =50 kV ε ≈4: *a* –air, d=0.4 mm, L=4 cm; *b* - He , d=1 mm, L=4 cm; *c* - He, d=0.4 mm, L=4 cm; *d* - He, d=1 mm, L=10 cm.

A sliding discharge uniformity depends on a gas type. A sliding discharge is more uniform in heavy inert gases than in helium. K=1 in Ar already at the dielectric thickness of *d*=2 mm.

Variation of a discharge gap geometry also influenced a discharge uniformity. In **Fig. 2.11**, *d* one can see the sliding discharge photo in He at the inter electrode distance of *L*= 10 cm. It can be seen that n ≈6,5 near the high voltage electrode. The increasing of *n* to 9 ch/cm took place at a

distance of >1,5 cm, and up to 17 ch/cm at a distance greater than 3 cm. Jumps of a channel density along a gap were absent at decreasing of U or $\partial U/\partial t$.

It was established that a decreasing of d increases an uniformity more substantially than a n increasing of ε in corresponding times number (**Fig. 2.9, b*; 2.11, c*)**.

In references [5-7] were experimentally obtained values of voltage pulse propagation velocity v, and voltage pulse rising velocity $\partial U/\partial t$ for discharges in He, Ne, Ar, Kr, Xe, N_2 and air. They showed that an average value of the expression $(1/(N v))(\partial U/\partial t)$ stays the same for each gas in a wide range of pressures and has the same dimension as of E/N, which is the following for the indicated above gases: E/N=2,0; 1,75; 2,3; 2,1 ; $14\cdot10^{-16}$ и $16\cdot10^{-16}$ V·cm^2. At that [5-7] для гелия $(1/(N v))(\partial U/\partial t)$ for helium changes insignificantly along a dielectric length with the discharge propagation over the dielectric from the high voltage electrode to the grounded one. Thus in conditions of [6-7] this value was $2{,}3\cdot10^{-16}$ V·cm^2 at 1 cm from the high voltage electrode and $1{,}5\cdot10^{-16}$ V·cm^2 at 8 cm from it , this says that breakdown conditions are improving during the discharge development, that can be connected with the channel heating.

Theoretical estimates.

Role of electrical and physical parameters.

Let us suppose that a main mechanism of electron production in conditions of undertaken experiments during the initial moment of the voltage wave coming was a direct ionization of atoms or molecules by electron impact. At that an electron concentration n_e in a plasma layer near a dielectric is proportional to initial concentration n_e (0) and changes in time by a following law:

$$n_e(t) \sim n_e(0)\cdot exp\left(\int_0^t \nu_i(E/N)\,dt\right) \qquad (2.13)$$

where ν_i – is ionizing frequency of atomic particles by the electron impact is an exponential function of E/N parameter (E — electric field strength in a plasma N is a gas density near a dielectric surface).

Atoms and molecules in excited metastable are accumulated after the voltage wave coming with a discharge developing time, It leads to increasing of an ionization from an excited states. The electron concentration rises in this case by the explosion type [7]

$$\frac{d\,n_e(t)}{d\,t} \sim n_e^{\,1+\alpha},\ \alpha>0$$

increasing initial non uniformity greatly. By increasing of the ionization from excited states role one can explain non uniform of high current discharge stade development observed in the experiments,

when it is realized with a delay at $U_{min} \le U \le$ (**Fig. 2.7**), and also with increasing of its duration at $U > U_{max}$.

Basing on this consideration it is easier to organize the high current sliding discharge in gases where the role of excited states is not important. The role of excited states and stepwise processes in nitrogen and air is important, so it is much more difficult to organize the uniform sliding discharge in them than in some other gases, considered above.

A frequency of a direct ionization ν_i increases more sharply with increasing of *E/N*, then a frequency of an ionization from excited states [7]. At that even a small increase of *E/N* parameter leads to an essential increasing of relative role of direct ionization processes, insuring improvement of a discharge uniformity. In a sliding discharge plasma on the first stage one has the following equation for *E/N* according to [1,5] :

$$E/N = (1/N)\sqrt{\left\{U/\left[\Delta + \frac{d}{\varepsilon}\cdot\frac{4\pi\sigma + \partial\ln(\partial U/\partial y)/\partial t}{\partial\ln(u - \Delta\,\partial U/\partial y)/\partial t}\right]\right\}^2 + \left(\frac{\partial U}{\partial t}\cdot\frac{1}{v}\right)^2}, \qquad (2.14)$$

where σ - is the plasma conductivity in a layer near a dielectric; Δ is a thickness of this layer; *v* – is a velocity of the voltage wave propagation velocity. The first term in the radicand describes the field strength in the normal direction to the dielectric surface (along *y* axis), the second – along the discharge gap (along *z* axis).

When the plasma layer conductivity is small ($\sigma << \frac{1}{4\pi}\frac{\partial ln}{\partial t}\left(\frac{\partial U}{\partial t}\right)$**)**, then according to (4)

$$E/N \cong (1/N)\sqrt{\left\{U/\left[\Delta + \frac{d}{\varepsilon}\right]\right\}^2 + \left(\frac{\partial U}{\partial t}\cdot\frac{1}{v}\right)^2}. \qquad (2.15)$$

E/N in accord with (5) can be increased by increasing of *U*, *∂U/∂t*, *ε /d* or decreasing *N*, Δ. The sliding discharge uniformity improvement was observed in the experiments at the increase of the voltage at the high voltage electrode and the voltage velocity of rising, increase of *ε/d* (**see Fig. 2.7, 2.9, 2.10**) and decrease of *N*.

We have to note that the increase of *U*, *∂U/∂t*, *ε /d* and 1*/N* according to (4) essentially influences the discharge uniformity (due to the increase of *E/N)*, if the plasma conductivity σ is small, what takes place in an initial moment of a voltage wave front coming. *E/N* decreases when the plasma layer conductivity becomes essential, and is determined mainly by the value $E/N \cong (1/(N\nu))(\partial U/\partial t)$ [1,5], which varies weakly (for~20%) at variation of parameters *U*, *∂U/∂t*, *v*, *d* and *N* [5].

The fact that *d* decreasing essentially increases the uniformity than the increase of ε in the corresponding number of times can be explained in the frames of the applied model if the dependence of Δ via *d* (see (2)), obtained for the second stage is true for the first discharge stage as well.

Plasma influencing on channel parameters of channels distributed over a dielectric surface.

At an analysis of sliding discharge channel development it is necessary to account both the complicated kinetics of processes in a gas mixture in a channel developing during a breakdown over a dielectric surface and the channel heating as well.

The channel growth takes place during times much smaller than those of the gasdynamical, at which the pressure equalization takes place, so at the heating analysis one can consider that concentrations of atomic particles (molecules and/or atoms) are constant during the whole processes of energy putting in, and the temperature rises in accordance with [8]

$$\frac{7}{2} N k_B \frac{dT}{dt} = \frac{\bar{I}\,\overline{U}}{S h}, \qquad (2.16)$$

where k_B- is the Boltzmann constant, $\bar{I}$, $\overline{U}$ - average values of the discharge voltage and current during the discharge pulse time Δt , *h* is channel diameter, and S is the surface area of the discharge, or

$$T = T_0 + \frac{\bar{I}\,\overline{U}\,\Delta t}{S h \frac{7}{2} N k_B}. \qquad (2.17)$$

Accounting that the temperature in the channels changes significantly during the pulse one can consider that the initial and the final discharge sizes are formed at different conditions. In this approach we do not consider the longitudinal channel evolution when different instabilities (overheating and field types) leading to the channel splitting can develop.

A radius R_0 of a plasma can be estimated according to [16] by a formulae

$$R_0 \approx \sqrt{6 D_e \tau}\,, \qquad (2.18)$$

here D_e is the electron diffusion coefficient (at their motion from the channel), τ is the time of the electron elimination in plasmachemical (elementary) processes.

Electron balance equation in the discharge channel accounting possible surface vaporized particles and inert gas additions to air in one dimensional approach has a form

$$\frac{dN_e}{dt} = \nu_i \cdot N_e - k_{att} N_{O2} N_e - \alpha_{disrec} N_e N^+ - \alpha_{tr} N_e^2 N^+ - \frac{6 D_e}{R_0^2} + (k_{\det} N + k_{\det}^* N^*) \cdot N^-, \qquad (2.19)$$

here ν_i, k_{att}, α_{disrec}, α_{tr}, k_{det}, k_{det}^*, respectively are the ionization frequency of atomic particles by electrons; dissociative attachment frequency of electrons to the oxygen molecule $e+O_2 \rightarrow O^- + O$, $k_{att}=10^{-11}$ cm^3/s at E/N=1.7 $\cdot 10^{-16}$ V$\cdot$cm^2 (in the region of air breakdown); rate constant of the dissociative ionization of electrons and molecular ions $e + M_2^+ \rightarrow M + M$, for oxygen molecule, for example, $e + O_2^+ \rightarrow O + O$, $\alpha_{disrec} = 2\cdot 10^{-7}\cdot(300/T_e)^{0.7}$ cm^3/s; rate constant of the three body recombination of electrons and ions $e + e + M^+ \rightarrow M + e$, $\alpha_{tr}=9.05\cdot 10^{-20}\cdot(300/T_e)^{4.5}$ cm^6/s; rate constant of the electron detachment from the negative oxygen ion $O_2^- + O_2 \rightarrow O_2 + e + O_2$ with sharply temperature dependence $k_{det} = 8.10^{-10}\cdot\exp(-6035/T)$, cm^3/s; and rate constant of the electron detachment from the oxygen negative oxygen ion at collision with electronically excited molecule $O_2(\Delta) + O_2^- \rightarrow e + O_2 + O_2$, where $k_{det}^* = 2.10^{-10}$, cm^3/s (negative ions of atomic oxygen O^- quickly changes into the molecular ones O_2^- in the result of the charge exchange reactions).

According to estimates the main put into electron elimination gives dissociative attachment of electrons to oxygen molecules at $N_e \square 10^{13}$ cm^{-3}, the process of electron detachment decreases the efficiency of this process.

The initial channel radius when there is no the surface vaporization and of heating is determined from the equation obtained with a help of formulas (2.18), (2.19) :

$$R_{01} \approx \sqrt{6D_e(T_0)/(k_{att}N_{o2})}, \qquad (2.20)$$

and the final radius when there is the surface vaporization and of heating is determined from the equation obtained also with a help of formulas (8), (9)

$$R_{02} = \sqrt{6D_e(T)/(k_{att}N_{O2} - (k_{det}N + k_{det}^*N^*)\cdot N^-/N_e)}. \qquad (2.21)$$

According to formulas (10) and (11) if the plasma is formed in the cold air then $R_{01}\approx 0.12$ mm; if the gas heating up to 2000 K took place then $R_{01}\approx 0.32$ mm without accounting of detachment and $R_{01}\approx 0.42$ mm at $N^-/N_e \sim 0.1$. At that we used the data from [10] для D_e(T=300 K, E/N=1.7 $\cdot 10^{-16}$ V$\cdot$cm^2)=1.5$\cdot 10^3$ cm^2/s, D_e(T=2000 K, E/N=1.7 $\cdot 10^{-16}$ V$\cdot$cm^2)=1.1$\cdot 10^4$ cm^2/s. Formulas (2.20) and (2.21) show that heating of a channel multiples its initial radius by several times, so as it follows from (2.17) the increase of the putted in power leads to uniformity of the discharge distribution over the surface.

Formulas (2.20) and (2.21) also show that additions of inert gases into air mixture and easily ionized additives lead to diminution of the attachment role and to the increase of the detachment processes role, and also they can lead to the uniformity of the discharge distribution over the surface. This is in agreement with conclusions of the references [10-11].

PART III. Theoretical studies of plasma boundary layer on the plate surface influencing on parameters of the supersonic flow over the plate surface (Task 3, Task 4).

§3.1. Gasdynamic characteristics of a gas in the boundary layer at an initiation of a shock wave by the sliding discharge at a supersonic velocity of the oncoming flow.

Characteristics of a plasma boundary layer created by the sliding discharge at late stages after energy release were considered in references [27,28], it means that they were considered after all gasdynamic processes taking place during the discharge development. However there is an essential interest to the initial stage of the gasdynamic processes development. This stage takes place directly after finishing of the energy release process in the sliding discharge.

It is well known [8] that gasdynamic disturbances appear in a gas medium in a form of shock waves at the sliding discharge initiation on the surface of a plate. They appear practically immediately in comparison with the gas kinetic times of temperature rise in a thin gas layer, in which the sliding discharge develops. This temperature rise leads to a substantial rise of the pressure in the layer and respectively to variation of the gas density. One can say that the closed gas volume with the higher temperature, pressure and density (in comparison with the ambient gas medium) is created during the discharge developing time. The pressure shock induces a shock wave which propagates normally to the substrate surface. The energy release area is totally inside the boundary layer region in the case when the sliding discharge is created on the surface of the plate flown around by the supersonic flow [28]. So the appearing shock wave will propagate from the surface of the flown around body in a region under the jump of compression. The propagation of the shock wave and of the decompression region located behind the compression region will lead to changing of the flow characteristics in the region below the compression region and its turn to parameters changing of a gas flowing around a plate.

Parameters of the shock wave and of the decompression wave appearing after the termination of the sliding discharge in the boundary layer can be determined in the case when one knows the gas parameters under the jump of the compression and characteristics of the high temperature boundary layer. For the determination of these parameters let us determine the gas flow characteristics under the compression jump in the case when the sliding discharge is created in the boundary layer over the surface flown around by a gas flow.

We consider the case when the sliding discharge is created on the side surface of the plane wedge with the opening angle α, see **Fig.3.1**. We consider the wedge specially, because in real conditions of experiments it is practically impossible to achieve the ideal condition with the absolute coincidence of the direction of the flow and the dielectric surface.

A compression shock with the incidence angle β ($\mu \le \beta \le \pi/2$, where $\mu = \arcsin(1/M)$, M –is the Mach number) is formed at the supersonic flow around the plane wedge, and β is determined by a velocity of the incident flow.

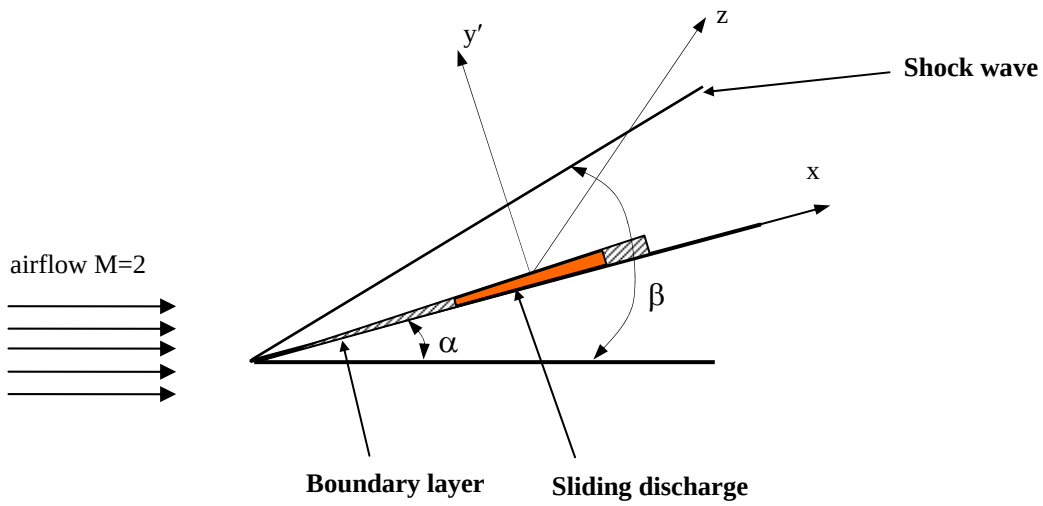

Fig. 3.1.

Let us determine parameters of the gas, which is not disturbed by the sliding discharge action under the compression shock. The gas motion through the compression shock satisfies to conservation laws of mass, momentum and energy. This allows to determine a pressure, density and a temperature at known M and β .

§3.2. Gas parameters determination at the compression shock

A ratio of a gas parameters before and after the compression shock are determined by the incident flow Mach number M and the incidence angle o of the shock β. Let us represent these equations obtained from the kinematics and dynamics equations at the oblique compression shock [29]. Changing of the momentum during the unit time through the unit area of the shock equals to the pressure forces momentum during the same time. One can obtain the following equation from the equation of the momentum change:

$$m\cdot(V_n - V_{n1}) = \rho\cdot V_n\,(V_n - V_{n1}) = P_1 - P \quad , \qquad (3.2.1)$$

here m – is the gas mass; V_n - is the normal component of the incident gas flow velocity to the plane of the compression shock; V_{n1} - is the normal component of the gas flow velocity propagated through the compression shock to the plane of the compression shock; ρ - is the gas density in the incident flow; P – is the gas pressure in the incident flow; P_1 - is the gas pressure in the flow propagated through the compression shock .

Accounting that:

$$\rho V_n = \rho_1 V_{n1} \qquad (3.2.2)$$

we obtain

$$\left(\frac{P_1}{\rho_1 \cdot V_{n1}} - \frac{P}{\rho \cdot V_n} \right) = V_r - V_{n1} \ . \qquad (3.2.3)$$

One has the following equation from the energy conservation equation

$$\frac{\gamma}{\gamma - 1} \cdot \frac{P}{\rho} + \frac{V^2}{2} = \frac{\left(V^2\right)_{lim}}{2} .$$

Taking the limiting velocity before the shock as the constant

$V^2_{lim}/2 = const = (\gamma./(\gamma\text{-}1))(RT_0)$,

where R= 8.32 J/(mole K) is the universal gas constant, $\gamma = 1.4$ – is the adiabatic coefficient, one obtains

$$\frac{\gamma}{\gamma - 1} \cdot \frac{P}{\rho} + \frac{V^2}{2} = \frac{\left(V^2\right)_{lim}}{2} \qquad (3.2.4)$$

before the shock, and

$$\frac{\gamma}{\gamma - 1} \cdot \frac{P_1}{\rho_1} + \frac{V_1^2}{2} = \frac{\left(V^2\right)_{lim}}{2}$$

after the shock. (3.2.5)

From (3.2.4) and (3.2.5) follows that

$$P/\rho = (\gamma\text{-}1)/\gamma) \cdot (V^2_{lim} - V^2_{\tau})/2 - (\gamma\text{-}1)/\gamma) \cdot (V^2_n/2) \qquad (3.2.6)$$

$$P_1/\rho_1 = (\gamma\text{-}1)/\gamma) \cdot (V^2_{lim} - V^2_{\tau 1})/2 - (\gamma\text{-}1)/\gamma) \cdot (V^2_{n1}/2),$$

where V_τ - is the tangential velocity component. Accounting that $V_\tau = V_{\tau 1}$, and that the limiting velocity V_{lim} is connected with the critical sound velocity C_{cr} as

$$C^2_{cr} = V^2_{lim} (\gamma\text{-}1)/(\gamma + 1)$$

One obtains

$$(V_n - V_{n1}) = C^2_{кр} - V^2_{\tau} (\gamma\text{-}1)/(\gamma + 1). \qquad (3.2.7)$$

Here all values but V_{n1} are known since they are determined by the parameters of the undisturbed flow before the shock and by the given incident angle of the shock β. There is no the flow discontinuity at the transition through the compression shock, so the one second flow rate through the unit area of the shock has not to be changed according to the mass conservation law, and one

$$\rho V \sin\beta = \rho_1 V_1 \sin(\beta - \alpha)$$

or

$$V_{n1} = ((\gamma -1) / (\gamma + 1)) ((V^2_{lim} - V^2 + V^2_n)/ V^2_n)) \qquad (3.2.8)$$

Inserting (3.2.8) into (3.2.2) gives

$$\rho / \rho_1 = V_{n1} / V_n = ((\gamma -1) / (\gamma + 1)) [((V^2_{lim} - V^2)/ V^2_n)) + 1] \qquad (3.2.9)$$

So from the energy conservation equation, written using the flow velocity and the sound velocity **a** with accounting that (V/ **a**) = M , one can obtain

$$\rho / \rho_1 = 1/[((2/(\gamma + 1))(1/M^2 \sin^2 в) +((\gamma-1) / (\gamma + 1)] \qquad (3.2.10)$$

Variation of the pressure and temperature one can obtain from the momentum equation and the equation of the gas state. From the equation of the momentum changing with accounting that $\gamma P/\rho = C^2$, and ratio of velocities is $V_{n1} / V_n = \rho / \rho_1$ one obtains

$$P_1 /P = (2\gamma /(\gamma + 1)) M^2 \sin^2 \beta - (\gamma -1) / (\gamma + 1). \qquad (3.2.11)$$

Writing the equation of the state before and after the shock one

$$T_1 /T = (P_1 / P)(\rho / \rho_1) \qquad (3.2.12)$$

Dependencies P_1/P, ρ_1/ ρ, T_1 /T are presented in **Fig.3.2** for the case when the gas heat capacity is constant. Let us use well- known equation [29] for determining of the compression shock incidence angle

$$tg(\beta - \alpha) = tg \beta \cdot ((2/(\gamma + 1)(1/(M^2 \sin^2 \beta) + (\gamma - 1)/(\gamma + 1)) \qquad (3.2.13)$$

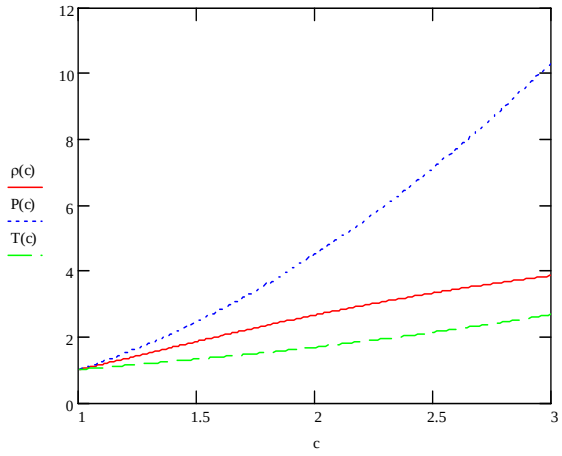

Fig.3.2. Dependencies of ratios variation with respect to a parameter Msin(β). Ratio of pressure - P_1/P_0, density - ρ_1/ρ_0 , and T_1/T_0 . $\rho(c)= \rho_1/\rho_0$, $P(c)= P_1/P_0$, $T(c)= T_1/T_0$

From (3.2.13) follows that there are two values for the angle in the range $0 \le \beta \le \alpha = \alpha_{max}$ at each fixed value of M. The smaller angle β values correspond to the supersonic velocity behind the shock, and the larger β values correspond to the subsonic velocity behind the shock.

§ 3.3. Gas parameters in the boundary layer near a plate surface

Represented above ratios allow to determine the gas parameters in the boundary layer, and it is necessary for the clarification of the flow disturbance picture before the compression shock at the initiation of the sliding discharge at the given plate section (**Fig.3.1**).

For determining of the gas parameters in the boundary layer and of the gas flow character at the shock wave origin it is necessary to know the gas parameters under the compression shock, namely, the density ρ_1, the temperature T_1, the pressure P_1 and the sound velocity C_1..

The gas parameters in the incident flow are designated by the index 0: ρ_0 , P_0, T_0, C_0.

We obtain values of the density, pressure and pressure from the equations (3.2.10), (3.2.11) and (3.2.12) at the following parameters of the incident flow: M=2, $\beta = 40^0$, $\alpha=10^0$, P_0 = 0.5 atm, $T_0 = 273^0$ K, $\rho_0 = 6.39\ 10^{-4}$ g/cm^3. β was obtained from (4.13) and we chose the smallest и выбрано value corresponded to the supersonic velocity under the shock. So the parameters under the compression shock are $\rho_1 = 9.585 \cdot 10^{-4}$ g/cm^3 , P_1 = 1.12 atm, $T_1 = 400^0$ K. The sound velocity under the compression shock is determined with a help of the equation $C^2 = \gamma R T_1$, and it equals to 332 m/s . Obtained data allows to get the gas parameters in the boundary layer. The gas pressure in the boundary layer equals to the gas pressure under the compression shock, and the density can be determined using the equation of the state at the known temperature T_1 and pressure. Let us use the graphs from [28] for a variation of the gas density and temperature over the boundary layer cross section at the velocity of the incident flow corresponding to M=2. Using these data we will suppose that the sliding discharge fills the boundary layer completely, at that the gas temperature and the density have values equal to the average gas temperature and density directly after the discharge termination.

At such suppositions one can consider that the surface layer in initial moment of time represents some gas volume with constant temperature and density values over the whole volume. Since the pressure at sharp temperature rise (after the discharge termination) also increases, then the heated gas begins to flow out of the volume previously filled by the discharge. It is the source of the originating shock wave.

Let us determine the shock wave motion character and the gas parameters after the shock wave front at the given gas parameters outside and inside the boundary layer.

For determining of the shock wave parameters (which moves away from the boundary layer) we suppose that the sliding discharge fills some region over the plate, which linear sizes are much larger than the boundary layer width (along and perpendicular to the flow in the (x,z) plane), see **Fig.3.1.**

Let us determine the front velocity of the shock wave moving away from the plate. The incident flow turns for the angle α directly after the shock. At that the flow velocity component $V_{y'}$ equals to 0. A direction of the shock way moving from the plate coincides with $V_{y'}$. If not to account a gas viscosity then it is possible to think that the shock wave propagates in a gas at rest with the parameters corresponding to those under the compression shock. The equation for the shock wave front velocity has the following form [30]

$$V_2 = \sqrt{\frac{(\gamma-1)((\gamma+1)G + 2\gamma c_v T_1)}{2}} + \frac{\gamma-1}{\gamma+1}\sqrt{\frac{(\gamma+1)(\gamma-1)G}{2}} \quad ,$$

here G –is the specific value of energy inputted to the gas at forming of the sliding discharge. We suppose that the whole energy transforms into heat.

The shock wave front velocity equals to 570 m/s, at the sound velocity under the compression shock equal to 335 m/s, and the sound velocity in the hot boundary layer equals to 896 m/s. The shock wave front velocity of time is higher than the sound velocity in the gas under the compression shock and is smaller than the sound velocity in the hot gas of the boundary layer during the initial moment of time.

Let us determine the flow character behind the shock wave front and the character of the shock wave front propagation. The shock wave front in our formulation moves in conditions of the back pressure of the counter gas from one side and the pressure decrease in the decompression wave conditioned by the wall presence at another side.

Let us use the data of the reference [8] for determining of the shock wave front velocity variation character. Interferograms and shadowgrams of the shock waves propagating from the substrate, at which the sliding discharge was realized are presented in [8]. Represented results show that the plasma layer of 1 – 1.5 mm width at the presence of the sliding discharge is localized near the substrate surface.

The gas mixture volume with the sizes 1.5 x 150 x 800 mm was heated up to the temperature 3400^0 K at the inputted energy to the discharge W = 250 J (at that the heat capacity of the mixture was $c_v = 1.33$ J K^{-1} g^{-1}). Averaged over the volume pressure reached P ~ 12.5 atm. The pressure jump of ΔP = 11.5 atm initiates the shock wave, which starts its motion from the substrate with the velocity of V ~ 1.2 km/s. The shock attenuates during first 10 μs, then it moves with the constant velocity V_0 ~ 667 m/s , and it corresponds to the Mach number M ~ 1.09 .

Analysis of represented results shows that shock wave front velocity changes in the gas at rest in accord with the law close to

$$V_{y'}(t) = V_0 (1 + S^{-t/\tau}) \qquad (3.2.15)$$

And limits to the value $V_{0,}$ where $\tau \approx 20$ μs and $S \approx 4 - 6$ **(Fig.3.3)**. We can use this approximation for $V_{y'}(t)$ in our case because of the conditions indicated above if we consider the gas to be the ideal one, i.e. we neglect the viscosity influence. The region where the gas moves according to this law is bounded by two planes. The outside plane represents the surface of the shock wave itself, and the internal one is the surface of the weak discontinuity. At that the velocity on it equals to zero due to presence of the wall. Let us determine the motion of the gas character in the decompression wave moving after the shock wave.

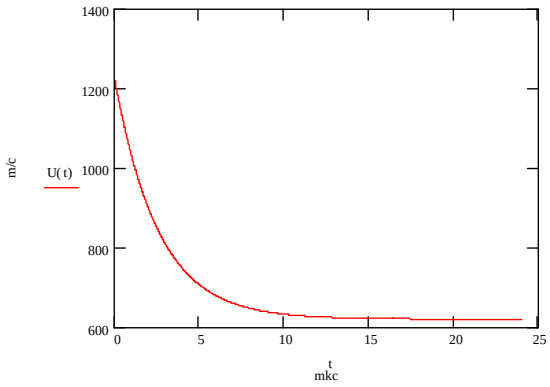

Fig.3.3. Shock wave front velocity variation dependence via time (according to the paper [3]).

A gas region is adjoined to the shock wave front, it moves after the front with the velocity of the front. Then there is the decompression wave. The gas in it moves in the same direction with the velocity changing from the value V_0 to zero near the wall according with the linear law. The pressure in this gas layer changes as follows, as it is shown in the reference [30]

$$P_1 = P_0\left(1-\frac{\gamma-1}{2}\cdot\frac{V(t)}{C_0}\right)^{2\gamma/\gamma-1}$$

from P_1 value to P_0 value near the wall, and V (t) – is the law of the shock wave front velocity variation (3.2.15). The profile of pressure variation is shown in **Fig.3.4**.

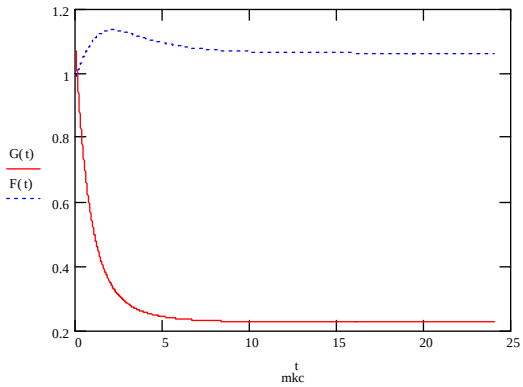

Fig.3.4. Dependencies of the pressure $G(t)=P/P_0$ and temperature $F(t)=T/T_0$) variation in the boundary layer via time. ($G(t)=P/P_0$, $F(t)=T/T_0$)

In the graphs of **Fig.3.4** one can see the results of temperature and pressure dependencies changing via time during the first 20 μs after the termination of the sliding discharge. So from the obtained results it follows that one will observe a gas flow directed perpendicular to a wall in a region of the boundary layer at the initiation of the shock wave by the sliding discharge. At that the changing of a pressure, density and temperature will be observed in the area of the boundary layer, and it will lead to the disturbance of the boundary layer structure. One can see in the graph of the temperature variation in the boundary layer that during first 10 μs (up to the moment when the shock wave front velocity becomes equal to the sound velocity under the compression shock) the temperature decreases from the initial value $T_{ПС}$ to the stationary level T_{C1}. This temperature change in the boundary layer leads to the changing of the boundary layer width and the resistance (drag) coefficient C_F . One can estimate the variation of the dynamic viscosity coefficient and of the gas density in thr layer [27] if he supposes that the gas temperature behind the shock wave front takes the value equal to the mean one over the boundary layer width

$$\mu_{C1} =. \mu_{CO} (T_{C1} / T_{CO})^K$$

and $$\rho_{C1} = \rho_{CO} (T_{CO} / T_{C1}),$$

where ρ_{CO} ,T_{CO} – are the density and the temperature in the boundary layer before the discharge forming, $\rho_{C1,}T_{C1}$ - the density and the temperature in the boundary layer by the moment when the front velocity of the shock wave is $V = V_O$, k – 0.6- 0.8, inserting obtained relations for a boundary layer width and the resistance (drag) coefficient one obtains [30]

$$C_F = 1.328/ Re^{1/2}$$

and $$\delta c1 / \delta co = (T_{ПС} / T_{П0}T)^{(1+ R)/2},$$

where Re- is the Reynolds number, C_F is the resistance (drag) coefficient. One can determine the resistance (drag) coefficient, the boundary layer width and other boundary layer parameters at the given temperature (**Fig.3.5**)

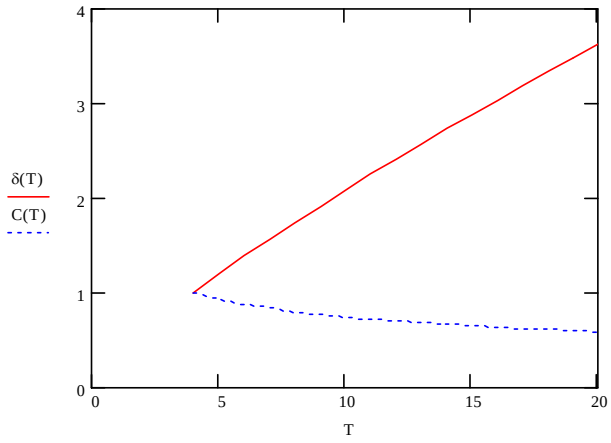

Fig.3.5 Dependencies of the boundary layer width $\delta(T)/\delta(T_0)$ and of the friction (drag) coefficient $C(T)/C(T_0)$ via time .

Graphs of $\delta(T)/\delta(T_0)$ and the resistance (drag) coefficient ratio $C(T)/C(T_0)$ dependencies for incompressible flow are represented with respect to T_C. One can see that the boundary layer width rises with the temperature rise and C_F decreases.

Represented results have approximate character and reflect the qualitative picture of the gasdynamic processes in the boundary layer at the shock wave initiation by the sliding discharge. For obtaining of quantitative results one requires experimental data for more precise definition of $\delta c1$, T_{C1} parameters and of the coefficients τ, S, k

§3.4. Influencing of the plasma layer on vortex structures in the gas flow

Let us consider a viscous flow around a thin plane when it is directed in infinity parallel to the side plane surface. In this case one can observe in the boundary layer the laminar, the turbulent and the mixed type of flows. The spontaneous destruction of the flow structure takes place on the external boundary of the viscous sub layer in the non-uniform near wall turbulence during the turbulent or mixed flow types. The substantial vorticity created on the wall develops in to distinct longitudinal vortices that later are drifted away from the near wall sub layer and carry the momentum to the external area [31]. In statistic models [32], with a help of which physical processes are described in the developed turbulent motion, is supposed that such a flow is originated by the hazardously changing set of vortices (i.e. disturbances, non uniformities or in other words the vortex elements), which sizes change in wide range. The sizes of the largest vortices by an order of the magnitude are equal to the size of the region occupied by the turbulent flow, the sizes of the smallest vortices are equal to the size of the region where transversally can be effectively realized the momentum transport under the molecular viscosity that leads to smoothing of the velocity gradients.

In references [33, 34] some questions connected with the viscous gas flow around the plasma sheet created by the sliding discharge are considered. The plasma sheet influence on the gas flow character along the surface and on the viscosity coefficient with respect to the gas ionization level in the plasma layer was considered in [33]. The questions connected with the sliding discharge development dynamics on the surface of the dielectric plate in the viscous flow were considered in [34]. The obtained results show that the plasma layer is formed over the flown around plate surface after the discharge termination. It has typical distributions of the temperature and the charge carriers over the boundary layer cross section, see Fig.1. In **Fig 3.6** one can see the temperature distribution T_0 and the charge concentration n_{eI} over the boundary layer cross section at the moment t_O immediately after energy release processes finishing in the sliding discharge [4].

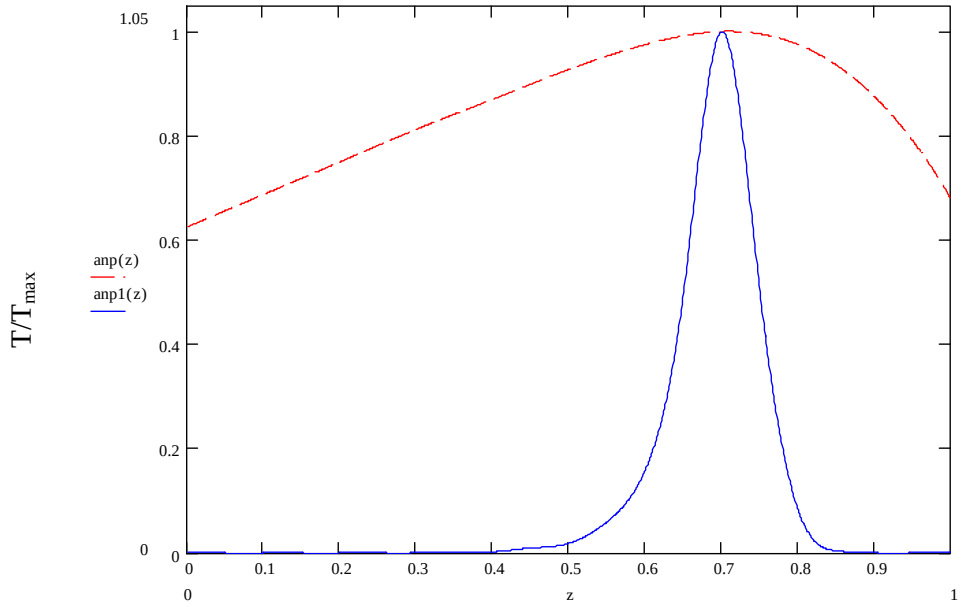

Fig.3.6. Normalized temperature T_0 (dashed curve) and the charge concentration (solid curve) distributions over the boundary layer cross section. (T_{max}=2700 K, $n_{e\,max}=5*10^{10}$ cm^{-3}).

For determination of the plasma region influence on the vortical structures the question about the scale of the smallest vortical formations with respect to Debye screening radius and the free path length of molecules becomes important. In this case it is necessary to account the molecular motion when the scale characterizing the fluid motion becomes very small. Some minimum size of the vortical formations was discovered in the turbulent flows. For example in the case of the flow in the cylindrical tube (Reynolds number Re~10^6, tube diameter Ø = 10 mm) the minimum diameter of the vortices was about 10^{-4} mm. At the same conditions the molecule free path length is of the order 10^{-5} mm in the gas flow. It follows from here that the mean molecule free path length is smaller than the size of vortices in the turbulent flows and this allows us to use the model of the continuous me um [2]. If one considers the vortex as the vortical tube, see **Fig.3.7**, and the value of the angular veloci **w** to bring in correspondence with the frequency and the v tex period to determine as $\mathbf{T_B = 2\,\pi/w}$, that it is possible to speak about the spectrum of the turbulent flow. The spectrum width can reach 10 kHz and more. If the ratio $\tau_v \sim T_v$ is realized (where τ_v – is the time constant characterizing the vortex evolution) then any vortex disappears after several turns. The vortex lifetime is comparable with the period of its rotation. Such a wide range of the vortices sizes variation is conditioned by the mechanism of the vortical tubes stretching. At that the vortices of approximately the same size are consequently transforms to the vortices of the next order of smallness. This process has a cascade character. Sizes of vortices sequentially decrease and the energy of the main flow is transported to the motion of smaller scales. The minimum size is reached when the vortices energy is scattered under the direct action of viscous tensions. Usually it is

considered that vortices of substantially different sizes do not influence directly each other. Vortices of comparable sizes can exchange energy. It was established that the viscosity weakly influence the motion and structure of the main turbulent flow. However its influence becomes decisive at the final stage of the turbulence energy dissipation, when velocity gradients in small vortices under the action of the viscous tensions [32].

Let us consider that the plasma area exists in conditions of the ambipolar diffusion mode after the end of processes accompanying the sliding discharge development. There is a vortex in the plasma layer that is characterized by the angular velocity w and by the radius R_v (see **Fig.3.7)**.

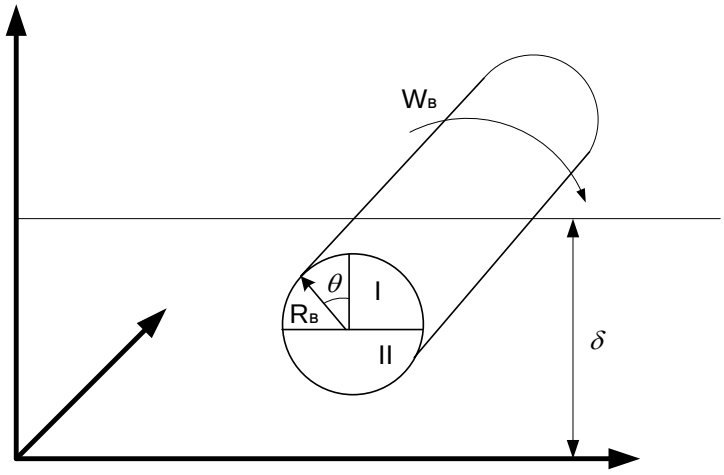

Fig.3.7. The scheme of the vortex location in the plasma layer of δ thickness.

Let us assume that the distribution of the charge carriers concentration on the cylinder of the unit length and of radius R_v in the time moment t_0 corresponds to the charge carriers concentration in the layer. The diffusion flow of charges in the one dimension case is directed normally to the wall, see **Fig.3.7** (against to the concentration gradient). The cylinder rotates in the direction indicated in the figure. Let us consider that the cylinder rotates as a single whole. Regions inside the cylinder (with low concentrations of carriers) will be brought to the area outside the cylinder (with higher concentration of carriers) at the cylinder rotation. The diffusion of carriers will take place from the region outside the cylinder to the area with the low concentration of carriers (inside the cylinder). The depth of charges penetration will be determined by the velocity of the cylinder rotation, electron diffusion velocity, the velocity of charges at the ambipolar diffusion and by the charges concentration gradient in the external area and the area inside the cylinder.

The accumulation of charges on the surface of the rotating cylinder takes place in the result of the diffusion, which is conditioned by the difference of charges in the external layer (with respect to the cylinder) and in the surface layer of the cylinder.

Let us estimate the charge value. This value is determined by the ratio of the linear velocity of the area located on the surface of the rotating cylinder ($u_л$) and the diffusion velocity of electrons (u_e), ions (u_i) and the charges velocity at the ambipolar diffusion (u_a). Electrons in the case of the fulfillment of the condition $u_e > u_л > u_a ; u_i$, (it means that the linear velocity is larger than the diffusion velocity of ions and the ambipolar diffusion velocity, but smaller than the diffusion velocity of electrons) will have time to penetrate to the area with low concentration at the turn of the cylinder and ions will practically stay at their places.

Let us determine the electric field value, the velocity of electrons and ions and their distribution in the plasma layer following the approach [35]. The directed velocity of charged particles is determined by the gradient of the concentration and temperature. For electrons it is much larger than for ions. Going of the charged particles to the wall and to the external area conditions the appearance of the volume charge sufficient for the transversal electric field E_A creation. This field leads to leveling the flows of electrons and ions, and the quasi-stationary state establishes in the plasma or the mode of the ambipolar diffusion. The equation determining the ordered motion of the charged particles has the follows form when it is possible to disregard the viscosity and in the absence of the magnetic field:

$$m_a (\partial u_a/\partial t) = Z_a eE - (1/n) \partial nT_a/\partial x + m_a \delta u_a/\delta t, \quad (3.4.1)$$

here - m_a is the mass of the particle (electron or ion);

n_a – concentration of neutral particles;

u_a – velocity;

Z_a = –1 for the electron and +1 for the ion;

$m\delta u/\delta t$ – the collision term accounting the friction of the charged particles on neutrals.

In conditions that:

1. the collision frequency of electrons and ions with neutrals is much higher than their collision frequency with each other: $\nu_{en} » \nu_{ee,} , \nu_{ei,} ; \nu_{in} » \nu_{ii} , (m_e /m_i) \nu_{ei}$;
2. the collision term of the equation in the low ionized plasma includes only the additives conditioned by the collisions of charged particles with the neutrals. For determination of the particles ordered velocity we will use the stationary solution of the equation (1). It is true in the case of the condition $\tau\nu_{an} »1$, when the typical time of the plasma parameters variation τ is much larger than the time between the collisions.

$$u_a = (e Z_a / \mu_a \nu_{an})E - D_a (dn_a/dx)/ n_a \quad (3.4.2)$$

here $D_a = T_a / (\mu_a \nu_{an})$ – is the diffusion coefficient of particles of the sort a (a=e;i) , ($T_e = T_i$),
$D_{at} = T_a / (\mu_a \nu_{an})$ - is the thermal diffusion coefficient of particles of the sort "a",

$\mu_{aa} \nu_{an} u_a$ - is the collision term (for the case when the collision frequency does not depend on velocity).

μ_{aa} - is the reduced mass (for electrons it is = m_e , and for ions = $m_i /2$).

The first term in the right hand side of the equation (2) describes the carriers motion under the electric field E. The second term determines the diffusion caused by the non uniformity of charged particle concentration. In [34] one can see the results of the temperature distribution calculations over the boundary layer cross section. From them follows that (grad n)/n >> (grad T)/T and the thermal diffusion is inessential, see Fig.1.

At this condition the equation for the ordered diffusion velocity of particles of the sort a has the form

$$u_a = – D_a (\text{grad } n)/n \qquad (3.4.3)$$

Let us additionally assume that the main mechanism of the charges elimination is connected with their recombination at the wall and in the external layer. In this case for conservation of the quasi stationarity it is necessary to have the variation of electron and ion concentrations equal in each element of the volume. The condition of the quasi stationarity undertaking reduces to the equality of the flows divergences:

$$\text{div} (n_e u_e) = \text{div} (n_i u_i). \qquad (3.4.4)$$

This equation in the one-dimensional case is equal to the equality of the ordered velocities of electrons and ions

$$u_e = u_i$$

At the existence of the volume charge in the central region under the action of the charge electric field the directed velocities of electrons and ions can be represented in the form:

$$u_e = u_a - b_e E_0 , \quad u_i = u_a - b_i E_{0,}$$

here b_e , $b_{i,}$ - are the mobilities of the electrons and ions ($b_a = e / \mu_a \nu_{an}$, e- is electron charge). b_i - $e/\mu_i \nu_{in}$ is the ion mobility, ν_{aH} - is the collision frequency of charges with neutrals.
The collision frequency of electrons with neutrals can be determined as [36]

$$\nu_{en} = 9 \times 10^9 P_0, \text{ s}^{-1}$$

where P_0 – is air pressure in Torrs.

At that the condition (4) leads to the equality

$$\text{div}[n (b_e + b_i) E_0] = 0$$

The ordered velocity of electrons and ions in this case can be expressed in the form

$$u_e = -D_e (\text{grad } n)/n - b_e E_0 ;$$

$$u_i = -D_i (\text{grad } n)/n - b_i E_0 .$$

Equating these velocities we obtain the ambipolar electric field, which is automatically formed in the plasma for leveling of flows of differently charged particles:

$$E_a = (D_i - D_e)/(b_e + b_i) \ (\text{grad } n)/n \qquad (3.4.5)$$

Or accounting that $D_e \gg D_i$, $b_e \gg b_i$ and $D_a / b_a = T_a / e$ one can accept

$$E_a \approx - (D_e / b_e) \ (\text{grad } n)/n = (T_a / e) \ (\text{grad } n)/n. \qquad (3.4.6)$$

If we know the electric field strength then it is possible to determine the ordered velocity of the ambipolar motion of the charged particles:

$$u_e = u_i = - D_a(\text{grad } n)/n , \qquad (3.4.7)$$

$$D_a = (D_e b_i + D_i b_e)/ (b_i + b_e),$$

where D_a - is the coefficient of the ambipolar diffusion.

Since $D_e \gg D_i$, $b_e \gg b_i$ and $D_a / b_a = T_a/e$ then, $D_a \approx D_i + D_e b_i / b_e$

or $D_a \approx D_i + T_e/ T_i$. So, $D_i < D_a < D_e$.

Expressions for the ambipolar velocity and the ambipolar electric field strength can be expressed in the following form in conditions when the collision frequencies do not depend on velocity

$$u_a = - (\text{grad } (D_a n))/n = -\text{grad}(n(T_e + T_i))/n \ \mu_{ia} \nu_{ia};$$

$$E_a = - \text{grad } (n T_e))/ en.$$

Represented equations for the directed velocity of the charged particles and the electric field allow to obtain the equation for the charge carriers distribution in the plasma layer.

From the equation of the particle balance (1) at the indicate above conditions one has

$$\partial n_a/\partial t + \text{div } (n_a u_a)= \delta u/\delta t.$$

Assuming that the collision frequencies of electrons and ions with atoms do not depend on the velocity and the relative temperature gradients are much smaller than the relative gradients of charged particles concentrations one obtains the following balance equation:

$$\partial n/\partial t - D_a \Delta n = \delta u/\delta t.$$

At boundaries of the plasma region the concentration of charges is equal to zero, the electron and the ion temperatures are constant, and the balance of particles is determined by the process of the direct ionization. The collision term $\delta u/\delta t = \nu^I n$ determines the efficiency of ionization and recombination processes. For the stationary case ($\partial n/\partial t = 0$), we get

$$D_a \Delta n + \nu^I n = 0,$$

where $\nu^I = \langle n_a s^i_{eH} u \rangle$ - is the mean ionization frequency determinate by the electron distribution function over the energy, s^i_{eH} - is the cross section of inelastic collisions.

In the case when the electron distribution function does not depend on the concentration the equation proves to be linear. The partial solution of at the given above initial and boundary conditions is the function:

$$n = n_0 \cos\left(\sqrt{\frac{\nu^I}{D_a}} \cdot x\right), \qquad (3.4.8)$$

where n_0 – is the concentration of charges in the central region.

The concentration equals to zero at the boundary at $x = \delta/2$ (δ – is the boundary layer width), when the cosine argument equals to zero. From here one finds

$[(\nu^I / D_a)\delta/2)]^{1/2} = \pi/2.$

The condition of stationarity of the concentration is the equality of velocities of appearance of charged particles and their diffusion leaving of the plasma region in the form:

$$\nu^I = D_a \pi^2 / \delta^2.$$

The penetration length of electrons $l = u_e t$ (t is determined by the rotational velocity of the cylinder) to the area with the lower concentration of charges does not exceed the Debye radius, or $l \approx R_D$.

So if to consider the vortex as the unit whole in the form of the cylinder of the unit length then it could be considered as the rotating dipole. The dipole moment is determined by the charge carriers density in the plasma layer and the cylinder radius. The cylinder of the unit length with the surface discharge density $g \sim \cos\Theta$ in the field E has the dipole moment P equal to [37]

$$P = E_a R^2{}_v / 2 ,$$

where – R_v is the vortex radius.

The dipole with this moment rotates in the ambipolar field E_a. The maximum value of the dipole moment is reached for the vortex, which radius corresponds to the value R_v at w=0. With the increase of the radius and velocity the value of the dipole moment of the vortex of the given radius drops.

The value of the surface charge can be determined from the equation:

$$g = en_0(\pi/2)wR_v L\left[\left(\int_0^{T/2} \sin wt\,dt\right)\times\left(\int_0^{T/2}(u_e \pm wR_v \cos wt)dt\right)\times\left(\int_0^{T/2} \sin\left(\frac{\pi}{2}\sin wt\right)\cos wt\,dt\right)\right]$$

Here under the sign of the first integral stands the value determining the law of the area variation crossed by the diffusion flow at the selected direction of charges motion and rotation of the vortex of L length (it changes during the motion as $S=LR_w\cos(wt)$). Under the sign of the second integral stands the value determining the law of the linear velocity of electrons variation and determining the penetration depth (velocities of charges motion in the first and second quarters of the cylinder

are respectively equal to: u_{ei}^{I}, $u_{ei}^{II}= (u_e \pm wR_v\cos(wt))$. Under the sign of the third integral stands the value determining the law of the charges density variation at the vortex rotation (variation of the charge density at the vortex rotation for the distribution $\Delta n= n_0\sin(wt)\ \cos\{(\pi/2)\sin(wt)\}$. The integration takes place from some initial time moment t=0 till the time moment equal to the half of the vortex rotation period.

From here one can determine the surface density of charges on the cylinder of R_v radius and the dipole moment, see **Fig.3.8**. In **Fig.3.8** are represented results of calculations of the form of the distribution of the surface charge in the upper half plane at the vortex rotation with the angular velocity w_v and the dependence of the variation of the charge value via w_v .

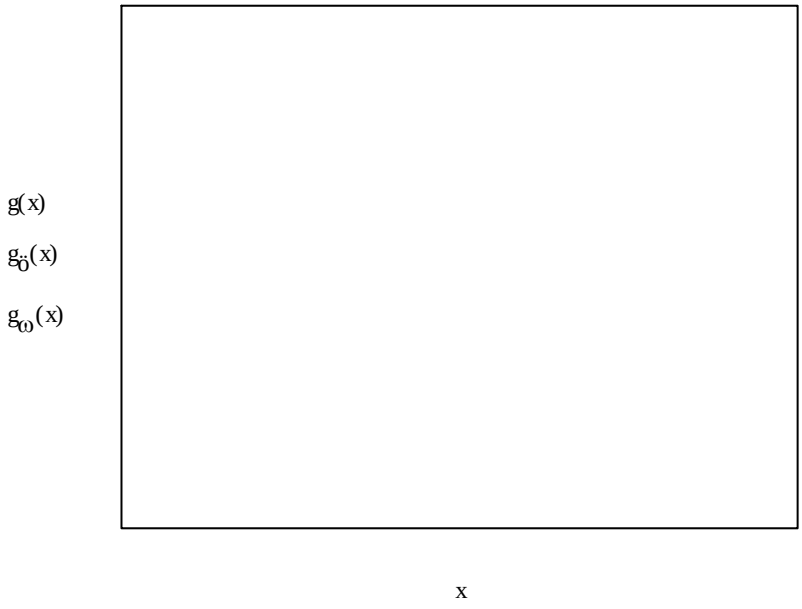

Fig.3.8. The solid line corresponds to the surface charge density distribution with respect to the angle at $R = R_B$, $w = w_B$; the dashed line corresponds to the dependence of the charge value variation via w_v, the dotted line – is the distribution of the surface charge density of $\cos\theta$ type.

So the stable charge distribution forming the dipole is created due to the energy of the rotating vortex.

Let us estimate the energy losses of the vortex with the dipole moment P, rotating in the field E_a. The value of the kinetic energy losses of the rotating disc W_k in the case when it is possible to disregard the viscous friction is determined by the energy losses at the dipole rotation in the constant field E_a. The energy losses W at the dipole rotation in the uniform electric field during the single turn are equal

$$W_p = 4PE_a$$

The temporary dependence of the energy value variation of the vortex rotating with the angular velocity w and radius R_v at the given value of the dipole moment P is represented in **Fig .3.9**.

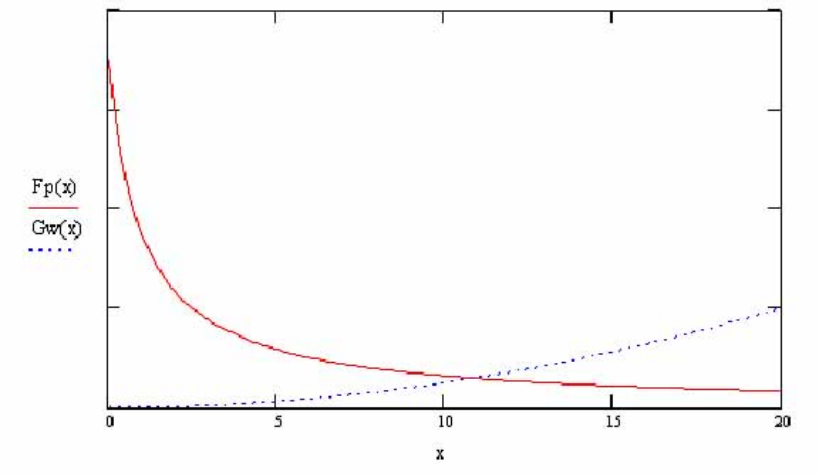

Fig.3.9. Energy value variation dependence W_k via w (pointed curve) and the dipole energy (solid curve) at the given R_v. Frequency along the x axis is in Hz.

§3.5.Turbulent disturbances spectrum at tangential break formation in a boundary layer at sliding discharge initiation in a gas flow

Processes dynamics arising at the slide discharge initiation on a surface of a dielectric plate streamlined by a gas flow was discussed in references [1-4, 37,38,39]. There is also an interest in consideration of a flow character at the boundary between a cold gas and low temperature plasma layer (which is a hot gas) created by the sliding discharge in the boundary layer on a plate surface. Instantaneous equalization of electron and neutral temperatures takes place during energy release process in the sliding discharge. A time of temperatures equalization can be estimated as [39]

$$T_{pl} \sim \tau_{en} \approx M/(2\nu_{en} m_e) ,$$

here m_e is the electron mass, M is a mass of neutrals, ν_{en} -is collision frequency between electrons and neutrals ($\nu_{en} = 4\ 10^9\ (P_o)^{1/2}\ s^{-1}$, here P_o is a gas pressure in Torr [35]).

$\tau_{pl} \sim 10^{-8}$ s at a gas pressure ~ 1 atm and temperature $T_{pl} \approx 3000$ K [4]. An establishing time of the gas motion in the boundary layer at the temperature corresponding to T_{pl} is determined by the plasma layer width $\delta_{pl} \approx \delta_{cold}$ (here δ_{cold} is the boundary layer width on a plate surface in a flow of the cold gas) and by thermal velocity of the gas molecules V_T

$$\tau_{est} \sim \delta_{pl}/V_T.$$

The establishing time is $\tau_{est} \approx 6\ 10^{-7}$ s (at $\delta_{pl} \sim 1$ mm and $V_T \approx 1500$ m/s).

At that the character of motion in the plasma layer is determined by a viscosity (with the coefficient $\acute{\eta}_T$) corresponding to T_{pl}. It is known that a viscosity rises with rising of the temperature. The viscosity coefficient $\acute{\eta}$ variation dependence on temperature, at consideration of collision cross

section S(v) as independent of velocity in our temperature range (S(v) =const), one can represent in the form

$$\acute{\eta}_T = \text{const}(T)^{1/2} \qquad (3.5.1)$$

The boundary layer width in some cross section x in a gas with the viscosity corresponding to the temperature T_{pl} can be defined with a help of the following equation [36]

$$\delta = C\,(x\ \acute{\eta}_T / V_\infty)^{1/2}, \qquad (3.5.2)$$

here V_∞ - is velocity of the incident flow, C = Const

So the boundary layer width for the gas with the viscosity coefficient $\acute{\eta}_T$ rises in the given cross section as

$$\delta_{pl} = \text{const}\ (T)^{1/4} \qquad (3.5.3)$$

The sliding discharge initiated in the boundary layer on a plate surface streamlined by by a gas flow l boundary of which co l flow or it is inside the ned during the time period τ_{est}. Respectively a new thickness of the boundary layer δ_T and a new velocity distribution over the boundary layer cross section has to correspond to this viscosity value at the given velocity of the incident flow V_∞. As a result the gas velocity inside the high temperature layer drops down sharply during τ_{est}, and the cold gas velocity stays the same equal to V_∞ on the external boundary, see Fig. 3.10.

Fig.3.10. A scheme of the cold gas boundary layer location ($\delta_{pl} = \delta_{cold}$) – high temperature layer and δ_{hot} is the boundary layer of the hot gas (at the condition that the plate is streamlined by the hot gas with the velocity $V = V_\infty$).

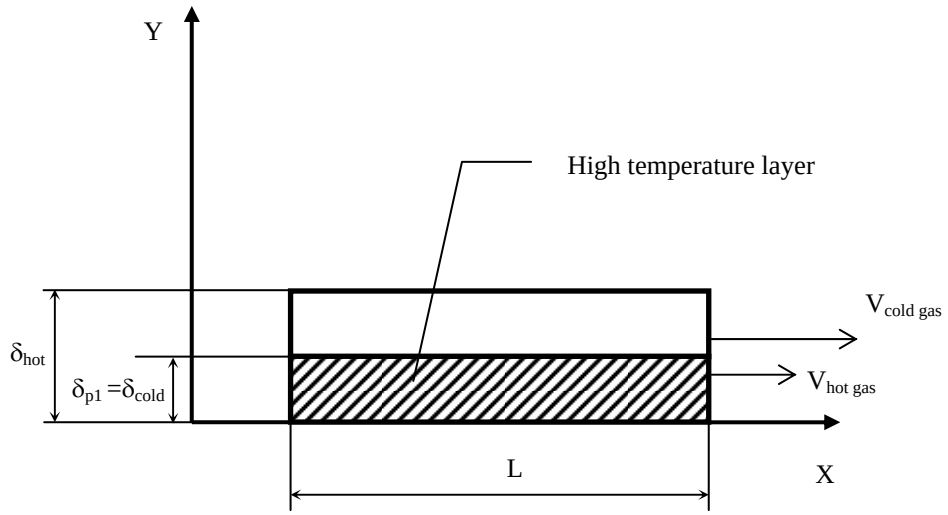

Thus the tangential break is formed at the boundary of cold and hot layers in which the gas velocity has a jump.

Later this boundary spreads with typical time defined by the flow velocity at the external boundary and by diffusion in the flow. We consider this boundary sharp for following estimates.

Let us determine the velocity variation scale on the division boundary. For the given boundary layer δ_{cold} cross section there is a graph in [36] of the velocity variation at the viscosity coefficient ή corresponding to the cold gas. Let us use the same graph for determination of the flow velocity at the boundary between the hot and the cold regions, the velocity distribution of the gas with the viscosity $ή_T$ can be obtained by the scale variation over the abscissa axis.

Let us determine δ_{pl} for determination of the velocity jump at the same gas temperature as in [39]. One can from (4) at T_{pl} = 3000 K that δ_{pl} rose by ~ 1.8 times, has by this value rises the scale over the abscissa axis in the graph of Fig.3.11.

The velocity value on the hot gas external boundary is $V_y \approx 0.82\ V_\infty$ (at $y = \delta_{cold}$). So the tangential break is formed at the separation boundary of the cold and the hot gases, at that the velocity jump value is $\approx 0.2V_\infty$. The formation of the tangential break takes place during the time $\sim \tau_{est}$ small compared with typical times of flow (streamlining the plate) characteristics variation, ($V_\infty/L \sim 10^{-3}$ s).

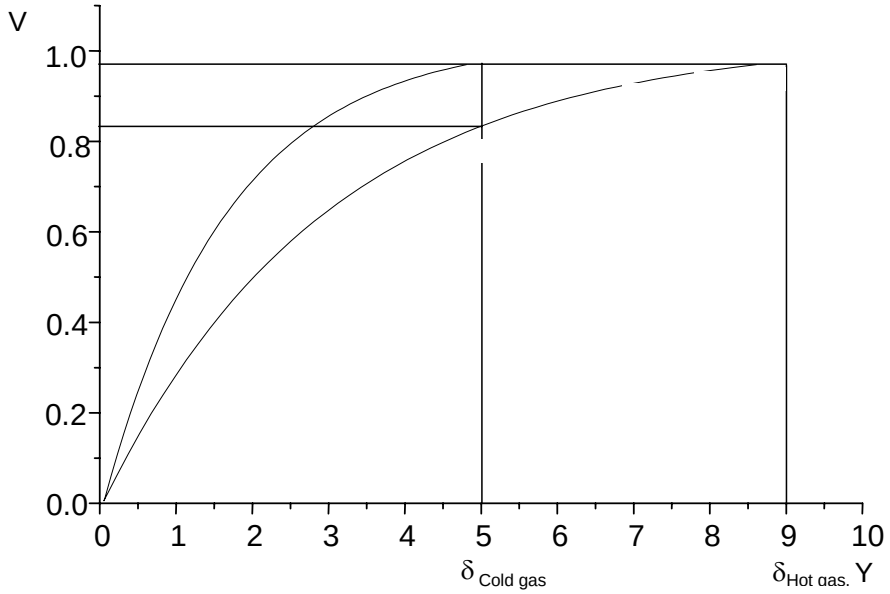

Fig. 3.11. Flow velocity variation over the boundary layer cross section of the cold gas –continuous line, flow velocity variation over the boundary layer cross section of the hot gas –dashed-dotted line

.

Let us represent the velocity variation at the division boundary in a form of some function of time as in [42]

$$V(t) = V_b \quad \text{at} \quad t > 0 \qquad (3.5.4)$$

$$V(t) = 0 \quad \text{at} \quad t < 0$$

Spectral density absolute value of the function V(t) at that is given by an expression

$$S(w) = V_b\,(1/w) \qquad (3.5.5)$$

In our case V(t) spectrum of frequencies is limited from below by the frequency $w_0 \approx V_b/L$, where V_b is the flow average velocity at the separation boundary, and L is the plasma layer length (see. Fig.1). The scale of the disturbance is limited by the boundary layer width δ_{pl} in the area of high frequencies, so $w_{max} \approx V_b/\delta_{pl}$. Let us consider that the velocity distribution on the separation boundary can be presented in a form of periodical functions row. Since the envelop of the continuous spectrum (the absolute value of the spectral density) of the non periodical function and the envelop of the linear spectrum of the periodical function (obtained from the non periodical one by its continuation with a period T) coincide by their forms and differ only by their scales [41]. Then the first harmonic amplitude is $A_1 \sim V_b$, and amplitudes of consequent harmonics will fall as 1/n (here n = 1,2,3,4…..k). Let us determine the disturbances spectrum envelope at the plasma area down the flow considering the separation boundary of the cold and of the hot gases to be the flat one, the flow velocity at the boundary from the hot gas side to be $V_{hot\ gas} = 0$, the flow velocity at the boundary from the cold gas side to be $V_{cold\ gas} = V_b$ and representing the velocity jump at the boundary in the form of periodic functions row as

$$V_n = A_n e^{\,i(k_n x - w_n t)}, \qquad (3.5.6)$$

here k_n – is a wave number.

Let us consider the gain factor of disturbances for each of harmonics to be linear on the whole extent of the gain area (the whole length of the plasma layer). The equation determining a dependence of w on k has a form [36]

$$w_n = k_n V_b\left(\rho_1 \pm i\sqrt{\rho_1\rho_2}\right)/\left(\rho_1 + \rho_2\right) \qquad (3.5.7)$$

here ρ_1,ρ_2 are densities of the cold and the hot gases respectively.

If to consider that the maximum velocity amplitude value A_n is limited by the value V_b, then inserting (7) and (6), and supposing that $\rho_1 = \rho_2$, one obtains

$$V_n = (V_{rp}/n)\, e^{\,[\pi((Vrp/\lambda_n)\ t} \qquad (3.5.8)$$

Here λ_n - is the wavelength of the harmonic w_n, and t is determined by the flow velocity V_b and by plasma layer length L ($t = L / V_b$). The maximum energy obtaining by each vibration type from the external flow will be limited by the value $\sim V^2_b$ [36]. Starting from this one can find the saturation time t_{sat}, necessary for the velocity amplitude of the given vibrations type to get the maximum value V_b.

$$V^2_n = V^2_b = (\,(V_b/n)\, e^{\,[\pi((Vb/\lambda n)\ t}\,) \qquad (3.5.9)$$

$$t_{sat} = Const\left(\sqrt{\ln(n)}\right)/n \qquad (3.5.10)$$

Inserting (10) to (8) one obtains spectrum components amplitude values at the outlet from the plasma area of the length L, see Fig.3.12. In Fig.3.12. one can see the normalized graphs of the disturbances spectrum at the outlet from the break area (t = 1), the disturbances spectrum representing the velocity jump (t = 0) and dependencies t_{sat} on w_n.

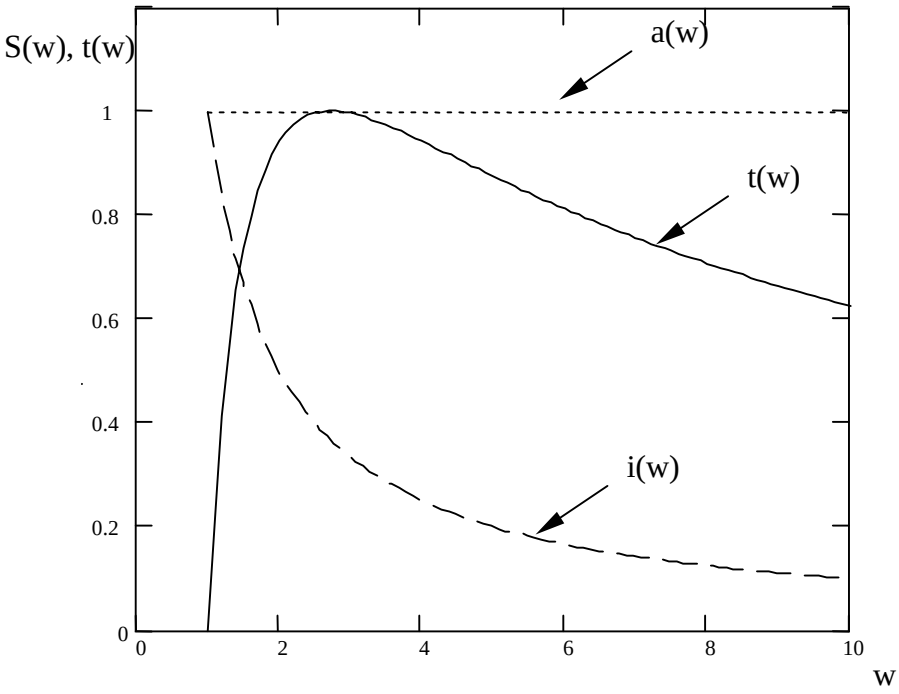

Fig.3.12.The graph of the disturbances spectrum at the outlet from the break area (t = 1) – the dashed line.
The graph of the disturbances spectrum representing the velocity jump (t = 0) – dashed-dotted line.
The graph of t_{sat} via w_n dependence - continuous line.

PART4. Numerical simulation (Task 3, Task 4)

§ 4.1. Technique of sliding discharge numerical simulation on basis of heat source model

Numerical model and codes for study of sliding discharge in supersonic flow have been developed on basis of local heat source model of discharge. Test calculations of flow over plate in the presence of steady-state and pulse-periodic heat deposition in near wall region have been performed. Effect of gas heating on skin-friction has been analyzed.

_Numerical model and codes for study of sliding discharge in supersonic flow have been developed. Discharge is simulated by near wall non-steady heat deposition. Thermally equilibrium chemically frozen gas-phase model of the heated air is used in codes. Turbulent flow is described by the Favre-averaged Navier-Stokes equations with additional source term in the energy equation. The Boussinesq approximation for the Reynolds stress tensor and two-equations $k-\omega$ turbulence model for calculation of turbulent transport coefficients are used. The adiabatic wall condition was used in calculations.

Some results of test calculations of turbulent flow over flat plate are presented. The effect of steady-state and pulse-periodic heat deposition in near wall region on skin-friction is analyzed.

Gas-phase model

Basic assumptions

1. The air is considered as an ideal one-temperature O_2 - N_2 mixture with the constant species mole fractions $X_{O2}=0.21$ and $X_{N2}=0.79$.
2. Navier-Stokes approximation is employed to calculate molecular viscous fluxes
3. Turbulent mean flow is described by Favre averaged [43] pressure p, velocity vector $\vec{u}$, and temperature T.
4. The Boussinesq approximation for the Reynolds stress tensor and Wilcox two-equations $k-\omega$ model [44] for calculation of turbulent transport coefficients are used.
5. Effect of discharge on gas flow is modeled by the local heat deposition.

State equation. The gas state equation is given by

$$p=\rho R_u T/M \qquad ,$$

where ρ is density, R_u is a universal gas constant, and M is a average molecular weight of the mixture.

Thermodynamic model. The rotational and vibrational energy modes of air molecules are described by the equilibrium "rigid rotator - harmonic oscillator" model with characteristic vibrational temperatures $T_{v,O2}$ = 2228 K and $T_{v,N2}$ = 3336 K. The internal energy per unit mass e and the heat capacity c_p are defined by expressions

$$e = \frac{5}{2}\frac{R_u}{\bar{M}}T + \frac{R_u}{\bar{M}}\sum_k \frac{T_{v,k}X_k}{\exp(T_{v,k}/T)-1}; \qquad c_p = \frac{7}{2}\frac{R_u}{\bar{M}}T + \frac{R_u}{\bar{M}}\sum_k \frac{(T_{v,k}/T)^2\exp(T_{v,k}/T)X_k}{[\exp(T_{v,k}/T)-1]^2};$$

Molecular transport model. Molecular stress tensor $\hat{\tau}_M$ (momentum fluxes tensor with reversed sign) is given by

$$\hat{\tau}_M = \mu_M \hat{\varepsilon},$$

where components of tensor of deformation rates $\hat{\varepsilon}$ are determined as

$$\varepsilon_{ij} = \frac{\partial u_i}{\partial x_j} + \frac{\partial u_j}{\partial x_i} - \frac{2}{3}\frac{\partial u_k}{\partial x_k}\delta_{ij},$$

and molecular viscosity is approximated by power law $\mu_M = a_\mu T^{0.683}$.

Heat flux $\vec{q}_M$ is given by expression

$$\vec{q}_M = -\lambda_M \frac{\partial T}{\partial \vec{r}},$$

where molecular heat conductivity is determined through μ, specific heat capacity c_p ,and molecular Prandtl number $\mathrm{Pr}_M = 0.7$

$$\lambda_M = \frac{\mu_M c_p}{\mathrm{Pr}_M}$$

Turbulent transport model. Turbulent (Reynolds) stress tensor $\hat{\tau}_T$ and turbulent heat flux $\vec{q}_T$ are expressed as

$$\hat{\tau}_T = \mu_T \hat{\varepsilon}, \quad \vec{q}_T = -\lambda_T \frac{\partial T}{\partial \vec{r}},$$

Eddy viscosity μ_T and turbulent heat conductivity λ_T are determined through turbulent mixing energy k and specific dissipation rate ω

$$\mu_T = \rho\frac{k}{\omega}, \qquad \lambda_T = \frac{\mu_T c_p}{\mathrm{Pr}_T}$$

The values of turbulent energy k and specific dissipation rate ω are defined from two differential equations:

$$\frac{\partial \rho k}{\partial t}+\frac{\partial}{\partial x_j}\left(ru_j k-(\mu_M+\sigma_T^*\mu_T)\frac{\partial k}{\partial x_j}\right)=b_k,$$

$$\frac{\partial \rho \omega}{\partial t}+\frac{\partial}{\partial x_j}\left(ru_j \omega-(\mu_M+\sigma_T\mu_T)\frac{\partial \omega}{\partial x_j}\right)=b_\omega,$$

where

$$b_k=\mu_T\hat{\varepsilon}_{ij}\frac{\partial u_i}{\partial x_j}-\beta_T^*\rho\omega k, \quad b_\omega=\gamma_T\rho\hat{\varepsilon}_{ij}\frac{\partial u_i}{\partial x_j}-\beta_T\rho\omega^2,$$

$\beta_T^*=0.09$, $\gamma_T=0.56$, $\beta_T=0.075$, $\sigma_T=0.5$, $\sigma_T^*=0.5$.

It is assumed that turbulent Prandtl number is $\mathrm{Pr}_T=1$.

Governing equations and numerical method

Governing equations. The integral form of two-dimensional governing equations in the Cartesian coordinates (x,y) for above gas-pase model are written as

$$\frac{d}{dt}\int_S \mathbf{U}dS+\int_{\delta S}\vec{n}\cdot\vec{\mathbf{F}}dl=\int_S \mathbf{\Omega}dS,$$

where S is a fixed control domain in a plane (x, y), δS is a boundary of domain , $\vec{n}=(n_x,n_y)$ is an unit outward normal to δS, U is a set of conserved variables per unit volume, $\vec{\mathbf{F}}=\vec{\mathbf{F}}^{inv}+\vec{\mathbf{F}}^{vis}$ represents a sum of the inviscid and viscous fluxes of U through the domain boundary and $\mathbf{\Omega}$ consists of the source terms. For considered gas-phase model these vectors are given by

$$\mathbf{U}=\{\rho,\rho u,\rho v,\rho e_0,\rho k,\rho\omega\}^{\mathrm{T}};$$

$$\vec{\mathbf{F}}=\begin{Bmatrix}\rho\vec{u}\\ \rho\vec{u}u+p\vec{n}n_x\\ \rho\vec{u}v+p\vec{n}n_y\\ \rho\vec{u}h_0\\ \rho\vec{u}k\\ \rho\vec{u}\omega\end{Bmatrix}+\begin{Bmatrix}0\\ -\vec{\tau}_x\\ -\vec{\tau}_y\\ \vec{q}_h-u\vec{\tau}_x-v\vec{\tau}_y\\ \vec{q}_k\\ \vec{q}_\omega\end{Bmatrix};$$

$$\mathbf{\Omega}=\{0,0,0,b_h,b_k,b_\omega\}^{\mathrm{T}}.$$

Here u,v are the components of velocity vector $\vec{u}$, $e_0=e+0.5(\vec{u}\cdot\vec{u})$ is a total energy per unit mass, $h_0=e_0+p/\rho$ is a total enthalpy, b_h is heat source power,

$$\vec{\tau}_x = (\tau_{xx}, \tau_{xy}), \quad \vec{\tau}_y = (\tau_{yx}, \tau_{yy}), \quad \hat{\tau} = \hat{\tau}_M + \hat{\tau}_T = (\mu_M + \mu_T)\hat{\varepsilon}$$

$$\vec{q}_h = \vec{q}_L + \vec{q}_T = -(\lambda_M + \lambda_T)\frac{\partial T}{\partial \vec{r}},$$

$$\vec{q}_k = -(\mu + \sigma_T^* \mu_T)\frac{\partial k}{\partial \vec{r}}, \qquad \vec{q}_\omega = -(\mu + \sigma_T^* \mu_T)\frac{\partial \omega}{\partial \vec{r}}$$

Numerical method. The governing equations are solved on the structured mesh through a finite volume approach. At this approach the finite difference equations system consists of numerical analogs of the conservation equations for the quadrilateral cells covering the computation domain and the difference approximation of the boundary conditions. This method yields an approximate solution $\mathbf{Z} = \{p, u, v, T\}$ in a center of each cell and in a center of each cell side lying on the wall. The cells are built by intersection of the two discrete curve sets. The inviscid fluxes $\mathbf{F}_G^{inv}$ through cell sides are calculated from result of the exact Riemann problem solution $\mathbf{Z}_G = \Re(\mathbf{Z}_G^L, \mathbf{Z}_G^R)$ where $\Re$ is the Riemann problem solver. The left and right interfacial values $\mathbf{Z}_G^L$ and $\mathbf{Z}_G^R$ are defined by the limited one-dimensional extrapolation of $\mathbf{Z}$ from the cell-centers to the cell sides. The numerical viscous fluxes $\mathbf{F}_G^{vis}$ through cell sides are evaluated using the central and one-sided difference formulas of the second order accuracy. For time-marching integrating of Navier-Stokes equations the implicit Runge-Kutta scheme of second order of accuracy is used. On every time step
the flowfield parameters are computed due Gauss-Seidel line relaxation numerical technique.

Test calculations.

The test calculations were performed for flow over plate with length of 50 cm and thickness of 0.02 cm at free stream Mach number M_∞ = 2.0, total pressure $p_0 = 1\text{atm}$, and total temperature $T_0 = 300K$. The non-slipped, unblown, and adiabatic wall model was used in calculations. Corresponding boundary conditions on the wall are expressed as

$$u_w = 0, \quad v_w = 0, \quad \left.\frac{\partial T}{\partial n}\right|_w = 0,$$

where n is distance along normal to plate surface. For turbulence model parameters it was assumed that

$$k_w = 0, \quad \omega_w = \frac{6\mu_{M,w}}{\rho_w \beta_T \Delta_w n},$$

where $\Delta_w n$ is n-size of first near wall cell. Values of k and ω in free stream are specified by two conditions

$$k_\infty / 0.5u_\infty^2 = 10^{-7}, \quad (\mu_T / \mu_M)_\infty = 0.03$$

The mesh 400x200 adapted to flow peculiarities was employed. The grid cells were condensed near plate surface so that in a laminar sublayer region not less than 10 grid points were placed.

Fig.4.1 shows the distribution along plate Reynolds number Re_θ calculated through momentum thickness θ and conditions on outer edge of the laminar boundary layer. The value Re_θ=300 often is used as criterion of laminar-to-turbulent transitions beginning. Fig.4.1 indicates that transition (without heat supply) begins at x ≈ 2.6 cm if this criterion to use. Fig.4.2 shows distributions of local skin-friction coefficient along plate for steady-state laminar and turbulent flow models without heat deposition. It is seen that used $k-\omega$ turbulence model also predicts laminar-to-turbulent transition that location depends from specified free stream and wall values of turbulence parameters. For considered numerical boundary conditions for k and ω transition occurs some above in interval $0.9 \le x \le 2.0\,\mathrm{cm}$.

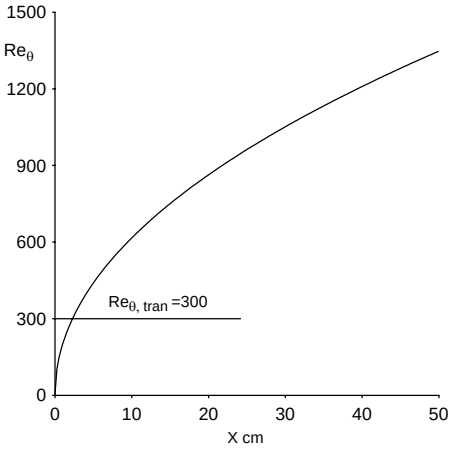

Fig.4.1. Reynolds number calculated through momentum thickness

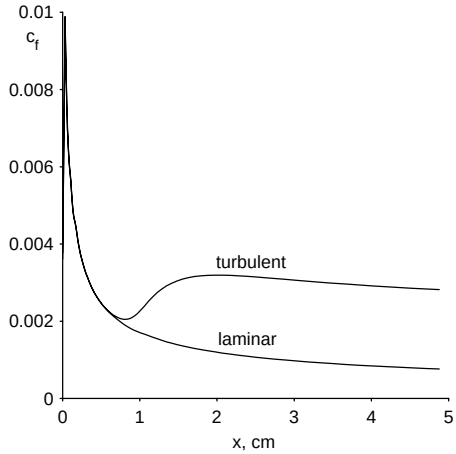

Fig.4.2. Local skin-friction for laminar and turbulent flows

The pulse-periodic heat deposition with pulse length $1\,\mu s$, frequency 100 kHz and constant power P_w= 2000 W/cm was considered. It was assumed that

heat supply is uniform into space region $10 \le x \le 20$ cm , $0 \le y \le 0.2$ cm , where x, y are distances from the plate heading and plate surface accordingly. The heat supply is started in initially steady-state turbulent stream.

Fig. 4.3 shows the predicted time distributions of total skin-friction coefficient C_f for plate section $10 \le x \le 50$ cm . The value of C_f is defined by expression

$$C_f = \int_{x_b}^{x_e} \tau_w dx / 0.5 \rho_\infty V_\infty^2 (x_e - x_b),$$

where τ_w is the local skin-friction, ρ_∞ and V_∞ are the free stream density and velocity accordingly, $x_b = 10$ cm, $x_e = 50$ cm. For comparison on this Figure coefficient C_f calculated for steady-state heat supply in the same space region with $P_w = 200\ W/cm$ is presented also. Presented data indicate that the heat supply leads to some decreasing of skin-friction. The value of C_f performs small high frequency oscillations near mean curve which approaches to the steady value of C_f. The relaxation time is about 1 ms. Time history of wall heating is shown in Fig.4.4

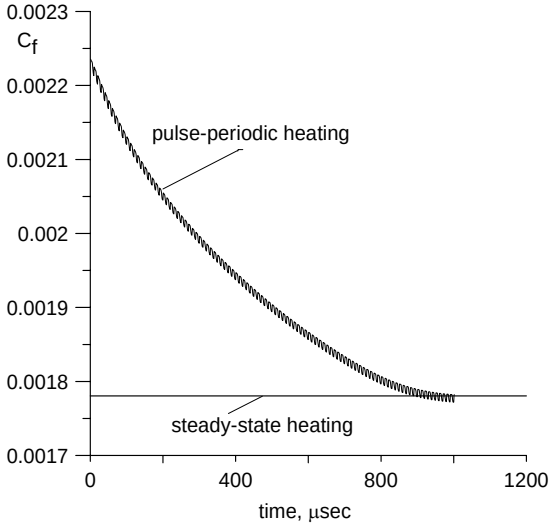

Fig.4.3. Time variation of total skin-friction coefficient

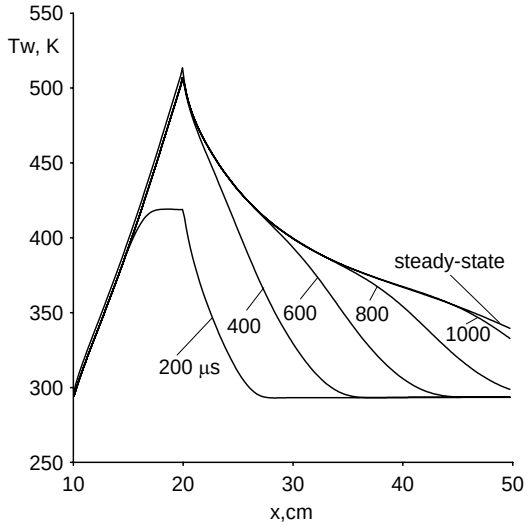

Fig.4.4. Time history of wall temperature distribution

§ 4.2. Numerical simulation of sliding discharge effects on the supersonic flow over flat plate

Calculations of flow over blunted plate length of 30 cm and thickness of 0.02 cm have been performed for free stream conditions close to planned in experiments on wind tunnel A-7: Mach number M_∞= 2.0, total pressure $p_0 = 2.4\,\text{atm}$, and total temperature $T_0 = 300K$. The pulse-periodic heat deposition modeling sliding discharge has been considered. In calculations pulse length t_p was 0.3 and $1\mu s$, forms of pulses were rectangular or triangular, pulse frequency f_p was 10 kHz, total heat supply during one impulse (cycle) Q_p= 10^{-2} J/cm. Two cases of space heat supply distribution were researched. In first case heat supply was distributed uniform into near wall space region $5 \le x \le 10\,\text{cm}$, $0 \le y \le 0.1\,\text{cm}$ where x, y are Cartesian coordinates attached to plate surface. This case heating distribution corresponds to the longitudinal sliding discharge. In the second case heat supply was distributed also uniform into space region $5 \le x \le 30\,\text{cm}$, $0 \le y \le 0.1\,\text{cm}$. This case corresponds to the transversal sliding discharge. The heat supply was started in initially steady-state turbulent stream. Parameters of considered variants of heat sources modeling gas discharges are listed in Table1.

Table1. Parameters of heat source

Case	t_p,μs	f_p, kHz	Q_p, J/cm	pulse form	space region of heat supply
1	1	10	10^{-2}	rectangular	$5 \le x \le 10\,\text{cm}$, $0 \le y \le 0.1\,\text{cm}$
2	0.3	10	10^{-2}	rectangular	$5 \le x \le 10\,\text{cm}$, $0 \le y \le 0.1\,\text{cm}$
3	1	10	10^{-2}	triangular	$5 \le x \le 10\,\text{cm}$, $0 \le y \le 0.1\,\text{cm}$
4	1	10	10^{-2}	rectangular	$5 \le x \le 30\,\text{cm}$, $0 \le y \le 0.1\,\text{cm}$

Calculations have been carried out using described in previously report [2.1] gas phase and gas-wall interactions models, and the same numerical technique.

Fig. 4.5 shows the predicted in considered cases time distributions of total skin-friction coefficient C_f for plate section $0 \le x \le 30\,\text{cm}$. The value of C_f is defined by expression

$$C_f = \int_{x_b}^{x_e} \tau_w dx / 0.5\rho_\infty V_\infty^2 (x_e - x_b),$$

where τ_w is the local skin-friction, ρ_∞ and V_∞ are the free stream density and velocity accordingly, $x_b = 0\,\text{cm}$, $x_e = 30\,\text{cm}$. For comparison on this Figure coefficients C_f calculated without heat supply and for steady heat supply in the same space region with power $P_w = 100\ W/cm$ are presented also. This value of heating power is equal to averaged through cycle power of considered pulse-periodic heat supply $Q_p f_p$.

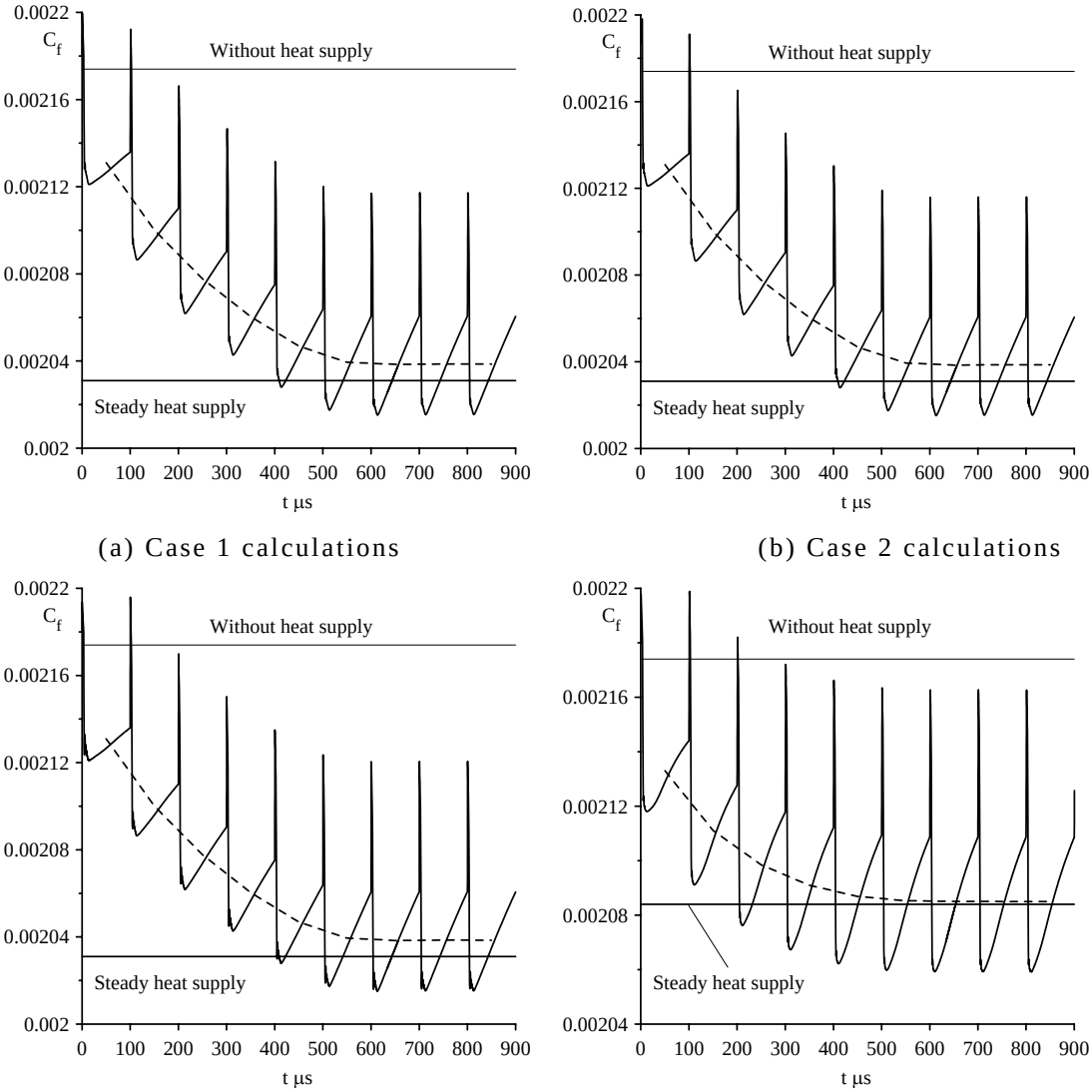

(a) Case 1 calculations

(b) Case 2 calculations

(c) Case 3 calculations

(d) Case 4 calculations

Fig.4.5. Time variation of total skin-friction coefficients

Presented data indicate that the heat supply leads to some decreasing of skin-friction. The value of C_f performs oscillations of relatively high amplitude near mean curve shown dotted line which approaches with time to the value of C_f for steady gas heating. The relaxation time for all investigated cases is about 0.6 ms.

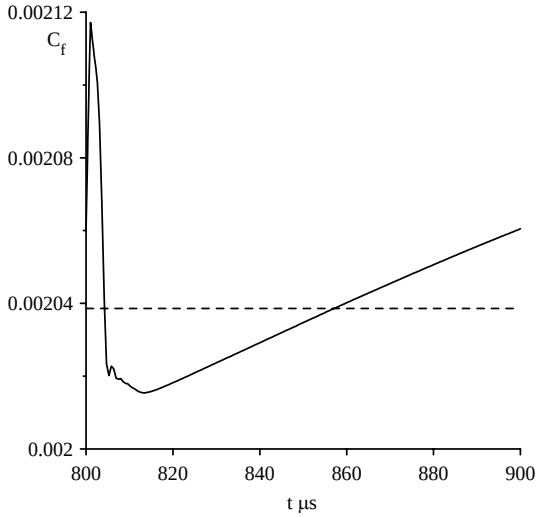

Fig. 4.6. Time variation of global skin-friction coefficient during one cycle for case 1.

Fig.4.6 shows time distribution of C_f during one cycle $800 \le t \le 900 \mu s$ for case 1. It is seen that into cycle value of C_f during heat supply fast increases further also fast decreases to bellow of cycle average level and again relatively slowly increases to above of cycle average level.

Comparison of cycle averaged global skin-friction predicted for considered cases is shown on Fig.4.7

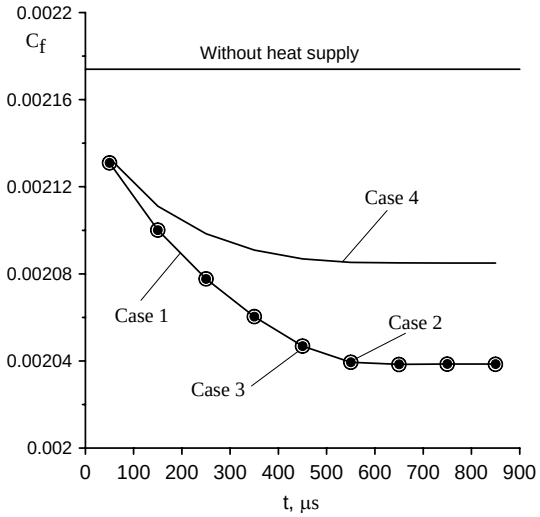

Fig.4.7. Comparison of cycle averaged global skin-friction coefficients predicted for different cases heat deposition

It is seen that results obtained for cases 1-3 practically coincide, that is, effects of pulse length and form on C_f value is negligible. For equal values of heat deposition short heat source gives larger viscous drag reduction then long heat source.

Time history of local skin-friction coefficients c_f, wall temperature and pressure distributions along plate surface are presented on Fig. 4.8- 4.10 Corresponding data for case without gas heating are shown by dotted lines.

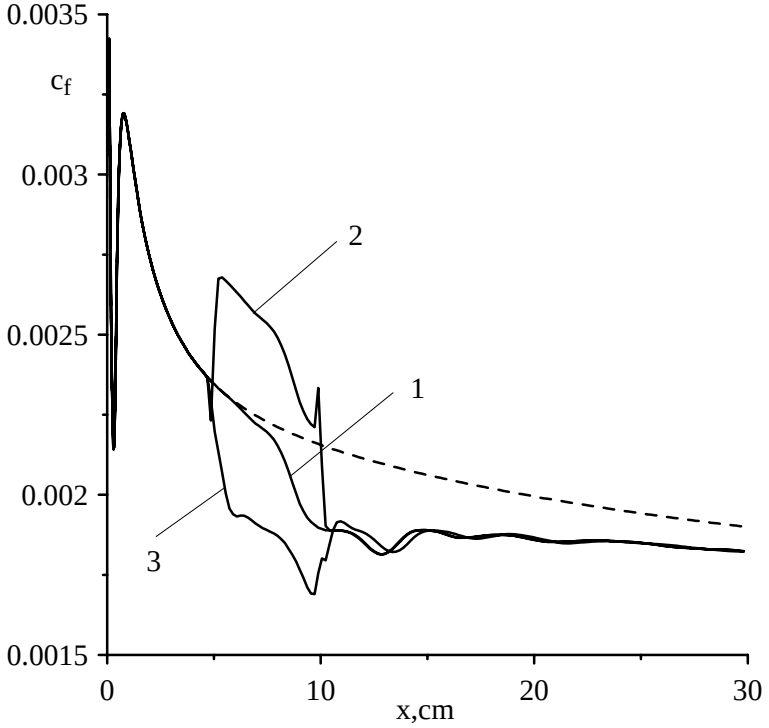

Fig.4.8. Time history of local skin-friction distribution along plate surface for case 1. 1- t = 800 μs, 2 – t = 801 μs, 3 – t = 812 μs

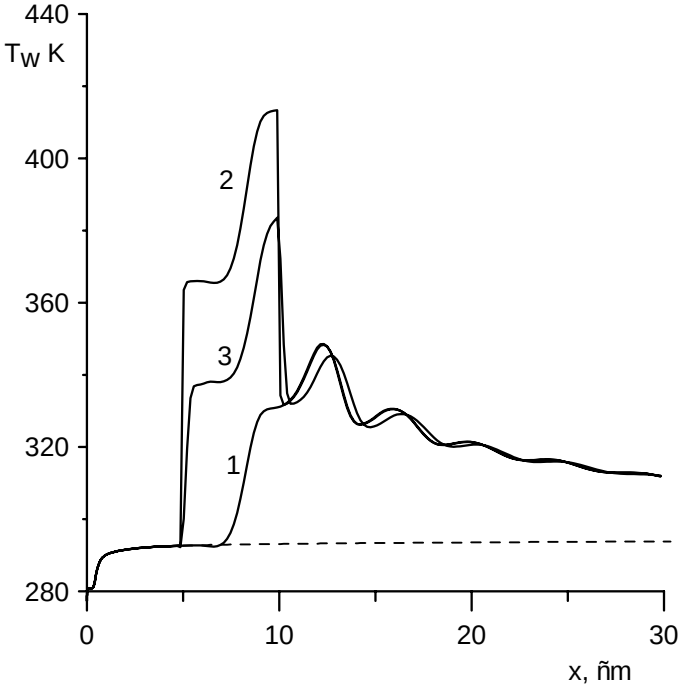

Fig. 4.9. Time history of wall temperature distribution along plate surface for case 1. Denotation as on Fig. 4.8

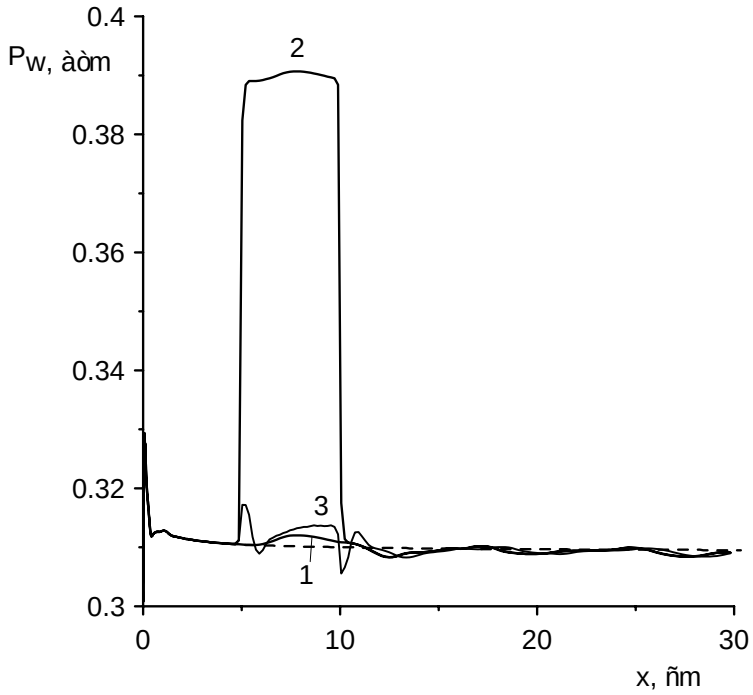

Fig. 4.10. Time history of wall pressure distribution along plate surface for case 1. Denotation as on Fig. 4.8

It is seen that heat supply produces significant local perturbations of gas flow parameters in heat supply region. Local skin-friction coefficient increases to 15%, wall pressure to 26%, and gas temperature on 120 K. After heat supply stopping skin-friction decreases to level below of one without heat supply. Wall temperature also decreases but remains above of its value without gas heating. Pressure perturbations practically damps to cycle end.

Space distributions of density, temperature and turbulent energy in the near wall region for different instants of time are displayed in Figs. 4.11-4.13

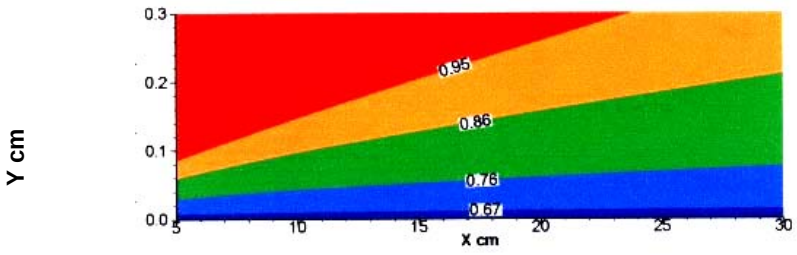

(a) Density, t = 0 μs

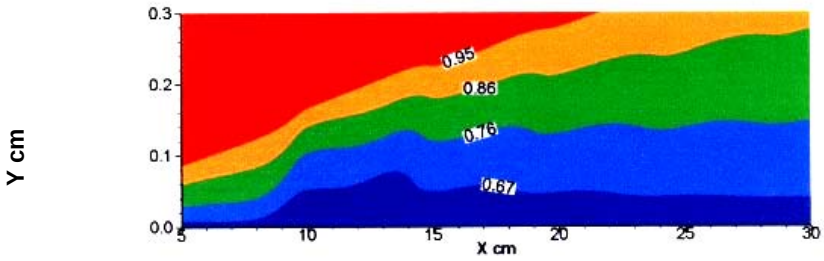

(b) Density, t = 800 μs

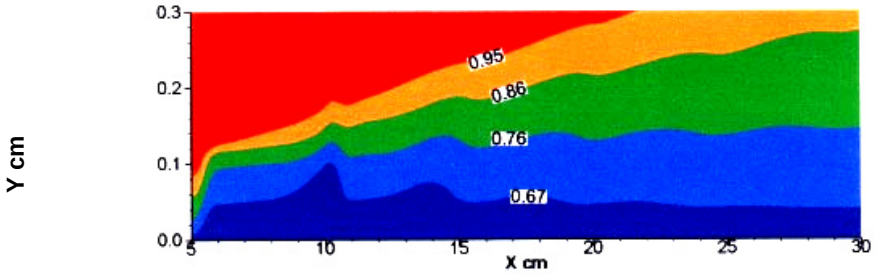

(c) Density, t = 801 μs

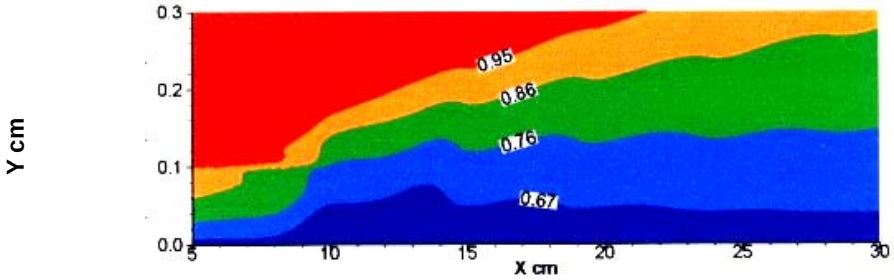

(d) Density, t = 812 μs

Fig. 4.11. Time history of ρ/ρ_∞ near wall contours for case 1

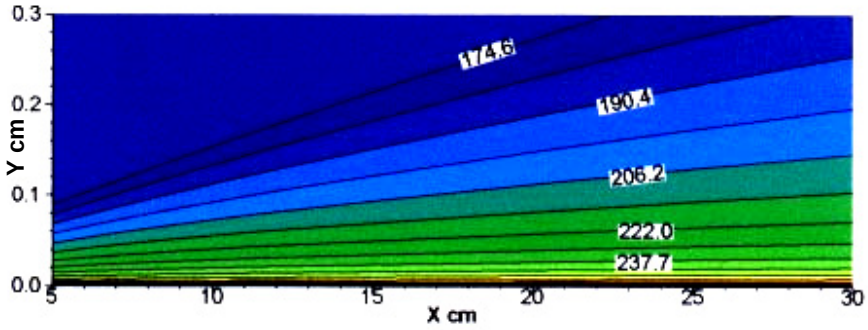

(a) Temperature, t = 0 μs

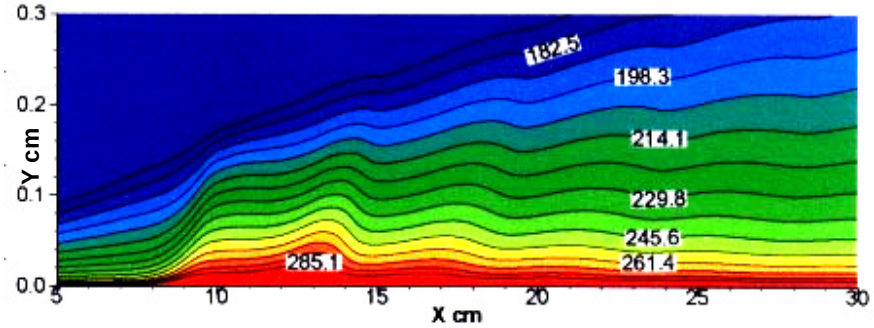

(b) Temperature, t = 800 μs

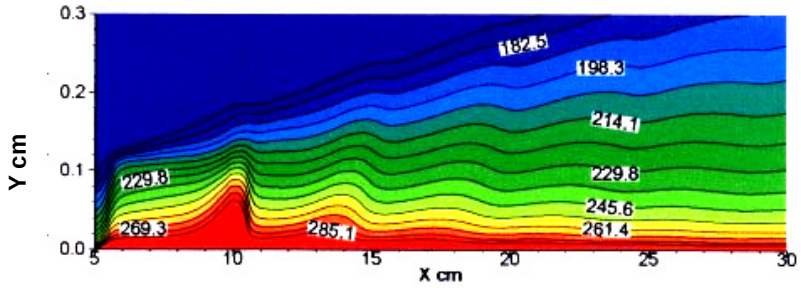

(c) Temperature, t = 801 μs

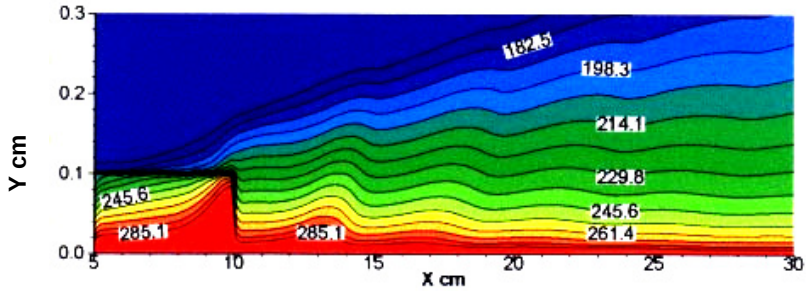

(d) Temperature, t = 812 μs

Fig. 4.12. Time history of gas temperature near wall contours for case 1

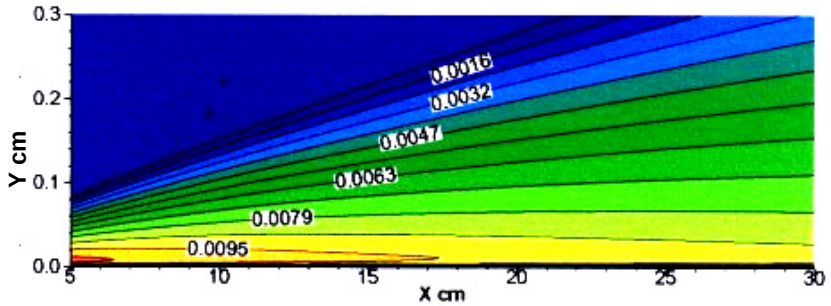

(a) Turbulent energy, t = 0

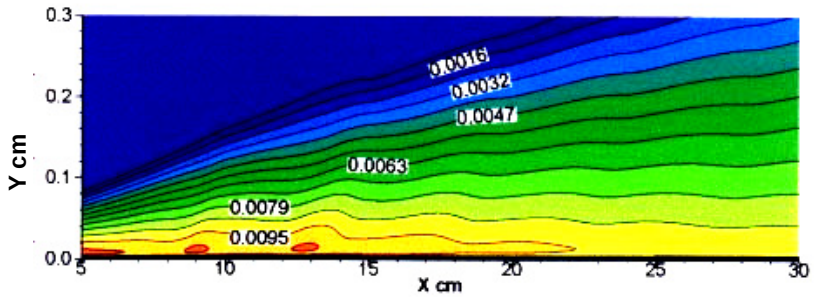

(b) Turbulent energy, t = 800 μs

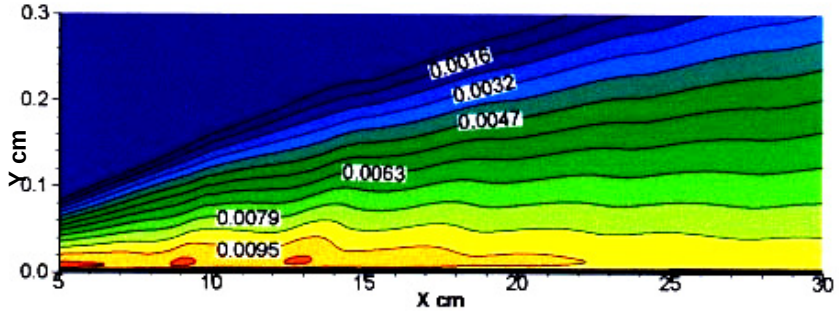

(c) Turbulent energy, t = 801 μs

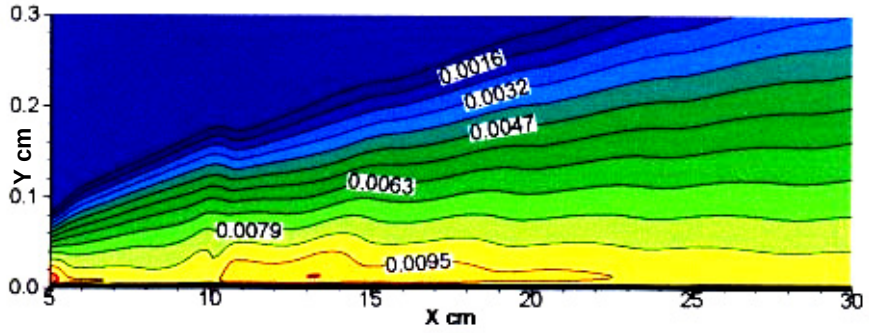

(d) Turbulent energy, t = 812 μs

Fig. 4.13. Time history of turbulent energy $k/0.5u_\infty^2$ near wall contours for case 1

§ 4.3. Numerical simulation of sliding discharge effects for Mach numbers M_∞ = 0.8, and M_∞ = 3 on trans- and supersonic flows over flat plate

Some results of parametric calculations of flow over flat plate for wind tunnel experiments conditions at Mach numbers M_∞ = 0.8, and M_∞ = 3.0 are given. The effects of heat deposition on skin-friction and near wall flow structure are studied.

Calculations of flow over blunted plate length of 30 cm and thickness of 0.02 cm have been performed for free stream conditions of planned experiments in wind tunnel A-7:

1) Mach number M_∞ = 0.8, total pressure $p_0 = 1.2$ atm, and total temperature $T_0 = 300K$;
2) Mach number M_∞ = 3.0, total pressure $p_0 = 3.7$ atm, and total temperature $T_0 = 300K$.

The pulse-periodic heat deposition modeling sliding discharge has been considered. In calculations pulse length t_p was $1\,\mu s$, form of pulses was triangular, pulse frequency f_p was 10 *kHz*, total heat supply during one impulse (cycle) $Q_p = 10^{-2}$ J/cm. Heat supply was distributed uniform into space region $5 \le x \le 10$ cm, $0 \le y \le 0.1$ cm, where x, y are Cartesian coordinates attached to plate surface. This case heating distribution corresponds to the longitudinal sliding discharge. The heat supply was started in initially steady-state turbulent stream.

Calculations have been carried out using described in previously report [2.1] gas phase and gas-wall interactions models, and the same numerical technique.

Fig.4.14 shows the predicted for M_∞ = 0.8 time distributions of total skin-friction coefficient C_f for plate section $0 \le x \le 30$ cm. The value of C_f is defined by expression

$$C_f = \int_{x_b}^{x_e} \tau_w dx / 0.5\rho_\infty V_\infty^2 (x_e - x_b),$$

where τ_w is the local skin-friction, ρ_∞ and V_∞ are the free stream density and velocity accordingly, $x_b = 0$ cm, $x_e = 30$ cm. For comparison on this Figure coefficients C_f calculated without heat supply C_f^0 and for steady heat supply C_f^{st} in the same space region with power $P_w = 100\ W/cm$ are presented also. This value of heating power is equal to averaged through cycle power of considered pulse-periodic heat supply $Q_p f_p$. Similar data predicted for M_∞ = 3.0 are shown on **Fig. 4.15**

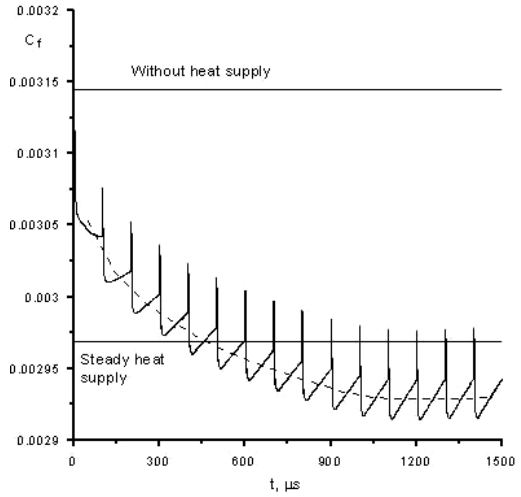

Fig.4.14. Time variation of total skin-friction coefficients for M_∞ = 0.8

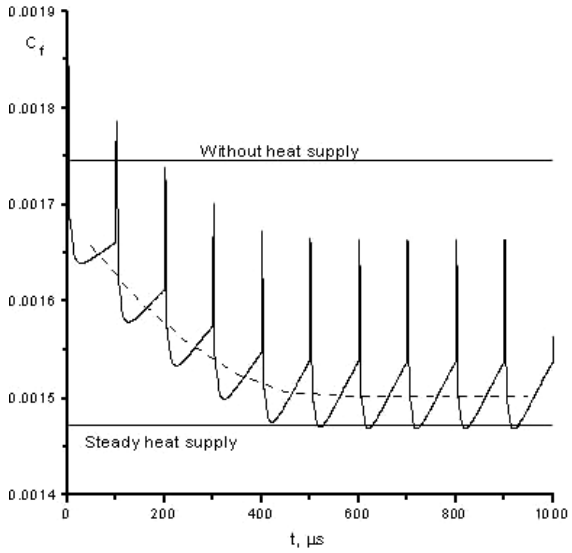

Fig.4.15. Time variation of total skin-friction coefficients for M_∞ = 3.0

Presented data indicate that the heat supply leads to decreasing of mean skin-friction. The value of C_f performs oscillations of relatively high amplitude near mean curve shown dotted line. With time averaged value of C_f approach to certain constant value $C_{f\infty}$. The relaxation time is about 1.0 ms for M_∞ = 0.8 and 0.5 ms for M_∞ = 3.0. It is seen that for M_∞ = 0.8 asymptotic value

of C_f is above of the total skin friction C_f^{st} predicted for steady gas heating, and it is below of C_f^{st} for $M_\infty = 3.0$.

Time history of local skin-friction coefficient c_f, wall temperature and pressure distributions along plate surface are presented in **Fig. 4.16 - 4.18** for $M_\infty = 0.8$ and in **Fig.4.19 - 4.21** for $M_\infty = 3.0$. Corresponding data for cases without gas heating are shown by dotted lines.

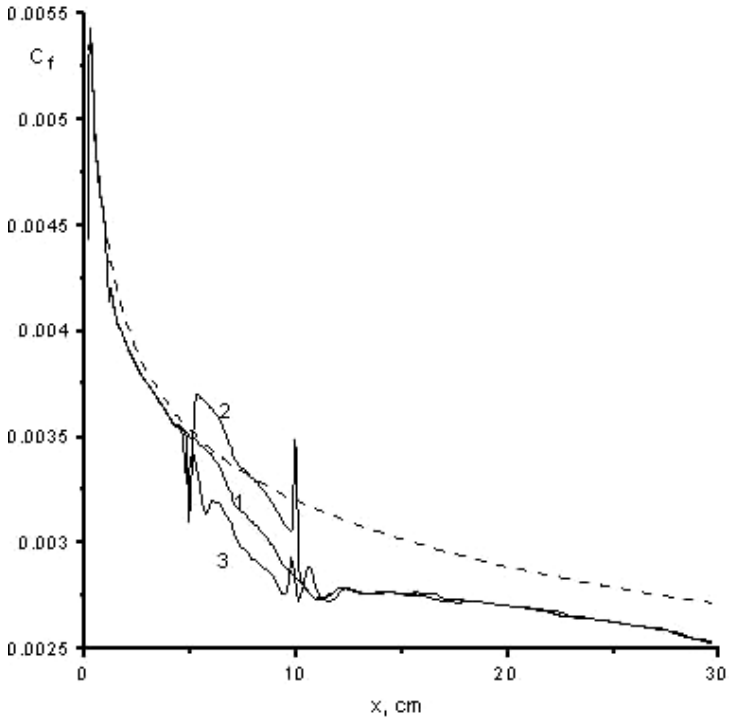

Fig.4.16. Time history of local skin-friction distribution along plate surface for $M_\infty = 0.8$.
1 t = 1200 μs, 2 – t = 1201 μs, 3 – t = 1212 μs

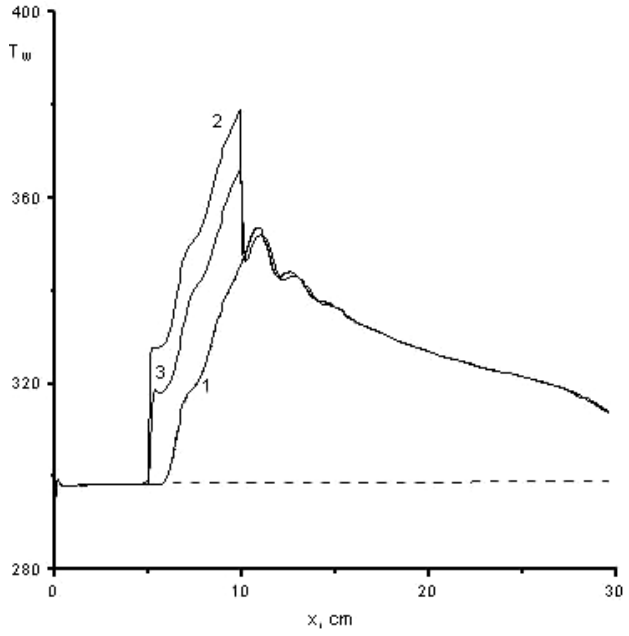

2

Fig.4.17. Time history of wall temperature T_w, K distribution along plate surface for $M_\infty = 0.8$.
Notations as on Fig. 2.3.

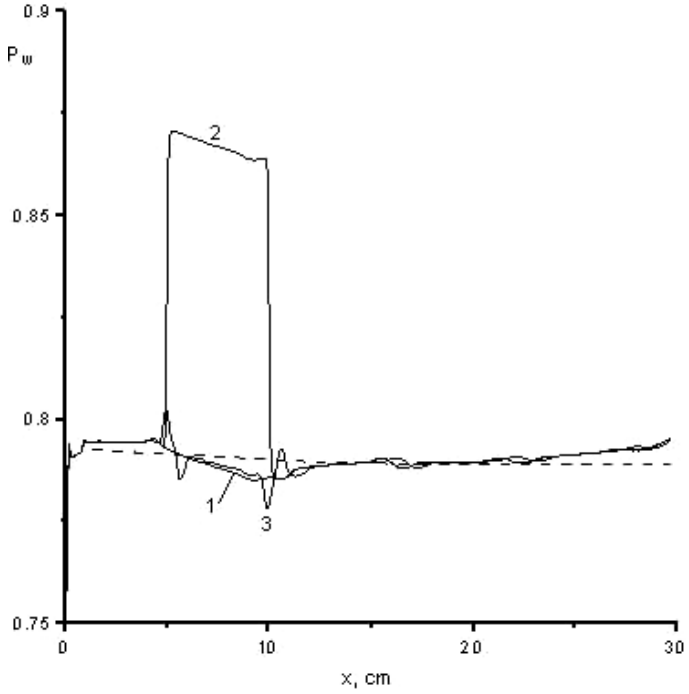

Fig.4.18. Time history of wall pressure p_w, atm distribution along plate surface for $M_\infty = 0.8$.
Notations as on Fig. 2.3.

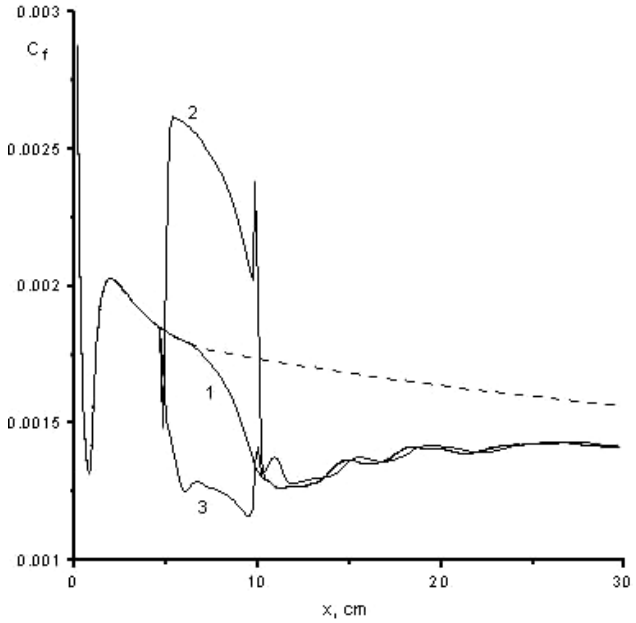

Fig.4.19. Time history of local skin-friction distribution along plate surface for M_∞ = 3.0
1 - t = 800 μs, 2 – t = 801 μs, 3 – t = 812 μs

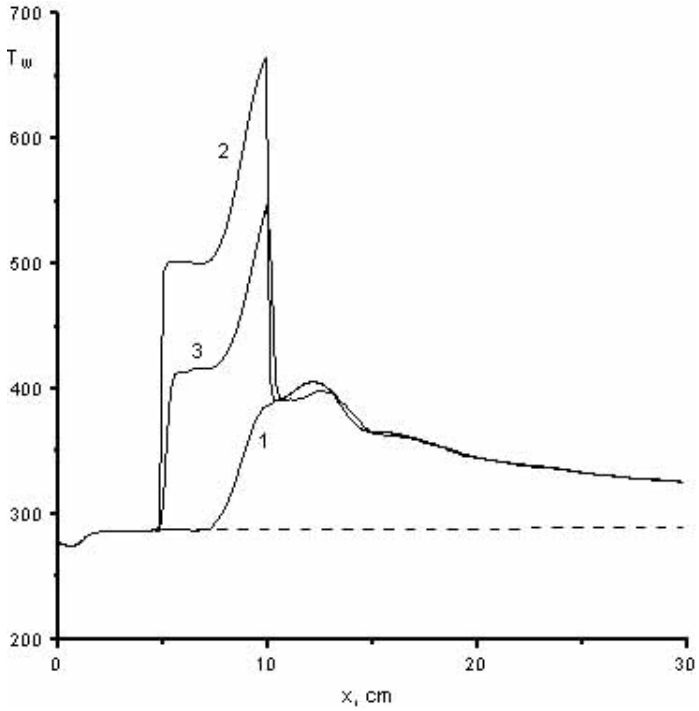

Fig.4.20. Time history of wall temperature T_w, K distribution along plate surface for M_∞ = 3.0. Notations as on Fig. 2.6.

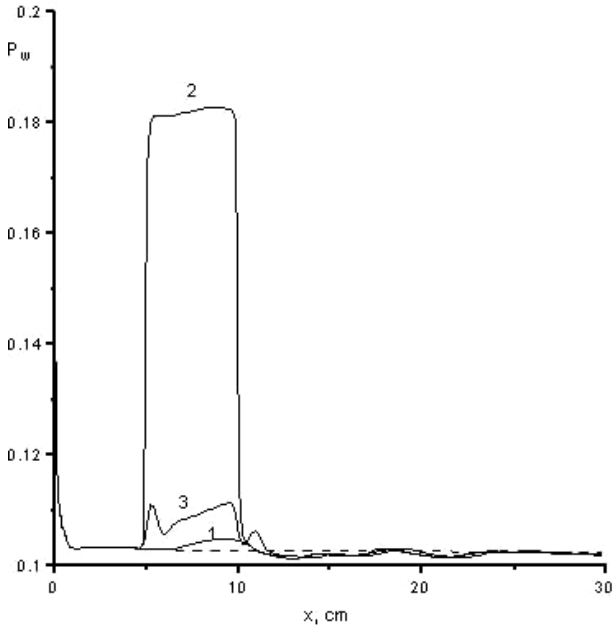

Fig.4.21. Time history of wall pressure p_w, atm distribution along plate surface for M_∞ = 3.0. Notations as on Fig. 4.19.

It is seen that gas heating produces significant local disturbances of gas flow parameters in heat supply region. These disturbances are greater for supersonic flow then for transonic. For M_∞ = 0.8 local skin-friction coefficient c_f changes within the limits of 10%, wall pressure p_w and temperature T_w increase to 10% and to 80 K accordingly. For M_∞ = 3.0 c_f changes within the limits of 45%, p_w increases in 1.8 time and T_w increases to 400 K. After heat supply stopping skin-friction decreases to level below of one without heat supply. Wall temperature also decreases but remains above of its value without gas heating. Pressure perturbations practically damp to cycle end.

Space distributions of density, temperature and turbulent energy in the near wall region for different instants of time are displayed in **Figs. 4.22 –. 4.27**

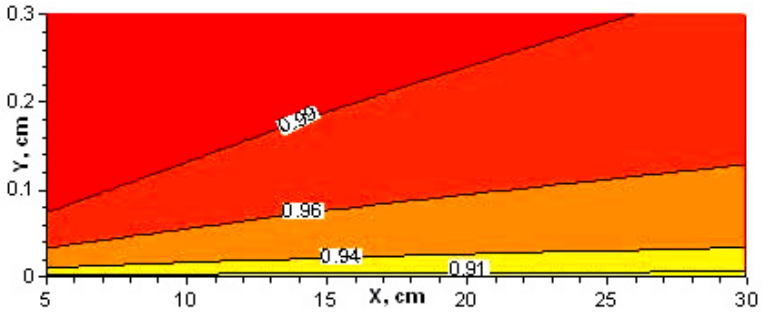

(a) Density, t=0

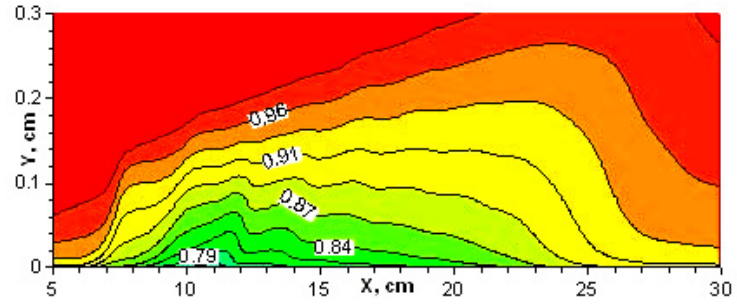

(b) Density, t=1200 μs

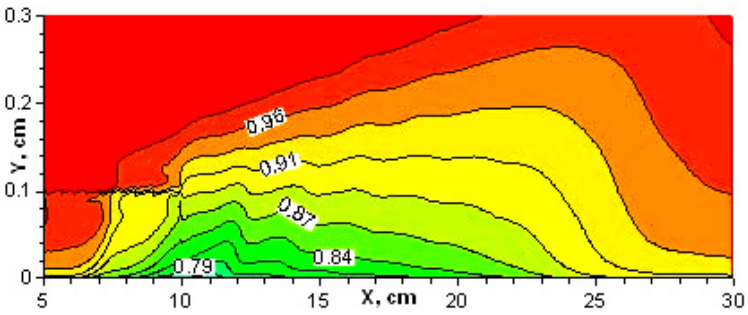

(c) Density, t=1201μs

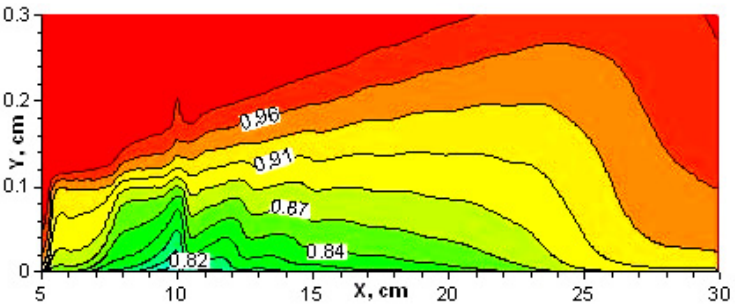

(c) Density, t=1212 μs

Fig.4.22. Time history of ρ / ρ_{∞} near wall contours for M_{∞} = 0.8

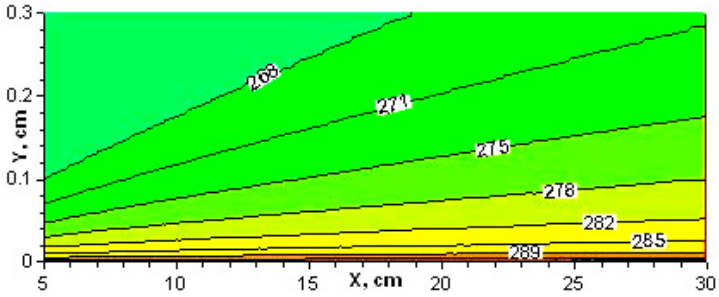

(a) Temperature t=0

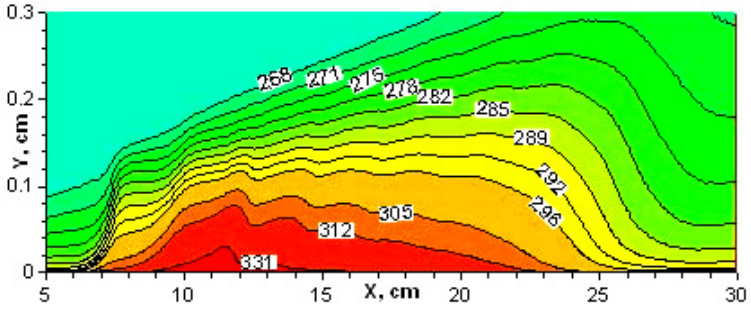

(b) Temperature t=1200 μs

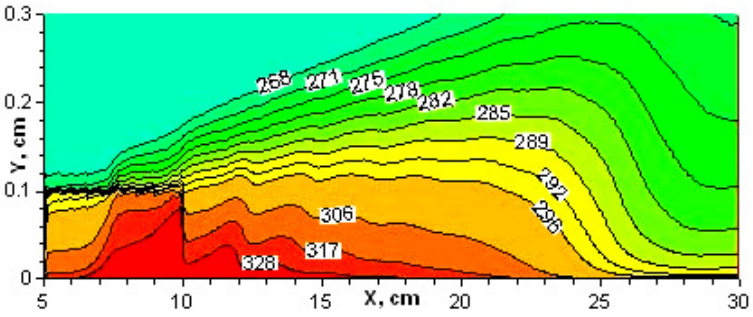

(c) Temperature t=1201 μs

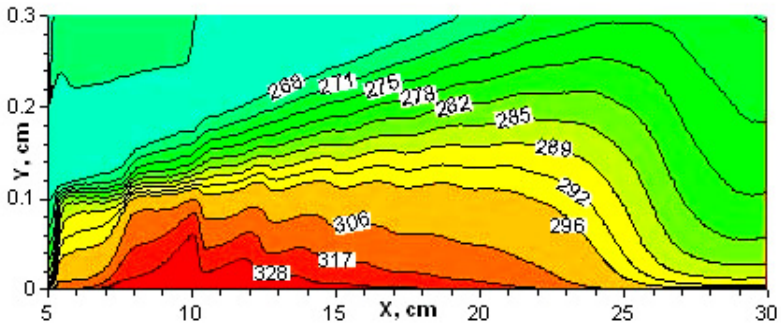

(d) Temperature t=1212 μs

Fig. 4.23. Time history of gas temperature T_w, K near wall contours for M_∞ = 0.8

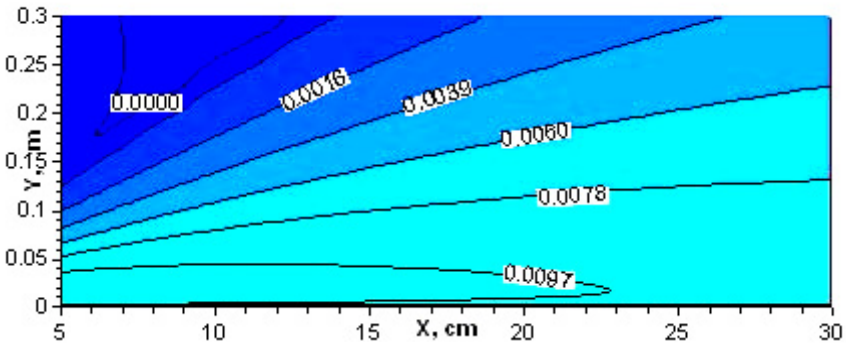

(a) Turbulent energy t=0 μs

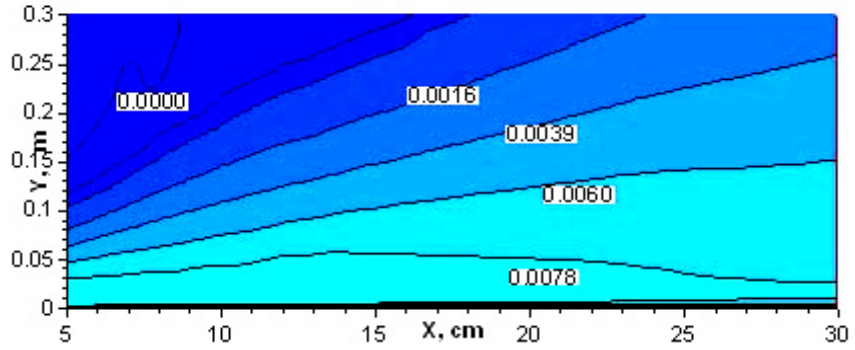

(b) Turbulent energy t=1200 μs

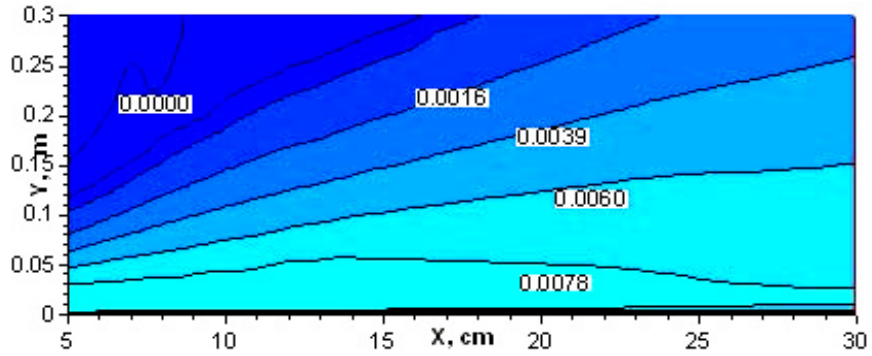

(c) Turbulent energy t=1201 μs

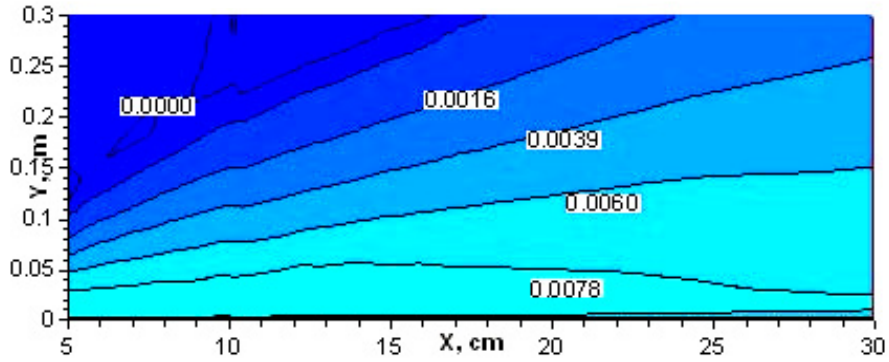

(d) Turbulent energy t=1212 μs

Fig.4.24. Time history of turbulent energy $k/0.5u_{\infty}^{2}$ near wall contours for M_{∞} = 0.8

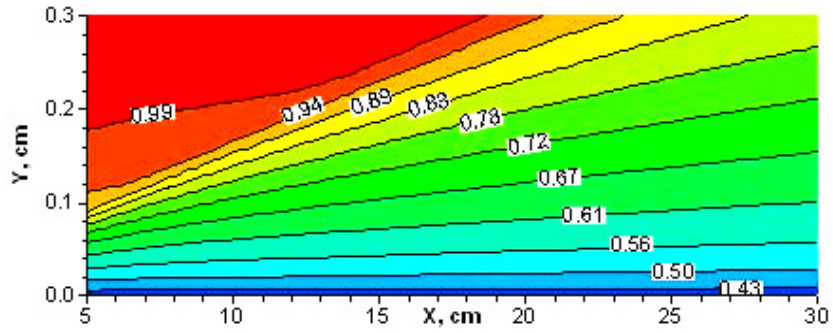

(a) Density t=0 μs

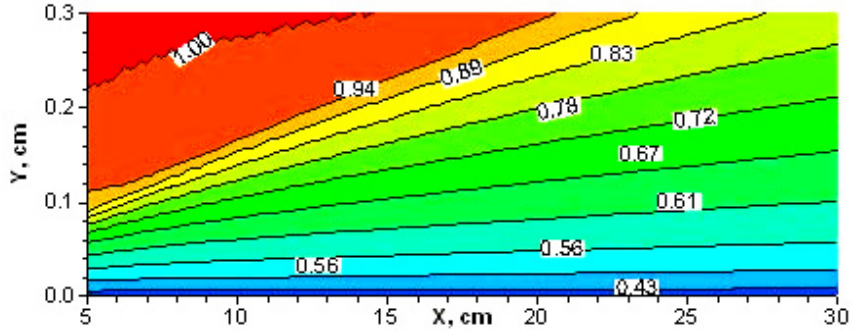

(b) Density t = 800 μs

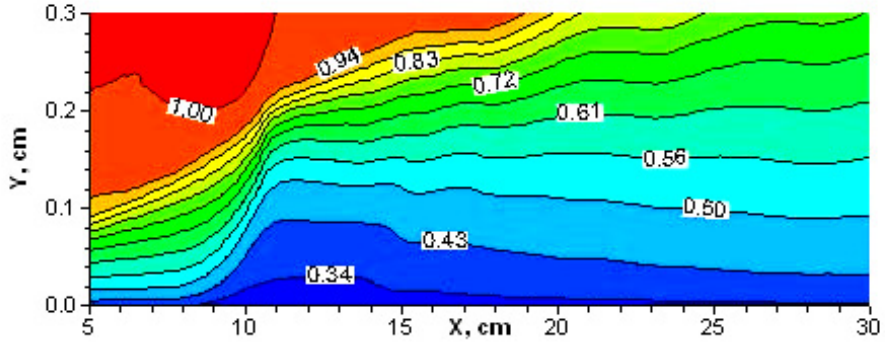

(c) Density t = 801 μs

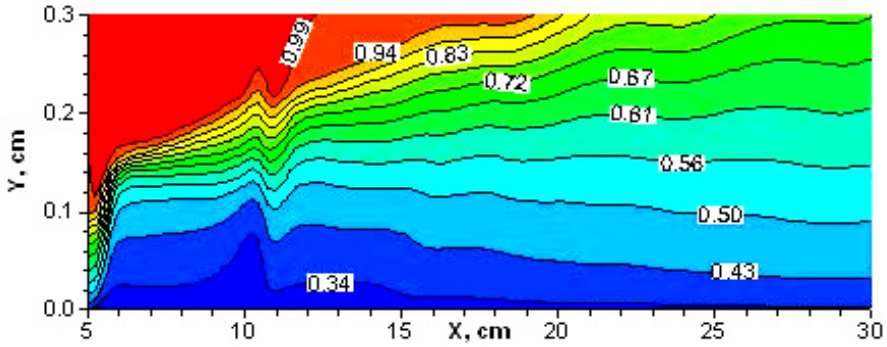

Fig.4.25. Time history of ρ / ρ_{∞} near wall contours for M_{∞} = 3.0

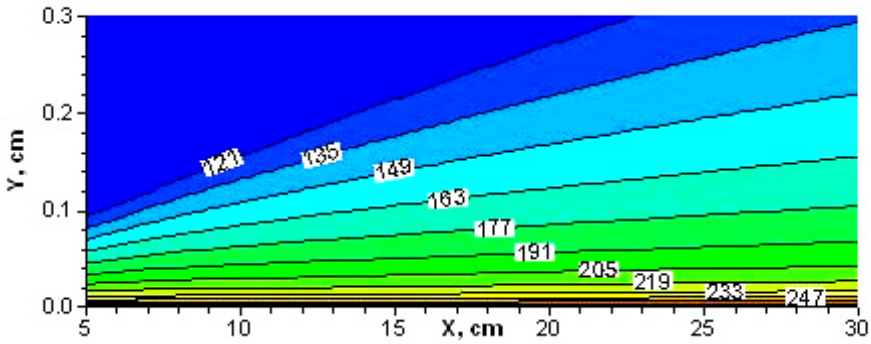

(a) Temperature t = 0 μs

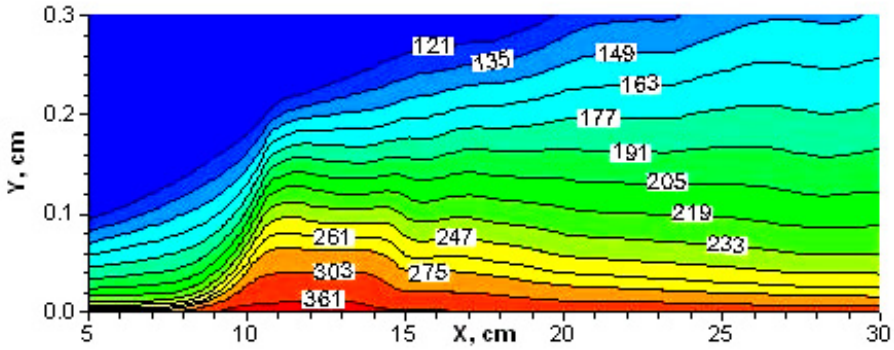

(b) Temperature t = 800μs

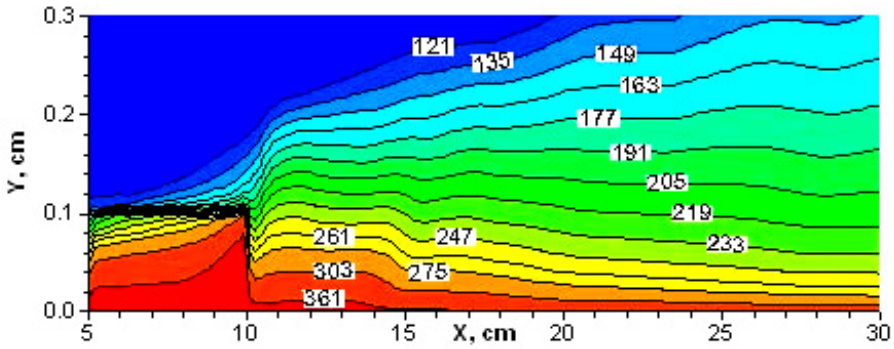

(c) Temperature t = 801 μs

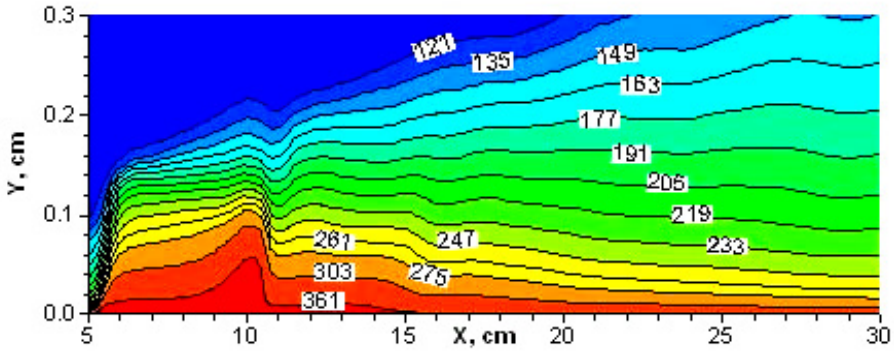

(d) Temperature t = 812 μs

Fig. 4.26. Time history of gas temperature T, K near wall contours for M_∞ = 3.0

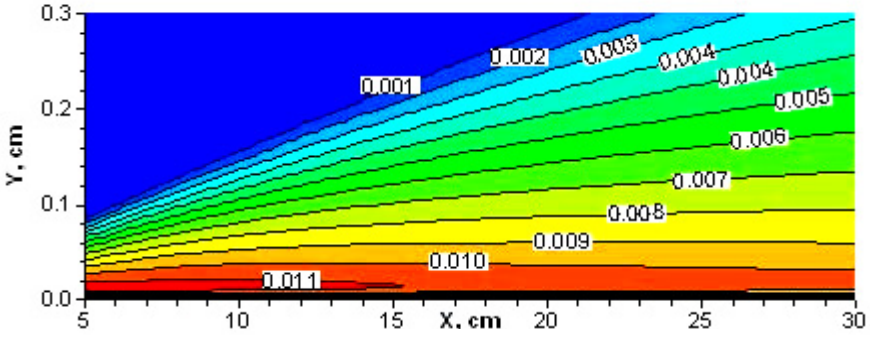

(a) Turbulent energy t = 0 μs

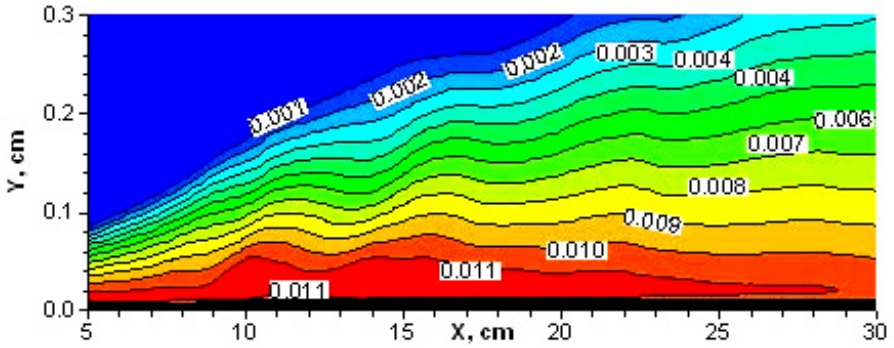

(b) Turbulent energy t = 800 μs

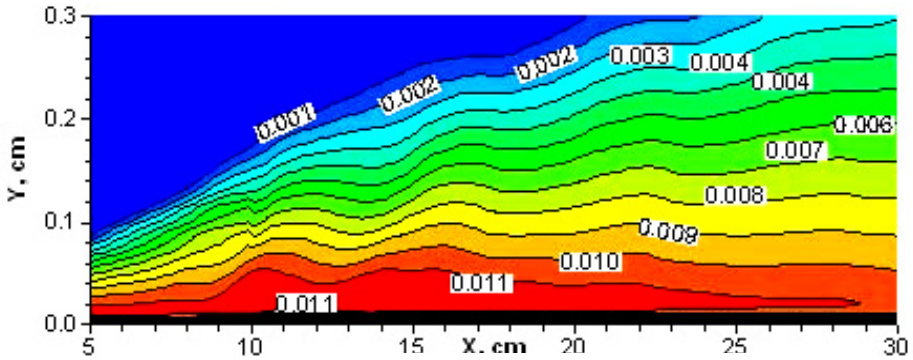

(c) Turbulent energy t = 801 μs

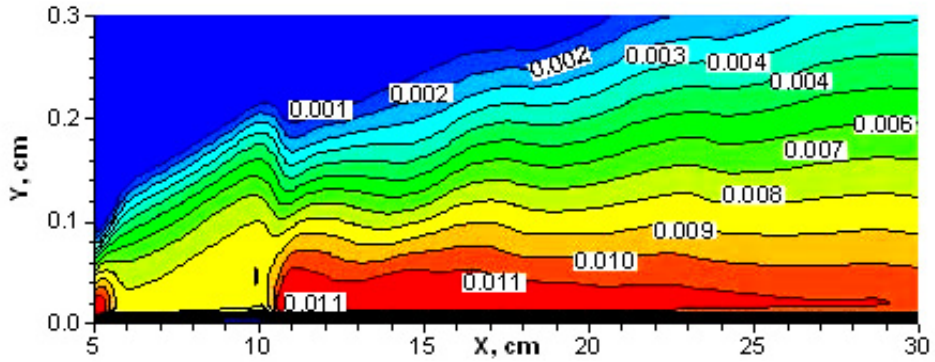

(c) Turbulent energy t = 812 μs

Fig.4.27. Time history of turbulent energy $k/0.5u_\infty^2$ near wall contours for M_∞ = 3.0

4.4. Numerical simulation of sliding discharge effects on trans- and supersonic flows over flat plate using lag model of turbulence.

4.4.1. Lag turbulence model

Turbulent (Reynolds) stress tensor $\hat{\tau}_T$ are expressed as

$$\hat{\tau}_T = 2\mu_T\hat{\varepsilon}\,,\ \mu_T = \rho\upsilon_T \quad ,$$

where μ_T is eddy viscosity and components of the tensor of deformation rates $\hat{\varepsilon}$ are determined as

$$\varepsilon_{ij} = \frac{1}{2}\left[\frac{\partial u_i}{\partial x_j} + \frac{\partial u_j}{\partial x_i} - \frac{2}{3}\frac{\partial u_k}{\partial x_k}\delta_{ij}\right],$$

Kinematical eddy viscosity υ_T is determined in combination with turbulent energy k and specific dissipation rate ω from three differential equations:

$$\frac{\partial \rho k}{\partial t}+\frac{\partial}{\partial x_j}\left(\rho u_j k-(\mu_M+\sigma_T^*\mu_T)\frac{\partial k}{\partial x_j}\right)=b_k,$$

$$\frac{\partial \rho \omega}{\partial t}+\frac{\partial}{\partial x_j}\left(\rho u_j \omega-(\mu_M+\sigma_T\mu_T)\frac{\partial \omega}{\partial x_j}\right)=b_\omega,$$

$$\frac{\partial \rho \upsilon_T}{\partial t}+\frac{\partial}{\partial x_j}\left(\rho u_j \upsilon_T\right)=b_\upsilon,$$

where

$$b_k=\mu_T\hat{\varepsilon}_{ij}\frac{\partial u_i}{\partial x_j}-\beta_T^*\rho\omega k,\quad b_\omega=\gamma_T\rho\hat{\varepsilon}_{ij}\frac{\partial u_i}{\partial x_j}-\beta_T\rho\omega^2,\ b_\upsilon=a(R_T)\rho\omega(\upsilon_{TE}-\upsilon_T)$$

$$a(R_T)=a_0\left[\frac{(R_T+R_{T0})}{(R_T+R_{T\infty})}\right],\quad R_T=\frac{\rho k}{\mu_M\omega},\ \upsilon_{TE}=\frac{k}{\omega}$$

$\beta_T^*=0.09,\ \gamma_T=0.56,\ \beta_T=0.075,\ \sigma_T=0.5,\ \sigma_T^*=0.5,\ a_0=0.35,\ R_{T0}=1,\ R_{T\infty}=0.01.$

Turbulent heat flux $\vec{q}_T$ are expressed as

$$\vec{q}_T=-\lambda_T\frac{\partial T}{\partial \vec{r}},\ \lambda_T=\frac{\mu_T c_p}{\mathrm{Pr}_T}.$$

It is assumed that turbulent Prandtl number is $\mathrm{Pr}_T=1$.

4.4.2. Effect of turbulence model variation on skin-friction prediction

Calculations of flow over blunted plate length of 30 cm and thickness of 0.02 cm have been performed for two stream conditions of planned experiments in wind tunnel A-7:

3) Mach number $M_\infty=0.8$, total pressure $p_0=1.2$ atm, and total temperature $T_0=300K$;
4) Mach number $M_\infty=3.0$, total pressure $p_0=3.7$ atm, and total temperature $T_0=300K$.

The pulse-periodic heat deposition modeling sliding discharge has been considered. In calculations pulse length t_p is of 1 μs, form of pulses is triangular, pulse frequency f_p is 10 *kHz*, total heat supply during one impulse (cycle) $Q_p=10^{-2}$ J/cm. Heat supply was distributed uniform into space region $5\le x\le 10$ cm, $0\le y\le 0.1$ cm, where x, y are Cartesian coordinates attached to plate surface. This case heating distribution corresponds to the longitudinal sliding discharge. The heat supply was started in initially steady-state turbulent stream.

Calculations have been carried out using described in previous report [2.1] gas phase and gas-wall interactions models, and the same numerical technique.

Fig. 4.28. shows the predicted for M_∞ = 0.8 time distributions of total skin-friction coefficient C_f for plate section $0 \le x \le 30$ cm. The value of C_f is defined by expression

$$C_f = \int_{x_b}^{x_e} \tau_w dx / 0.5 \rho_\infty V_\infty^2 (x_e - x_b),$$

where τ_w is the local skin-friction, ρ_∞ and V_∞ are the free stream density and velocity accordingly, $x_b = 0$ cm, $x_e = 30$ cm. For comparison on this Figure coefficients C_f calculated without heat supply C_f^0 and for steady heat supply C_f^{st} in the same space region with power $P_w = 100\ W/cm$ are presented also. This value of heating power is equal to averaged through cycle power of considered pulse-periodic heat supply $Q_p f_p$. The averaged through period values of C_f are shown on Figure by dotted line. Similar data predicted for M_∞ = 3.0 are shown on Fig. 4.29.

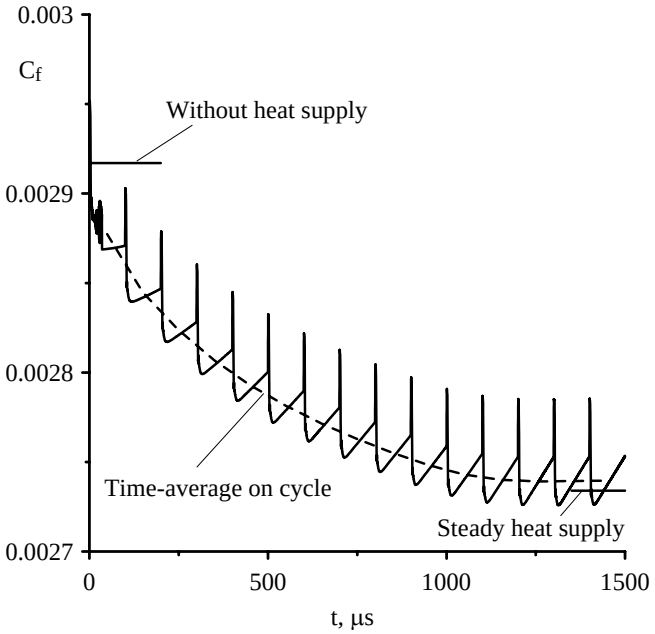

Fig.4.28. Time variation of total skin-friction coefficients for M_∞ = 0.8

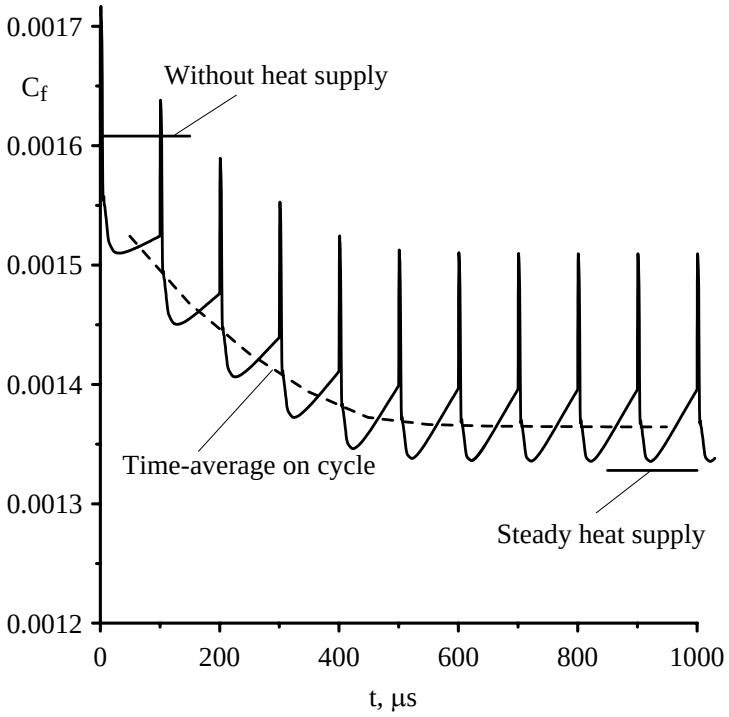

Fig.4.29. Time variation of total skin-friction coefficients for M_∞ = 3.0

Comparison of steady-state and averaged values of C_f predicted by baseline turbulence model and lag model are presented on Figs. 4.30 and 4.31. for M_∞ = 0.8 and M_∞ = 3.0 accordingly. The results of computations with the baseline model are shown by red lines. It is seen that the lag model predicts more low values of C_f then baseline model for both steady und unsteady calculations. The relative positions of these quantities are not changed.

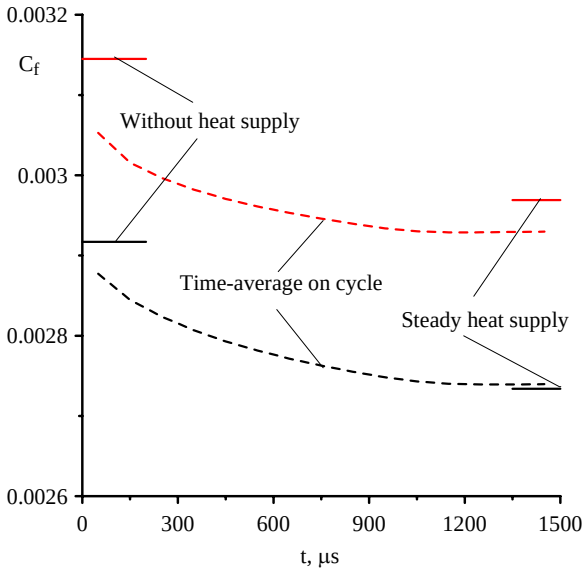

Fig.4.30. Comparison of steady-state and averaged values of C_f predicted by baseline (red line) and lag (black line) $k-\omega$ turbulence models for M_∞ = 0.8

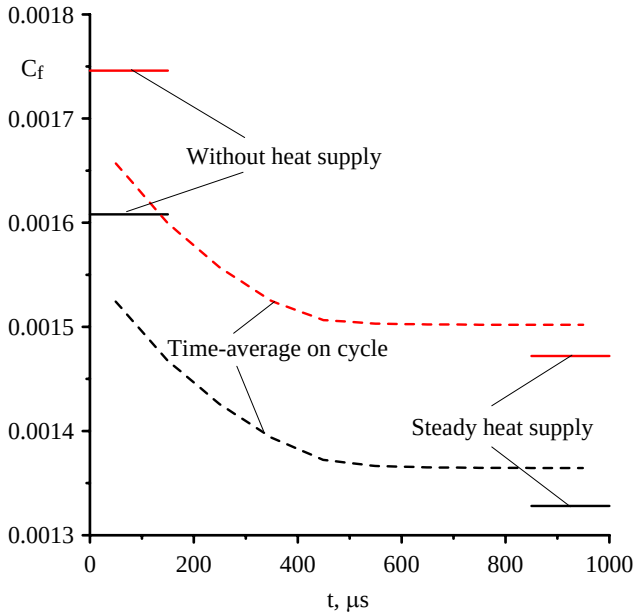

Fig.4.31. Comparison of steady-state and averaged values of C_f predicted by baseline (red line) and lag (black line) $k-\omega$ turbulence models for M_∞ = 3.0

Conclusions

In the present Report we represent results of theoretical and experimental investigations of sliding discharge applicability in problems of plasma aerodynamics.

Following results can be attributed to most important

1. Physical model of the sliding discharge was elaborated it allowed to reveal the following typical features of the sliding discharge. High current sliding discharge takes place in two stages. At the first stage, which is characterized by high uniformity, the linear capacity process of charging takes place. At the second stage takes place a self maintained breakdown of the inter electrode gap. In general case the *E/N* parameter depends on the linear dielectric capacity magnitude, gas pressure value over the dielectric, an amplitude and a velocity of applied voltage rising, etc. Changing of main parameters depends on the sliding discharge organization. An important difference of the sliding discharge over the dielectric surface from other discharges is the possibility of its realization at different *E/N* values, which depend or do not depend on plasma conductivity. Ionization processes at the front of the high current uniform sliding discharge, which condition the propagation of the voltage wave, are determined by the parameter $E / N \cong (1/(N v))(\partial U / \partial t) \approx const$.

The *E/N* value is determined by the sort of a gas, and is close to the maximum values of those in the pulse volume discharges.

Represented approximate analysis shows that the sliding discharge plasma layer of 1-1,5 mm width is heated up to the temperature $\Delta T \sim (2\text{-}3)\cdot 10^3$ K during the pulse time of the discharge of about hundreds of nanoseconds, obtained characteristics can be used as initial ones for the gasdynamic analysis.

The possibility of creation of rather uniform brightly luminous large size plasma surfaces with a help of the sliding discharge in incomplete and complete forms at rather moderate requirements to the feeding source allows to use this discharge for creation of plasma cathodes and heating devices, which can be applied in aerodynamics.

Obtained results show that kinetic energy losses of the vortex in the plasma layer are determined by the dipole moment value and the angular velocity of the vortex. They drop down proportionally to the value of the angular velocity for the vortex of the given radius. So creation of the plasma layer in the region of the turbulent floe leads to the effective suppression of the low frequency components of the turbulence spectrum, shifting it to the region of high frequencies, i.e. to the region where the effective dissipation of the vortices energy takes place due to the viscous friction forces.

In an area of laminar boundary layer there are created conditions leading to formation of tangential velocity discontinuity in the boundary layer at sliding discharge initiation. Spectral composition of velocity disturbances amplitudes covers wide area starting from some minimum value to the value equal to flow velocity V_b. In time this spectral composition transforms so that all the spectral components have the velocity amplitude ~ V_b, So one there is a rectangular envelope of signal spectrum at the outlet from the break area, i.e. all the spectral components have the velocity amplitude ~ V_b. From aforesaid follows that if one represents velocity jump in the area of the tangential break in a form of disturbances spectrum with frequencies from w_0 to w_n then the transformation of the initial spectrum can be observed in the area of the break in the result of disturbances development (from falling hyperbola to uniform distribution over the frequency axis). Undertaken estimates have sooner the qualitative character, since for more precise calculations one has to undertake an estimate of instabilities (developing in the break zone) energy losses, accounting of different scale instabilities rise dynamics, etc. Our goal was to indicate a possibility of tangential break appearance at the boundary between the hot and cold gas layers and to analyze disturbances development character in the break area.

Obtained results show that there is an opportunity of a boundary layer control from a laminar to a turbulent and visa versa, i.e. there is an opportunity to control a value of tangential tension.

2. Numerical study of sliding discharge effects on trans- and supersonic flows over flat plate are carried out using of local heat source model of discharge. The previously developed under the Project Navier-Stokes technique and codes for modeling of sliding discharge interactions with supersonic gas flows were used.

a. Calculations of flows over blunted plate length of 30 cm have been performed for two free stream conditions of planned experiments on wind tunnel A-7: 1) Mach number M_∞ = 0.8, total pressure $p_0 = 1.2\,\text{atm}$, and total temperature $T_0 = 300K$; 2) Mach number M_∞ = 3.0, total pressure $p_0 = 3.7\,\text{atm}$, and total temperature $T_0 = 300K$. The pulse-periodic heat deposition modeling sliding discharge has been considered. In calculations pulse length t_p was equal $1\mu s$, form of pulses was triangular, pulse frequency f_p was 10 *kHz*, total heat supply during one impulse (cycle) equal Q_p = 10^{-2} J/cm. It was supposed that heat supply is distributed uniform into near wall space region $5 \le x \le 10$ cm , $0 \le y \le 0.1$cm .

b. Effects of heat deposition on skin-friction and flow parameters were studied. Total skin-friction coefficient C_f for whole plate performs oscillations of relatively high amplitude near mean curve

that approaches with time to the asymptotic value $C_{f\infty}$. For M_∞ = 0.8 value of $C_{f\infty}$ is above of total skin-friction coefficient C_f^{st} for equivalent steady gas heating. For M_∞ = 3.0 $C_{f\infty}$ is below of C_f^{st} . The relaxation time is about 1.0 ms for M_∞ = 0.8 and 0.5 ms for M_∞ = 3.0. Reduction of asymptotic mean value of C_f is about 6.8% for M_∞ = 0.8 and about 14% for M_∞ = 3.0.

c. Heat supply produces significant local disturbances of gas flow parameters in heat supply region.. These disturbances are greater for supersonic flow then for transonic.

d. Numerical study of sliding discharge effects on trans- and supersonic flows over flat plate were carried out using of local heat source model of discharge. The lagged $k-\omega$ turbulence model is applied for calculations of the steady and unsteady flows over flat plate for wind tunnel experiments conditions at Mach numbers M_∞ = 0.8, and 3.0. This turbulence model has been proposed by Olsen and Coakley [2.4] to simulate unsteady flows.

. Comparison of steady-state and averaged values of C_f predicted by baseline turbulence model and lag model are shown that the lag model predicts lower values of C_f then baseline model for both steady und unsteady calculations. The relative positions of these quantities are not changed.

Results of the fulfilled numerical investigations confirm results of theoretical investigations and can be used for planning and interpretation of experiments on created experimental facility.

Investigations of sliding discharge plasma influence on a character and structure of a picture of the working model streamlining by an incident flow at the flow velocity corresponding to the Mach number M =3 have been carried out for the first time during the execution of this project. The sliding discharge was initiated on a surface of the working model in a boundary layer. Conditions have been determined at which stable development of the sliding discharge over a separation boundary of two dielectrics with different dielectric permittivity (two solid dielectrics and solid and liquid dielectrics) is observed. Sliding discharge characteristics in different conditions have been determined (at different pressures, in gas flow and without flow in wind tunnel). Pressure measurements on the working model surface has been made before and after a boundary layer disturbance by the sliding discharge. Change of gas flow around character was detected at minimal energy put of ~ 0.1 J/cm^3 to the discharge (boundary layer thickness change, inclination angle change of disturbances lines, turbulization of a boundary layer, changing of static pressure behind the excitation zone). We undertook investigation of gas flow streamlining character of two types of working models: a flat plane and a cylinder.

References

1. Quarterly technical report under CRDF Project RP0-1382-MO-03 for first quarter.

.2. Quarterly technical report under CRDF Project RP0-1382-MO-03 for second quarter.

.3. Quarterly technical report under CRDF Project RP0-1382-MO-03 for third quarter

4. Annual Technical Report of CRDF Project # RPO-1382-MO-03 (From June 2003 to June 2004)

5. Quarterly technical report under CRDF Project RP0-1382-MO-03 for fifth quarter.

6. Quarterly technical report under CRDF Project RP0-1382-MO-03 for sixth quarter.

7. Quarterly technical report under CRDF Project RP0-1382-MO-03 for seventh quarter.

8 Kovalev I.O., Kuz'min G.P., Nesterenko G.P. Pulsed CO_2 – lazers with plasma electrodes. Works of IOFAN. V. 52. Moscow. Nauka. 1996. P. 3-91.

9 Dashuk P.N., Chelnokov L.L., Yarysheva M.D. Characteristics of the sliding discharge over the surface of solid dielectrics with reference to high voltage commutators. Electronnaya tekhnika. Ser. 4. 1975. №.6. P. 9-17.

10 Folrat K. Spark light sources and high speed photography. In a book Physics of high speed processes. V.1. Moscow. Mir. 1971. 135 P.

11 Kovalchuk B.M., Kremnev V.V., Mesyats G.A., Yurike Ya. Ya. Development of the surface discharge over a dielectric with high dielectric permeability in a gas in the nanosecond range. Zhurnal Prikladnoi Mekhaniki i Tekhnicheskoi Fiziki. 1973. №1. P.48-55.

12 Reter G. Electron avalanches and a breakdown in gases. Moscow. Mir. 1968. 390 P.

13 Baranov V.Yu., Borisov V.M., Vysikailo F.I., Khristoforov O.B. Investigations of the uniform high current sliding discharge forming conditions. Teplofizika. Vysokhikh Temperatur. 1984. V.22. № 4. P. 661-666.

14 Babich L.P. On a nature of photo – ionizing radiation in initial stage of nanosecond gas discharges. Izvestiya Vuzov. Radiofizika. 1975. T.18. № 7. P. 1056-1058.

15 Dashuk P.N., Kulakov S.L. X-ray radiation of the nanosecond sliding discharge in a gas. Pis'ma v Zhurnal Tekhnicheskoi Fiziki. 1975. T.5. № 2. P. 69-72.

16 Bertsev V.V., Dashuk P.N., Lysakovskyi G.G. Volt-Coulomb characteristics of the sliding discharge. Izvestiya Vuzov. Energetika. 1963. № 6. P. 24-31.

17 Borisov V.M., Vysikailo F.I., Khristoforov O.B. Investigations of the uniform high current sliding discharge. Teplofizika. Vysokhikh Temperatur. 1983. V.21. № 5. P. 844-851.

18 Dashuk P.N., Sergeenkova E.A. Spectroscopic investigations of the sliding discharge characteristics in the streamer and spark stages. II All Union Sympos. on gas laser physics. Novosibirsk. 1975. P. 154.

19 Bashkin A.S., Grigoriev P.G., Oraevskyi A.P., Skvortsov A.B. Powerful UV –radiation source about 1 mcs duration for pumping of gas lasers. Kvantovaya Electronika. 1976. V.3. № 8. P. 1824-1826.

20 Grigoriev A.B., Dashuk P.N., Markov S.N. et.al. Low inductive Mega ampere current commutator with the sliding discharge. Pribory i Tekhnika Eksperimenta. 1976. №8. P. 151-153.

21 Andreev S.I., Zobov E.A., Sidorov A.N. Controlling method of the sliding sparks parallel channel system development and forming in air at atmospheric pressure. Zhurnal Tekhnicheskoi Fiziki. 1976. №3. P.12-17.

22 Daniel E.V. Development of the surface spark discharge channel. Zhurnal Tekhnicheskoi Fiziki. 1965. V.35. № 4. P. 769-771.

23 Vanyukov M.P., Daniel E.V. To the question of development of the surface discharge channel. Zhurnal Tekhnicheskoi Fiziki. 1967. V.37. N.8. C. 1529-1532.

24 Daniel E.V. Influence of the voltage polarity on of the surface discharge channel. Zhurnal Tekhnicheskoi Fiziki. 1968. V.38. N.7. P. 1181-1182.

25 Andreev S.I., Vanyukov M.P., Daniel E.V. Application of the surface spark discharges for pumping of OQG. Zhurnal Tekhnicheskoi Fiziki. V.37. N.8. P. 1527-1529.

26 Vanyukov M.P., Daniel E.V. Surface spark discharge as the light source. Optiko-mekhanicheskaya promyshlennost. 1969. № 5. P. 13-15.

27 Kuz'min G.P., Minaev I.M., Rukhadze A.A. Flow of viscous gas around a plasma sheet created by the sliding discharge. Teplofizika Vysokikh Temperatur, 2002, V. 40, № 3, P. 515.

28 Minaev I.M., Rukhadze A.A. On localization of the pulse periodic discharge near the dielectric flown around by viscous gas Teplofizika Vysokikh Temperatur, 2003.

29 Zeldovich Ya.B., Raizer Yu. P. Physics of shock waves and high temperature hydrodynamic phenomena. Moscow. Nauka. 1963.

30 Landau L.D., Lifshits E.M. Mechanics of continuous media. Moscow. Fizmatlit. 1954.

31 Krasnov N.F. Aerodynamics. Vysshaya Shkola, Moscow. 1980

32 Turbulence, Principles and applications. Editors W. Frost and T. Moulden. Mir. Moscow 1980.

33 Kuz'min G.P., Minaev I.M., Rukhadze A.A. Viscous gas flow around the plasma sheet created by the sliding discharge. Teplofizika Vysokhikh Temperatur, 2002, V. 40, № 3, P..515.

34 Minaev I.M., Rukhadze A.A. On the localization of the pulse periodic discharge on the dielectric flown around by the viscous flow. Teplofizika Vysokhikh Temperatur, 2003, V. 41.

35 Golant V.E., Zhilinsky A.P., Sakharov I.E. Foundations of plasma physics. Atomizdat. Moscow. 1972.

36 Brown. S. Elementary processes in gas discharge plasmas. Gosatomizdat. Moscow. 1961.

37 V.Buchkov, G.Kuz'min, I. Minaev, I.Timofeev, A.Rukhadze. Sliding discharge application in aerodynamics, 38 41st AIAA Aerospace Science Meeting and Exhibit, 6-9 January 2003, Reno, Nevada AIAA-paper 2003-0530.

39 Kuz'min G.P., Minaev I.M., Rukhadze A.A. Streamlining of plasma sheet by viscous gas flow. Teplofizika Vysokhih Temperatur, 2002, V 40, № 3, P.515.

40 Minaev I.M., Rukhadze A.A. On localization of viscous gas streamlined pulse periodic discharge on a dielectric. Teplofizika Vysokhih Temperatur, 2003.

41 Landau L., Liftshits E. Mechanics of fluids. Moscow. Nauka. 1982.

42 Gonorovsky I.S. Radiotechnical circuits and signals. Soviet Radio. Moscow. 1966.

43 Favre, A., "Equations des gas turbulents compressibles", Journal de Mecanique, 4, 1965.

44 Coakley, T.J. "Development of Turbulence Models for Aerodynamic Applications," AIAA Paper 97-2009, 1997

The Contractor, the Physical department of Moscow state university, hereby declares that, to the best of its knowledge and belief, the technical data delivered herewith

under CRDF Project #: RPO-1382-MO-03

"Modification of Aerodynamic Surfaces Using Plasma"
is complete, accurate, and
complies with all requirements of the contract."

"I certify that there were no subject inventions to declare as
defined in FAR 52.227-13, during the performance of this contract."

Dean of Physical department V.I. Trukhin

DATE: 22. July. 2005